# Parametric Optimization of Dynamic Power Cable Configurations

## for Floating Offshore Wind Applications

M.P. van der Tholen

Technische Universiteit Delft

TU Delft

# Parametric Optimization of Dynamic Power Cable Configurations

## for Floating Offshore Wind Applications

by

M.P. van der Tholen

in partial fulfilment of the requirements for the degree of

**Master of Science**
in Mechanical Engineering

to be defended publicly on Monday February 27, 2023 at 14:15.

| | | |
|---|---|---|
| Student number: | 4341775 | |
| MSc track: | Multi-Machine Engineering | |
| Report number: | 2023.MME.8762 | |
| Supervisors: | Dr. ir. X. Jiang | |
| | Dr.-Ing. S. Schreier | |
| Thesis committee: | Dr. ir. X. Jiang | TU Delft committee chair, 3mE |
| | Dr.-Ing. S. Schreier | TU Delft committee member, 3mE |
| | Dr. ir. A. Jarquin Laguna | TU Delft committee member, 3mE |
| Date: | February 27, 2023 | |



TU Delft

# Preface

This thesis was written as a final assignment to obtaining a MSc. degree in Mechanical Engineering, track Multi-Machine Engineering, at Delft University of Technology. The objective of this Thesis is to give a complete overview of my research on the topic of parametric optimization of the dynamic power cable configuration. My work aims to contribute to the knowledge about the preliminary design of dynamic power cables for offshore wind turbines. The driving force behind formulating this research objective has been the importance of developments of floating offshore wind turbine and associated dynamic power cable technology. In the near future, floating offshore wind will be playing a crucial role in the transition towards more sustainable energy production.

Throughout the writing of this thesis, I have learned a great deal about how to individually complete a large research project. The process is very dynamic and lots of persistence is required to able to achieve the research objective. Frequent reconsideration of the research approach and goals is an important aspect of this process. My knowledge on simulation-based optimization and numerical modelling in a marine environment, the latter of which had previously not been part of my mechanical engineering background, has greatly improved. The gathered experience is undoubtedly going to be valuable throughout the rest of my career.

I would like to thank my daily supervisors Xiaoli Jiang and Sebastian Schreier for granting me their constant support and expertise. The feedback during the bi-weekly meetings has been invaluable. Further acknowledgements go out to the third member of the thesis committee, Antonio Jarquin Laguna, and the staff members of the Transport Engineering and Logistics research group, who have taught me the important skills needed to become an engineer. Finally, I would like to thank my family and friends for their unconditional support in a time filled with much hard work, blood, sweat and tears. I will be dearly missing the coffee breaks outside the master student study landscape on the fourth floor of the faculty.

*Max van der Tholen*
*Delft, February 2023*

# Summary

The combination of worldwide population growth and battle against climate change has created a pressing demand for more renewable energy sources. Offshore wind technology plays an important role in this energy transition. However, there are not enough available locations for conventional bottom-fixed offshore wind turbines, mainly due to water depth limitations. This has led to the rapid development of Floating Offshore Wind Turbines (FOWT), which are suitable for deployment in much deeper waters.

One of the critical components of a FOWT system is the inter-array power cable. This cable hangs freely down the water column and is therefore subjected to the dynamic loads from environment and floater movements. This cable is referred to as the Dynamic Power Cable (DPC). The harsh environmental loading makes the DPC is susceptible to mechanical failures during operation. There is a particular risk of fatigue damage to the copper conductor cores, due to the cyclic loading.

DPC technology is yet a fairly unexplored field of research. There is a demand for specific methods for the analysis and design of DPCs. This MSc thesis presents the development of a parametric DPC model for the analysis of the cable, along with a method for the optimization of the DPC configuration. The goal was to develop a method that can calculate an optimized preliminary cable configuration within reasonable computational time and which is applicable to a wide range of environmental scenarios, without requiring much expert knowledge or pre-analysis. The objective for the optimization was minimization of the fatigue damage.

An extensive literature study was conducted on the state-of-the-art of DPC design, analysis and optimization. This revealed the relevant loads, design requirements and designs parameters. The methodology for decoupled structural response and fatigue analysis was documented. The possibilities of blackbox optimization methods for the application with expensive simulation models were explored, and the progress on DPC optimization by previous authors was explained.

A global parametric model of a Lazy Wave Shape (LWS) DPC configuration was formulated using the software package OrcaFlex. This served as a basis for the calculation of structural response and fatigue damage on the DPC. The modelling choices were verified by conducting experiments and comparing the simulated results to analytically derived values. Finally, convergence and sensitivity studies were performed to tune the parameters for the simulations and investigate the influence of the global model parameters on the structural and fatigue behaviour of the DPC.

A model-based optimization method was presented. The design of experiment consisted of a static analysis of samples across the search space, after which a feasible search space was defined. The boundaries of the feasible search space were defined as a function of the water depth, which allows for application to scenarios with different water depths, without generation of infeasible samples. A radial basis function interpolant was used to construct a surrogate model on the sampled training data. The optimization problem was solved by applying an iterative search strategy, which gradually moved from exploratory to exploitative search, in an attempt to not prematurely converge to a local optimum. The surrogate model was updated with each iteration until the error between the surrogate model and the real model evaluation reached an error threshold. The workings of the proposed algorithm were verified by conducting experiments with a known test function.

Experiments were carried out to validate the optimization method, in terms of convergence, robustness and efficiency. Herein, different environmental case studies were formulated and several executions of the optimization algorithm were carried out. Additionally, a Grid Search (GS) was applied to the same case studies and a reference configuration from literature was analysed for fatigue damage. The two decision variables for optimization were the cable length between the Hang-off Point (HOP) and the start of buoyant cable section and the total number of attached Buoyancy Modules (BM).

The results show good convergence properties, when comparing the final solutions from the optimization and GS runs. Superior fatigue performance was registered compared to the reference configurations. In terms of efficiency, the proposed optimization method clearly outperformed the GS. The algorithm can potentially be improved if the optimization parameters are tuned and if slight alterations to the search strategy are made. The calculated fatigue results show that an optimized DPC configuration balances the fatigue stresses between the HOP and the buoyant section of the cable as much as

possible. Positioning the buoyant cable section close to the HOP dampens the motions and stresses at the HOP, but increases them at the buoyant section. A too large or too small total number of BMs can lead to increased fatigue stresses at the HOP or at either characteristic bends of the LWS DPC.

# Samenvatting

De combinatie van wereldwijde bevolkingsgroei en strijd tegen klimaatverandering heeft geleid tot een dringende vraag naar meer hernieuwbare energiebronnen. Offshore windtechnologie speelt een belangrijke rol in deze energietransitie. Er zijn echter niet meer voldoende locaties bechikbaar voor conventionele offshore windturbines, die op vaste funderingen staan, voornamelijk vanwege de beperkte waterdiepte waarin deze funderingen gebouwd kunnen worden. Dit heeft geleid tot de versnelde ontwikkeling van drijvende offshore windturbines (Engels: Floating Offshore Wind Turbine (FOWT)), die geschikt zijn voor inzet in veel diepere wateren.

Een van de kritieke onderdelen binnen een FOWT-systeem is de stroomkabel die de afzonderlijke windturbines verbindt. Deze kabel hangt vrij naar beneden door de waterkolom en ondervindt daardoor dynamische belastingen die veroorzaakt worden door het omliggende zeemilieu en de bewegingen van het drijvende platform. Een kabel van deze soort wordt een dynamische stroomkabel (Engels: Dynamic Power Cable (DPC)) genoemd. Door de zware dynamische belastingen is de DPC gevoelig voor mechanische storingen tijdens de operatie. Door de cyclische belasting ontstaat een groot risico op schade door vermoeïïng aan de koperen geleiders in de kabel.

DPC-technologie is momenteel nog een vrij nieuw onderzoeksgebied. Daarom is er vraag naar specifieke methodes voor de analyse en het ontwerp van DPC's. Deze MSc-scriptie beschrijft de ontwikkeling van een parametrisch model van een DPC, dienend voor de analyse van de kabel. Daarnaast wordt een methode voor de optimalisatie van de DPC configuratie gepresenteerd. Het doel hiervan was om een methode te ontwikkelen die, gebruikmakend van beperkte rekentijd, een geoptimaliseerde kabelconfiguratie kan berekenen en die toepasbaar is op een breed scala aan omgevingsscenario's, zonder dat daar veel vakkennis of vooranalyse voor nodig is. Het optimalisatiecriterium was het minimaliseren van de schade door vermoeïïng.

Een uitgebreide literatuurstudie is uitgevoerd naar nieuwste ontwikkelingen op het gebied van DPC-ontwerp, -analyse en -optimalisatie. Hieruit werd een overzicht van de de relevante krachten, ontwerpeisen en ontwerpparameters die van toepassing zijn op DPC's vastgelegd. Het uitvoeren van analyses voor ontkoppelde structurele respons en vermoeïïng werd gedocumenteerd. De mogelijkheden van blackbox-optimalisatiemethodes voor de toepassing op simulatiemodellen werden onderzocht en de reeds volbrachte onderzoeken op het gebied van DPC-optimalisatie werden uitgelegd.

Een globaal parametrisch model van een DPC-configuratie werd geformuleerd met behulp van het softwarepakket OrcaFlex. Dit model diende als basis voor de berekening van structurele respons en vermoeïïng op de kabel. De keuzes die zijn gemaakt in het opstellen van het model werden geverifieerd d.m.v. het uitvoeren van experimenten en het vergelijken van de resultaten uit deze simulaties met analytisch afgeleide waarden. Ten slotte zijn er convergentie- en gevoeligheidsanalyses uitgevoerd om de simulatieparameters jusit te kunnen afstemmen. Daanaast leverden de resultaten bevindingen op over de invloed van de modelparameters op de vermoeïïngsrespons van de DPC.

Een optimalisatiemethode die gebruik maakt van een benaderingsmodel werd beschreven. Het specifieke zoekdomein voor de optimalisatievariabelen werd bepaald door het herhaaldelijk uitvoeren van statische analyse over het gehele domein, voor verschillende waterdieptes. Zo konden de grenzen van het zoekdomein worden vastgesteld als lineaire combinaties van de waterdiepte. Daardoor is directe toepassing op verschillende waterdieptes mogelijk gemaakt, zonder dat daarvoor een uitzonderlijk uitgebreide steekproef nodig is. Voor interpolatie op de testdata werden Radiale Basisfuncties (RBF) gebruikt, waaruit het benaderingsmodel ontstond. Het optimalisatieprobleem werd opgelost d.mv. het toepassen van een iteratieve zoekstrategie, die progressief van globale naar lokale oplossingen zocht, in een poging om niet voortijdig te convergeren naar een lokaal optimum. Het benaderingsmodel werd tijdens elke iteratie bijgewerkt met het nieuw vergaarde data punt tot de error tussen het benaderingsmodel en en het echte model een bepaalde drempelwaarde bereikte. Tenslotte werd de werking van het voorgestelde optimalisatiealgoritme geverifiëerd d.m.v. het uitvoeren van experimenten met een volledig gedefiniëerde testfunctie.

Er zijn experimenten uitgevoerd om de voorgestelde optimalisatiemethode te valideren, m.b.t. convergentie, robuustheid en efficiëntie. Hiervoor werden verschillende casestudy's geformuleerd, waarop

het optimalisatiealgoritme meerder malen is toegepast. Daarnaast werd een Grid Search (GS) algoritme toegepast op dezelfde casestudy's en werd een referentieconfiguratie uit een andere publicatie geanalyseerd op schade door vermoeïng. De twee optimalisatievariablen waren de kabellengte tussen het ophangpunt (Engels: Hang-off Point (HOP)) en het begin van het drijvende gedeelte van de kabel en het totale aantal bevestigde drijvers (Engels: Buoyancy Module (BM)).

De vergelijking van uiteindelijke resultaten die voortkwamen uit de optimalisatie- en GS-experimenten wijst op goede convergentie-eigenschappen. Bovendien werden er bij de geoptimaliseerde cofiguraties betere vermoeïingsprestaties geregistreerd dan bij de referentieconfiguraties. Op gebied van efficiëntie presteerde de voorgestelde optimalisatiemethode duidelijk beter dan de GS-aanpak. Het voorgestelde optimalisatiealgoritme kan mogelijk worden verbeterd als de optimalisatieparameters beter worden afgestemd. Daarnaast zijn milde wijzigingen aan de zoekstrategie mogelijk die de kans op convergentie naar een lokaal minimum kunnen verkleinen. De berekende vermoeïingsresultaten laten zien dat, in het geval van een een geoptimaliseerde DPC-configuratie, de vermoeïingsspanningen zo gelijk mogelijk verdeeld worden tussen het HOP en het drijvende gedeelte van de kabel. Het dicht bij het HOP plaatsen van het drijvende kabelgedeelte leidt tot demping van de bewegingen en vermindering van de spanningen bij het HOP. Deze maatregel veroorzaakt echter ook grotere spanningspieken in het drijvende gedeelte van de kabel. De keuze voor een te groot of te klein aantal BM's kan leiden tot verhoogde vermoeïingsspanningen bij het HOP of in één van beide karakteristieke curves van de DPC.

# List of Symbols

| | | |
|---|---|---|
| $\alpha$ | Phillips parameter (JONSWAP) | - |
| $\beta$ | Minimum candidate selection distance parameter | - |
| $\Delta$ | Maximin distance to data points | m |
| $\Delta\sigma$ | Stress range | Pa |
| $\eta$ | Utilization factor | - |
| $\gamma$ | Peak enhancement factor (JONSWAP) | - |
| $\gamma_m$ | Material factor | - |
| $\hat{f}$ | Surrogate function | - |
| $\kappa_{MAX}$ | Maximum allowed curvature on the cable | $\mathrm{m}^{-1}$ |
| $\mathcal{D}$ | Feasible search space | - |
| $\mu$ | Dynamic viscosity | $\mathrm{kg\,m^{-1}\,s^{-1}}$ |
| $\rho$ | Fluid density | $\mathrm{kg\,m^{-3}}$ |
| $\rho_w$ | Density of water | $\mathrm{kg\,m^{-3}}$ |
| $\rho_{BM}$ | Density of buoyancy module | $\mathrm{kg\,m^{-3}}$ |
| $\rho_{cbl}$ | Density of DPC | $\mathrm{kg\,m^{-3}}$ |
| $\tau_e$ | Error threshold for stopping criterion | - |
| $A$ | Area | $\mathrm{m}^2$ |
| $c$ | Set of constraints | - |
| $C_a$ | Added mass coefficient | - |
| $C_d$ | Drag coefficient | - |
| $C_L$ | Lift coefficient | - |
| $D$ | Water depth | m |
| $D_0$ | Reference depth for wind-generated current | $\mathrm{m\,s^{-1}}$ |
| $D_C$ | Characteristic fatigue damage | - |
| $D_c$ | Effective conductor diameter | m |
| $D_D$ | Design fatigue damage | - |
| $D_i$ | Inner diameter of the bend stiffener | m |
| $D_o$ | Outer diameter of the bend stiffener | m |
| $D_{BM,i}$ | Inner diameter of buoyancy module | m |
| $D_{BM,o}$ | Outer diameter of buoyancy module | m |

| | | |
|---|---|---|
| $d_{BM}$ | Spacing between buoyancy modules | m |
| $d_{cur}$ | Current direction | ° |
| $D_{ftg}$ | Maximum annual fatigue damage | - |
| $d_{seabed}$ | Minimum distance between sag bend and seabed | m |
| $d_{surface}$ | Minimum distance between hog bend and water surface | m |
| $d_{wind}$ | Wind direction | ° |
| $DFF$ | Design fatigue factor | - |
| $e$ | Error between surrogate and real model | - |
| $E_{BS}$ | Young's modulus of the bend stiffener | Pa |
| $EA$ | Axial stiffness of the cable | N |
| $EI$ | Bending stiffness of the cable | N m$^2$ |
| $EI_{BS}$ | Bending stiffness of the bend stiffener | N m$^2$ |
| $f$ | Objective function | - |
| $F_b$ | Buoyancy force | N |
| $F_g$ | Gravitational force | N |
| $F_h$ | Hydrodynamic force | N |
| $F_L$ | Lift force generated by VIV | N |
| $f_p$ | Spectral peak frequency | s$^{-1}$ |
| $f_v$ | Vortex shedding frequency | s$^{-1}$ |
| $f_W$ | Wave frequency | s$^{-1}$ |
| $F_{wet}$ | Weight in water | N |
| $g$ | Gravitational acceleration | m s$^{-2}$ |
| $H$ | Height of the HOP above the seabed | m |
| $H_s$ | Significant wave height | m |
| $L$ | Total cable length | m |
| $L_1$ | Length of the first dynamic cable section | m |
| $L_2$ | Length of the buoyant cable section | m |
| $L_3$ | Length of the second dynamic cable section | m |
| $L_{BM}$ | Length of buoyancy module | m |
| $l_{ftg}$ | Minimum fatigue life | years |
| $L_{ST}$ | Length of the static cable section | m |
| $m$ | Mass | kg |
| $MBL$ | Minimum break load | N |
| $MBR$ | Minimum bend radius | m |

| | | |
|---|---|---|
| $N$ | Number of cable segments | - |
| $n$ | Number of initial samples | |
| $n_{BM}$ | Number of buoyancy modules | - |
| $OD$ | Outer diameter of the cable | m |
| $p_0$ | Ambient pressure | Pa |
| $p_h$ | Hydrostatic pressure | Pa |
| $ps$ | Phase shift | s |
| $R_i$ | Inner radius of the bend stiffener | m |
| $R_k$ | Characteristic resistance | Pa |
| $R_o$ | Outer radius of the bend stiffener | m |
| $Re$ | Reynolds number | - |
| $S_D$ | Design load effect | Pa |
| $S_{eA}$ | Characteristic stresses from accidental loads | Pa |
| $S_{eE}$ | Characteristic stresses from environmental loads | Pa |
| $S_{eF}$ | Characteristic stresses from functional loads | Pa |
| $t$ | Time | s |
| $T_p$ | Peak wave period | s |
| $T_s$ | Significant wave period | s |
| $T_z$ | Zero-crossing wave period | s |
| $T_{MAX}$ | Maximum allowed axial tension on the cable | N |
| $U$ | Current velocity | unit |
| $u$ | Flow velocity | $\mathrm{m\,s^{-1}}$ |
| $U_0$ | Surface current velocity | $\mathrm{m\,s^{-1}}$ |
| $U_{tide0}$ | Tidal current velocity at surface | $\mathrm{m\,s^{-1}}$ |
| $U_{tide}$ | Tidal current velocity | $\mathrm{m\,s^{-1}}$ |
| $U_{wind0}$ | Wind-generated current velocity at surface | $\mathrm{m\,s^{-1}}$ |
| $U_{wind}$ | Wind-generated current velocity | $\mathrm{m\,s^{-1}}$ |
| $V$ | Volume | $\mathrm{m^3}$ |
| $v$ | Velocity of body moving in fluid | $\mathrm{m\,s^{-1}}$ |
| $v_{wind}$ | Wind velocity | $\mathrm{m\,s^{-1}}$ |
| $w_{dry}$ | Mass per unit length | $\mathrm{kg\,m^{-1}}$ |
| $w_{wet}$ | Equivalent mass per unit length submerged in water | $\mathrm{kg\,m^{-1}}$ |
| $x$ | Set of decision variables | - |
| $x_{TP}$ | Horizontal distance to the termination point | m |

# List of Abbreviations

| | |
|---|---|
| **6DoF** | 6 Degrees-of-Freedom |
| **ALS** | Accidental Limit State |
| **BBO** | Blackbox Optimization |
| **BM** | Buoyancy Module |
| **BS** | Bend Stiffener |
| **CORS** | Constrained Optimisation using Response Surfaces |
| **CSF** | Curvature Stress Factor |
| **CSL** | Cable Segment Length |
| **DFF** | Design Fatigue Factor |
| **DoE** | Design of Experiment |
| **DPC** | Dynamic Power Cable |
| **DS** | Direct Search |
| **ETPC** | Electrolytic Tough Pitch Copper |
| **FEM** | Finite Element Modelling |
| **FLS** | Fatigue Limit State |
| **FOWF** | Floating Offshore Wind Farm |
| **FOWT** | Floating Offshore Wind Turbine |
| **FWEC** | Floating Wave Energy Converter |
| **GA** | Genetic Algorithm |
| **GS** | Grid Search |
| **JONSWAP** | Joint North Sea Wave Observation Project |
| **HOP** | Hang-off Point |
| **LHS** | Latin Hypercube Sampling |
| **LWS** | Lazy Wave Shape |
| **MBL** | Minimum Break Load |
| **MBR** | Minimum Bend Radius |
| **MCS** | Monte-Carlo Sampling |
| **RAO** | Response Amplitude Operator |
| **RBF** | Radial Basis Function |
| **SLS** | Serviceability Limit State |

| | |
|---|---|
| **SMO** | Surrogate Model Optimization |
| **S-N** | Stress-Life |
| **TDP** | Touchdown Point |
| **TP** | Termination Point |
| **TSF** | Tension Stress Factor |
| **ULS** | Ultimate Limit State |
| **VIV** | Vortex-Induced Vibrations |

# List of Figures

# List of Tables

# Contents

# 1 Introduction

The Dynamic Power Cable (DPC) is a relatively new piece of technology within the offshore renewable energy industry. It acts as the inter-array connector between floating renewable energy devices. Possible applications are the Floating Offshore Wind Turbine (FOWT) and the Floating Wave Energy Converter (FWEC). The free hanging nature of the DPC leaves it under exposure of dynamic loads caused by the environmental conditions. Amongst these are loads from motions of the floating platform, wave loads and loads from sea currents. These dynamic loads impose great design challenges, as the cables need to be resilient to both ultimate and fatigue failure, whilst still being able to fulfil their requirements for electricity transmission. Rather than changing the specifications of the cable itself, loads on DPCs can be mitigated by changing the configuration or 'shape' of the cable. A wide variety of research on the analysis of loads on DPCs has already been conducted, as well as parametric studies on their dynamic behaviour.

This MSc thesis presents a methodology to create a preliminary global design of a DPC configuration, making use of parametric optimization and using the background knowledge from previous research on dynamic power cable analysis, modelling and optimization. The focus herein lies on formulating a universally applicable DPC optimization model that is computationally efficient and attempts to minimize the fatigue damage on the cable. This is achieved by building a numerical model of a cable in a commercial hydrodynamic analysis software package and applying a surrogate model based blackbox optimisation algorithm to optimize the configuration of the DPC.

## 1.1. Background

Population growth has caused a rapid increase in energy demand. This trend is expected to continue over the next decades. By 2050, worldwide population is predicted to have grown by 2 billion to a total of 9.7 billion [1]. At the same time, the energy demand is expected to increase by 50% between 2020 and 2050 [2]. In contrast, emissions of greenhouse gases caused by fossil energy production need to be reduced in order to limit the impact on climate change. As decided in the 2015 Paris agreement [3], efforts must be made to hold the increase in global average temperature to well below 2°C, while pursuing a limit of 1.5°C. In order to reach these climate goals, the energy production using fossil fuels, which in 2019 still accounted for 84% of the total worldwide energy consumption [4], must be replaced by renewable alternatives. To be a able to achieve 'net zero' greenhouse gas emissions in 2050, two thirds of total energy supply must come from renewable sources such as wind, solar, bio, geothermal and hydro energy [5].

One of the issues that could endanger a successful energy transition is that opportunities to produce renewable energy onshore are not always readily available. Space restrictions and public resistance limit the amount of available wind and solar power to be harvested and hydro power is certainly not an option everywhere. This results in a necessity for offshore renewable energy sources, which can be in the form of offshore wind energy or ocean energy. European countries had approximately 25GW of offshore wind energy installed in 2020, which made up 11% of total wind energy production in Europe. Expectations are that until 2025, another 29GW of new offshore wind energy will be installed in Europe [6]. Ocean energy has the potential to provide enough electricity for the entire planet. Two noteworthy

technologies that can produce electricity with the use of ocean energy are wave energy converters and tidal energy converters. These have so far been mostly in development stage, with only 1.1MW of wave energy converter and 10.1MW of tidal energy converter technology active in European waters in 2020. Despite these small numbers, the steady productivity of the current projects is encouraging future developments in the sector [7]. Other ocean-based energy resources are ocean currents, salinity gradients and thermal gradients [8].

Most current offshore renewable energy technologies are situated in shallow waters near the coast, making use of bottom-fixed foundations. In the case of offshore wind turbines, the maximum water depth at which they can be built is limited by the substructure design. The maximum water depth for which the construction of fixed-foundation offshore wind turbines is feasible is 60 m [9]. This limitation can be problematic for coastal areas with a narrow continental shelf, where there is not enough room for large offshore wind farms near the coast. It also excludes the vast, deep water areas further from the coast, where higher average wind speeds offer great opportunity for large-scale offshore wind technology. In Europe alone, a potential of 4000 GW of wind energy is found in deep waters (50 m-220 m), which is about 80% of the total offshore wind energy potential [10]. For this reason, in recent years the development of floating offshore wind technology has taken a leap. FOWTs are positioned on top of a floating substructure held in place by mooring lines that are anchored to the seabed. Their application is therefore not limited to shallow waters only. The deployment of a Floating Offshore Wind Farm (FOWF) can be in deeper waters far from the coast (e.g. in the North Sea [10]), where there are high wind velocities, or in coastal areas with a steep bathymetry (e.g. parts of the Californian coast [11]). Another floating renewable energy technology is the FWEC. These can be installed in shallow or deep waters, but can harvest greater amounts of energy in deep waters, because of the higher energy content in deep water waves [12].

The electricity generated by floating renewable energy is transported to the mainland via a system of submarine power cables and energy collector hubs. A crucial part of this system is the inter-array power cable, often referred to as a “Dynamic Power Cable” (DPC), which inter-connects the floating structures and substations, as illustrated in Figure 1.1. This cable segment is under cyclic dynamic loading from the environment which makes it susceptible to mechanical failures, potentially much more so than a fixed static submarine cable. Therefore, DPCs must be designed differently than static cables, namely as flexible umbilicals that must be strong enough to withstand the dynamic loads exerted on them. The configuration of a DPC can be changed and designed to mitigate the effects of the dynamic loads and therefore limit the risk of damage occurring to the cable during operation. Research has shown that a change in configuration or ‘shape’ in which the cable is suspended can lead to significant reductions of internal stresses and fatigue damage [13].

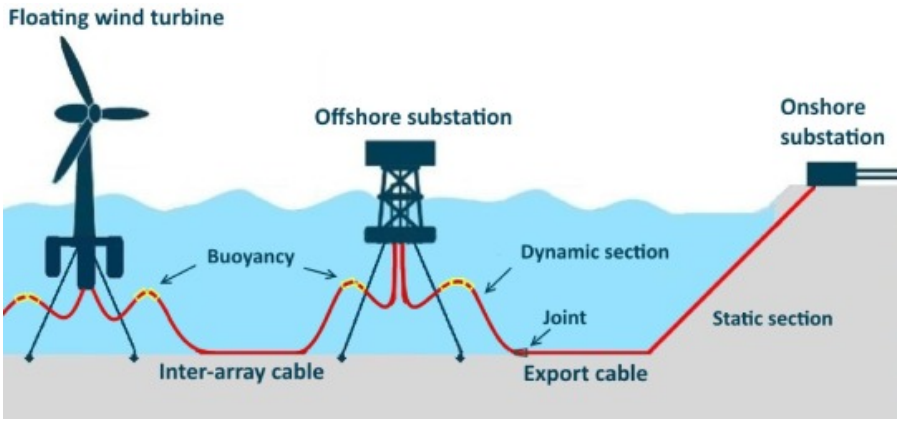


Figure 1.1: Overview of FOWF with DPCs [14]

## 1.2. Research Motivation

FOWT technology has great potential and is going to be playing a crucial role in meeting the 2050 climate goals. Even though an almost negligible amount of 100 MW of floating wind energy had been installed until 2020, 250 GW of floating wind energy is predicted to have been commissioned by 2050, making up 20% of the total future offshore wind industry [15]. By 2030, up to 494 MW of wave energy

can be installed [16]. How much of this will involve FWECs is unclear. However, it is evident that over the next decades floating renewable energy will play an important role in the energy transition. To ensure reliable operation of these systems, it is essential that extensive research is done about the behaviour and design of DPCs.

Currently, not much is known about the behaviour and failure of DPCs for renewable energy applications. The reason for that is the small number of these cables that are currently in operation and secrecy by the cable manufacturers. There is however a clearly increasing worldwide trend in failure of conventional submarine power cables, which leads to believe that future DPCs could also be affected. Power cable failures cause major financial losses in the offshore wind industry, with damaged cable section replacement costs varying between 0.72 and 1.87 million $ [17], not taking into account the financial losses from downtime of the offshore wind farms.

The number of available methods for the design of DPCs and their configurations is still limited. Experience in floating renewable energy design is often from the offshore and oil and gas industry. Floating platforms and flexible riser systems from this industry can be used as analogies for DPC systems. However, in order to accelerate the preliminary design of possible DPC configurations, dedicated methods for numerical analysis and design are required. Previous researchers have already made early efforts in preliminary DPC configuration design using some kind of optimization method. Poirette er al. [18] attempted to change the cable configuration in order to minimize the cable costs. Subsequently, Rentschler et al. [19] formulated a model for optimisation of the configuration with the objective to minimize fatigue, extreme loads and costs. The influence of individual decision variables (e.g. cable length) on the optimal performance of the configuration was analysed by Aninthaneni [20].

As mentioned, DPCs are subject to dynamic loading, which particularly increases the risk of fatigue failure. That being said, none of the previously conducted studies focus specifically on fatigue damage reduction. Additionally, there seems to be a lack of optimization models that facilitates the application of arbitrary environmental scenarios. Universal application of the model is difficult if the input variables of the model are restrictive and the computational cost is high. Based on these findings, there is demand for advanced models that can quickly calculate a fatigue-optimized preliminary cable configuration for arbitrary environmental scenarios.

## 1.3. Research Objective

The research objective of this MSc thesis is to develop a parametric model of a DPC in order to be able to optimize the configuration or 'shape' of the DPC. Optimization is performed by tuning the parameters that define the configuration of the DPC and evaluating the performance of the system in terms of a selection of objectives and constraints. The goal is to propose an optimization method that will allow for the fast calculation of the best possible preliminary DPC configuration for any arbitrary environmental scenario, without the need of extensive expert knowledge or pre-analysis. The main research question is formulated as:

> ***How can a parametric optimization model be developed to be used for the optimization of the dynamic power cable configuration?***

For a systematic approach to investigate the research objective, the following research sub-questions are in order:

> *What is the state-of-the-art of dynamic power cable configuration design?*
>
> *How can the global motions, loads and fatigue on dynamic power cables be calculated?*
>
> *What are the available methods for optimization of the dynamic power cable configuration?*
>
> *How can a parametric model of the dynamic power cable configuration be developed and what is the influence of the parameters on the performance of the system?*
>
> *How can parametric optimization be performed on the dynamic power cable configuration?*

## 1.4. Scope

A scope is defined to narrow down the research. The scope attempts to focus the research on relevant applications and simplified numerical models so that the simulations remain computationally feasible. The following limitations are introduced:

- *Optimization of the DPC configuration:* This research does not involve changing any of the cable's structural parameters, e.g. weight or stiffness. The assumption here is that those parameters are not independent and are provided by the cable manufacturer. The aim is therefore to optimize the parameters of the configuration, which involves global configuration variables, e.g. total cable length.

- *Global analysis and cable model:* Global analysis calculates the loads along the entire length of the cable, but not on a cross-sectional level. The cable is modelled as a solid, homogeneous cylinder. In other words, the individual components within the cable are not modelled separately. This approach allows for more computationally efficient cable simulations and offers a sound basis for the calculation of ultimate loads and fatigue on the cable.

- *Decoupled analysis:* In decoupled analysis, the motions of the floating platform are not influenced by those of the DPC or of its mooring lines. As a result, it is not necessary to accurately model the entire system, but only the DPC with 6 Degrees-of-Freedom (6DoF) input motions applied at the Hang-off Point (HOP). A coupled approach generally produces more accurate results, but relies on complex modelling of the entire system and is more computationally expensive. As will be explained in Section 3.1, in the case of DPCs decoupled analysis is likely to be sufficiently accurate, while allowing for a less complex, more computationally efficient model.

- *Application to FOWTs:* The projected growth figures that were given in Section 1.2 show that the FOWT is the dominant floating renewable energy source. This research will therefore be limited to application to FOWTs. Previous research and real-life cable specifications for this application are readily available, which aids this decision. That being said, in theory the model should also be applicable to other scenarios.

- *Investigation of the lazy wave cable configuration:* The lazy wave configuration is one of a number of available configuration types. Given that the lazy wave configuration is suitable for FOWT applications and reference literature for comparison is available, this research will be limited to the lazy wave configuration. A full overview of the available configuration types is given in Section 2.1.

- *Mechanical failure mechanisms during operation:* Electrical cables can be subject to mechanical, thermal, electrical and chemical failures. This also includes instant failures (e.g. impact with an anchor) or failures that develop slowly over time (e.g. electrical breakdown due to water treeing) [21]. These failure mechanisms can also occur during any stage of a cable's life. This research only takes spontaneous (not initiated by any human/wildlife interaction) mechanical failure mechanisms during the operational life phase into account. For a full overview of submarine cable failures, see [22].

- *Simplification of the loads:* Vertex-Induced Vibrations (VIV) (see Section 2.2.9) can cause oscillations of the DPC, which can contribute to the fatigue damage of the cable. In order to reduce modelling and computational efforts, these loads are not taken into account during this research. It must however be noted that for a more complete analysis of the fatigue damage, VIV must also be included.

## 1.5. Report Structure

This report is structured by using the sub-research questions as a guideline. The first chapters mainly focus on literature review of the state-of-the-art of DPC design, modelling and optimization, after which the exact modelling and optimization decisions that were made for the proposed optimization method are described. The remainder of the report consists of experimentation and results, as well conclusions and recommendations.

- *Chapter 2:* This chapter gives an overview of all the aspects that are involved in the design of the DPC configuration and answers the question *"What is the state-of-the-art of DPC configuration design?"*. This involves explanations of the configuration types and the important auxiliary components, loads on the cable and failure mechanisms. Based on this, certain design requirements can be made, which are summarized subsequently. The section is concluded with an overview of possible design parameters.
- *Chapter 3:* The behaviour of DPCs under hydrodynamic loading can be understood through thorough analysis. This section answers the question *"How can the global motions, loads and fatigue on DPCs be calculated?"* by chronologically going through the different types of global analysis that can be conducted on DPCs.
- *Chapter 4:* With optimization being the key aspect of this research, Chapter 4 investigates optimization methods that are suitable for the optimization of the DPC configuration. In spirit with answering the question *"What are the available methods for optimization of the DPC configuration?"*, different blackbox optimization methods are described and judged for suitability. The chapter is completed with an overview of the previous work on optimization of subsea umbilicals.
- *Chapter 5:* This chapter answers the question *"How can a parametric model of the dynamic power cable configuration be developed and what is the influence of the parameters on the performance of the system?"*. It first describes the parametric cable model and fatigue calculation model, after which the modelling aspects are verified. This is followed up by a convergence study and a parametric optimization study which give insight in the relevant simulation and configuration parameters.
- *Chapter 6:* A model-based optimization method is proposed with the objective of minimizing the fatigue damage on the DPC. The process of how the optimization algorithm is built up is described in an attempt to answer the question *"How can parametric optimization be performed on the dynamic power cable configuration?"*.
- *Chapter 7:* Case studies are formulated and experiments are carried out to test the proposed optimization model's performance. Validation of the optimization algorithm is done by testing the method's convergence, robustness and efficiency. The results of the fatigue calculations that are associated with the optimized configurations are analyzed and conclusions are drawn on what causes fatigue damage and how to prevent it.
- *Chapter 8:* The final chapter gives conclusions on the research and recommendations for future work. Additionally, the limitations of the current work are highlighted.

# 2

# Dynamic Power Cable Design

In order to ensure that a DPC is not overstressed and remains mechanically intact for its design life time, it is crucial to make a good design of the shape in which it is lowered through the water column. This shape is determined by the configuration of the DPC. The configuration has great influence on the stresses within the cable and therefore on its structural integrity. Years of research and experience from the offshore oil and gas industry have resulted in extensive knowledge on the design of flexible risers and their configuration. This knowledge is the basis for the design of DPC configurations. Both being slender structures operating in deep waters, the behaviour of risers and DPCs is assumed to be comparable.

This chapter answers the research sub-question *"What is the state-of-the art of DPC configuration design?"*. It begins by listing the available configurations that have been developed in the oil and gas industry. From their advantages and disadvantages and experience from previous DPC projects, the most suitable configurations for DPC applications are chosen and explained in more detail. The auxiliary components associated with those configurations are also explained, as they play crucial roles within the configuration design. Next, an insight is given on the loads that act on a DPC configuration. To understand the perils for a DPC's structural integrity, an overview of the relevant mechanical failure mechanisms is given. A set of design requirements and criteria, retrieved from standards, is then presented, after which the relevant configuration design parameters are explained. Finally, a conclusion is given, reflecting back on the research objectives of the chapter.

## 2.1. Available Configurations

The available configuration types are listed in Table 2.1, along with their most important properties, advantages and disadvantages. Of the different configuration types listed in this section, the most commonly studied and used in practice for the application of DPCs are the catenary and Lazy Wave Shape (LWS). The LWS tends to be the more favourable solution, because it experiences lower tension and bending stresses at the HOP, is less susceptible to fatigue failure and the motions of the floater and the Touchdown Point (TDP) are mostly decoupled (see Section 3.1). The lazy S concept tends to be a good solution for an application where multiple DPCs use the same buoy (the buoy is shown in Figure 2.1e), e.g. when leading to an offshore substation, or where there are very large floater motions [23]. The double wave configuration has been analysed against the lazy wave in shallow water only [24]. Therefore, its applicability to FOWTs in deep waters might be insignificant. An interesting configuration is the W-shape. It is an inter-array configuration that does not touch down on the seabed, but is suspended between two floaters, while aided by buoyancy modules. The Buoyancy Module (BM) is explained in more detail in Section 2.1.2. This configuration is suitable for scenarios where the floaters are close together with sufficient water depth. Note that most of the available configuration types are adopted from the subsea gas and oil industry, where there has been significantly more research on the different configurations. Figure 2.1 shows illustrations of the aforementioned configuration types.

| Configuration type | Properties | Advantages | Disadvantages |
|---|---|---|---|
| Catenary | Free hanging to the seabed | Simple installation<br>Cheapest solution | Floater motions are not decoupled<br>No lateral motion restriction<br>High tension at HOP<br>Bend control required at HOP |
| Lazy wave | Wave shaped<br>Added buoyancy modules | Simple installation<br>Relatively low-cost solution<br>Motions between floater and TDP are decoupled* | No lateral motion restriction<br>Buoyancy modules required<br>Bend control required at HOP |
| Tethered wave | Similar to lazy wave, but with a tether restraining the TDP | Motions between floater and TDP are decoupled<br>Tethering minimizes translation of the TDP | Complex installation of tether<br>Buoyancy modules required<br>Bend control required at HOP |
| Steep wave | Similar to lazy wave, but with subsea base for vertical connection of the cable | Motions between floater and TDP are decoupled<br>Movement at the TDP is restricted<br>Reduced horizontal distance between HOP and TDP | Buoyancy modules required<br>Bend control required at HOP and TDP<br>Expensive solution due to subsea equipment |
| Lazy S | Similar to lazy wave, but uses subsea buoy (midwater arch) instead of buoyancy modules | Motions between floater and TDP are decoupled<br>No limitation of floater motion<br>Reduced motion by cross currents<br>Sag bend location is carefully controlled | Midwater arch and tether required<br>Bend control required at HOP<br>Sag bend location is fixed<br>Expensive solution due to subsea equipment |
| W-shape | Suspended between two floaters without touching the seabed<br>Aided by use of buoyancy modules | Low-cost solution<br>Short cable length<br>Applicable over short distances | Buoyancy modules required<br>Accurate platform positioning and cable length required<br>Feasibility has not been fully proven |
| Double wave | Double lazy wave shape | Better performance than lazy wave, with regards to fatigue | Buoyancy modules required<br>Bend control required at HOP<br>Large horizontal distance between HOP and TDP |

Table 2.1: DPC configuration types [13], [23], [24], [25], [26]
*Explanation of coupled and decoupled motions in Section 3.1

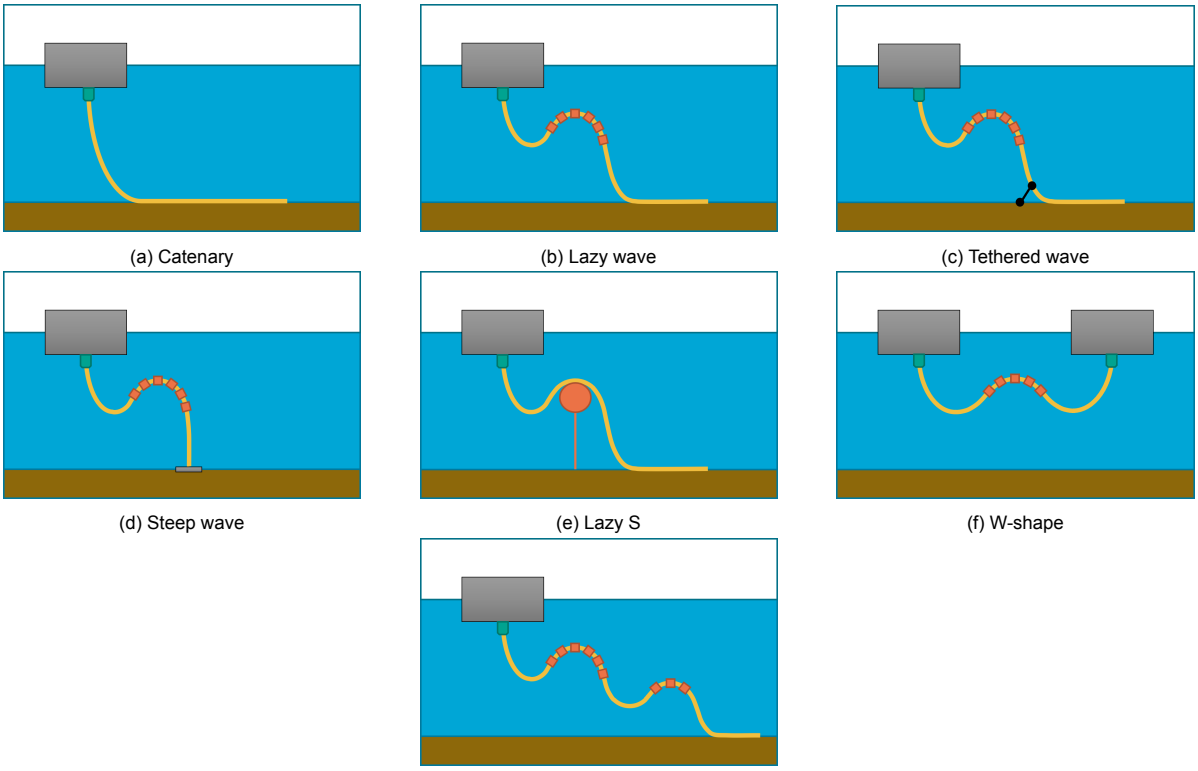

(a) Catenary (b) Lazy wave (c) Tethered wave

(d) Steep wave (e) Lazy S (f) W-shape

(g) Double wave

Figure 2.1: Available DPC configurations types

### 2.1.1. Floating Offshore Wind Application

To be suitable for DPC application in floating offshore wind industry, a configuration must be able to meet the following demands:

- *Suitable for deep waters:* FOWTs will operate in deep waters.
- *Sufficient prevention of large stresses at critical points:* In order to prevent cable failures stresses at critical points, such as the HOP, must be reduced.
- *Sufficient allowed floater offset:* FOWT platforms tend to have slack mooring systems, allowing for offsets from the original position.
- *Cost effective:* Due to the large amount of individual cables that must be installed in a full-scale offshore wind farm, cost effective configurations with easy installation procedures are preferred.

Considering the demands listed above the most suitable configuration types for renewable energy DPC applications are:

- Lazy wave shape
- W-shape

These configurations are suitable for deep water applications, reduce stresses at the HOP due to their buoyant elements, allow for some degree of floater offset and are also low-cost solutions, with their limited requirements for auxiliary components, cable length and simple installation. The LWS has already been deployed in practice at the Hywind FOWF in Scotland and at the Fukushima FORWARD FOWF in Japan. That being said, both projects are small scale with up to 5 FOWTs. The W-shape configuration is still in its conceptual phase, with very limited research and analysis conducted so far [27]. Early analysis on the influence on cable length and buoyancy on the W-shape has recently been conducted by Shi et al. [26]. Given the suitability of the LWS to scenarios where the floating platforms

are located relatively far apart, the remainder of this research will focus entirely the design of the LWS configuration.

In order to create said configuration, auxiliary components that are attached to the DPC are needed. Figure 2.2 shows the LWS DPC configuration suspended from a semi-submersible floating platform. The LWS configuration uses distributed BMs to create the floating arch section of the cable and a Bend Stiffener (BS) at the HOP to limit the bending stresses on the cable at that location. Other important locations on the LWS are the sag bend, hog bend, TDP and Termination Point (TP).

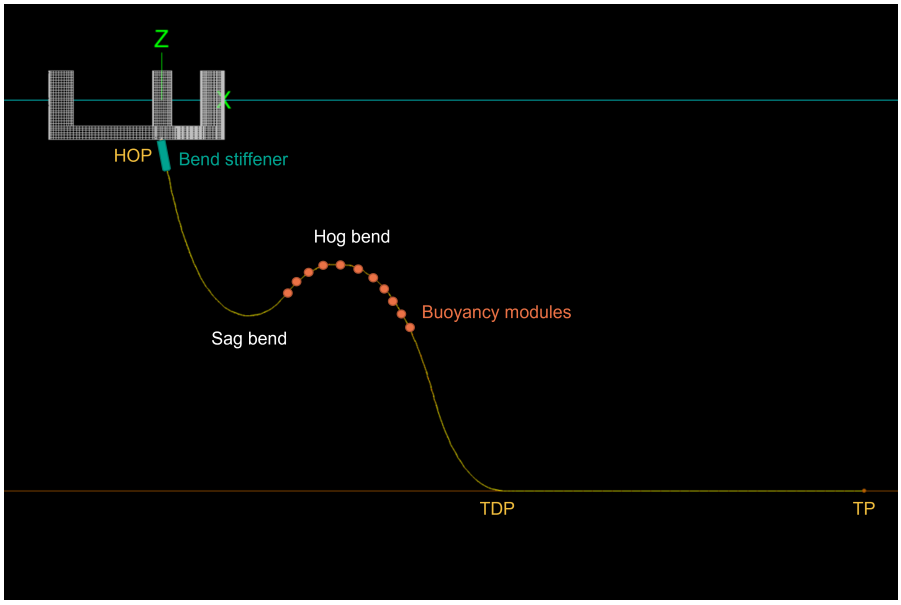


Figure 2.2: LWS cable configuration

### 2.1.2. Buoyancy Modules

Buoyancy modules provide the necessary buoyancy to create the desired shape of the configuration. They are made of two components: The internal clamp, which clamps around the DPC, and the buoyancy part, which consists of two halves held together by straps or bolts. The entire assembly is shown in 2.3. The BM halves are made of syntactic foam, which provides the buoyancy force. In order to prevent damage to the cable or slippage, the clamping system must be carefully designed for the circumference of the DPC. The external diameter, submerged weight and spacing of the BMs are all important parameters that influence total system's buoyancy [20].

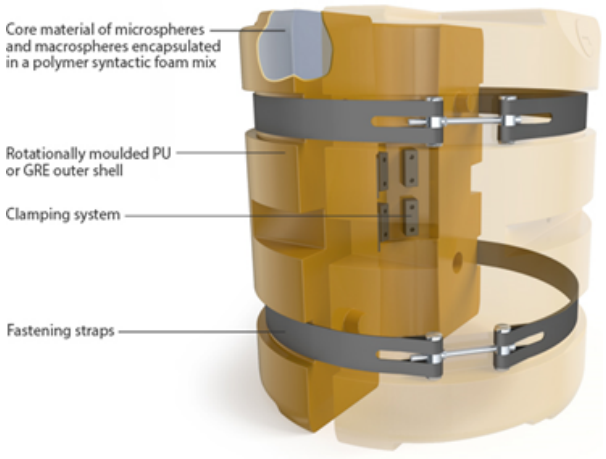


Figure 2.3: Buoyancy module system [28]

### 2.1.3. Bend Stiffeners

Bend stiffeners are cone-shaped sleeves around the DPC that provide additional bending stiffness and therefore prevent over bending of the cable. They are mostly used at the HOP, where bending stresses can become critical. A BS consists of a conical elastomer moulding with internal steelwork, which promotes load transfer to the attachment point. The BS must be designed to withstand both tension and bending loads, determined from a set of representative sea state scenarios [29]. Therefore, BSs with different dimensions and stiffnesses must be used for specific applications. The primary design requirements for BSs are the following [30]:

- The DPC must not experience overbending in extreme loading conditions.
- The fatigue limits of the DPC must not be exceeded.

The primary design constraint of a BS is its length. The reasons why a short BS design is preferred are [30]:

- A longer BS usually leads to increased shear force and bending moment at the BS's attachment point to the steel structure of the floater.
- Production and installation costs and difficulty significantly increase with a larger BS.
- Connection of a longer BS to the floater is more difficult, due to its larger diameter base.

Figure 2.4a shows the typical configurations of the HOP, along with the attached BS. The DPC is connected to the steel structure of the floater with a flange (A). In some cases an additional I or J tube (B) is placed in between the BS (C) and the flange. A picture of the real-life assembly can be seen in Figure 2.4b.

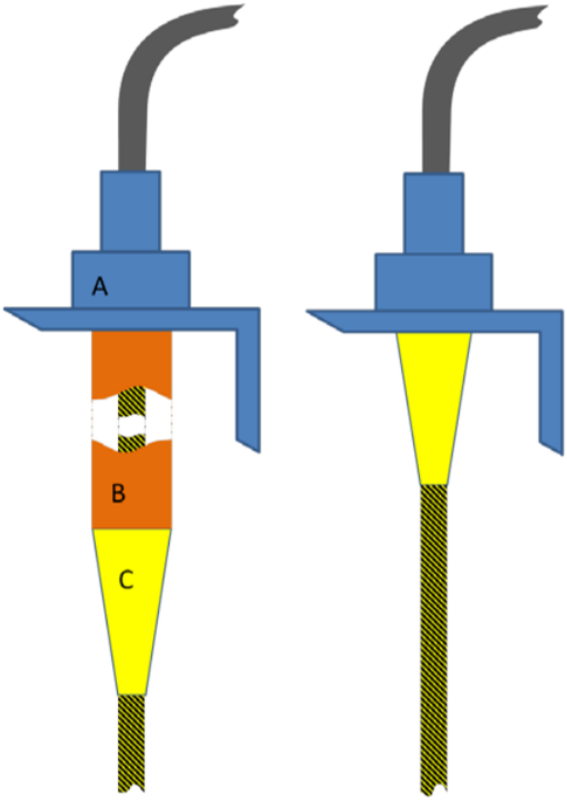


(a) Typical configurations of the HOP [29]

(b) Real-life bend stiffener and attachment [31]

Figure 2.4: Bend stiffener system

## 2.2. Loads

During its operational lifetime, a DPC will be subject to several different types of loads. These loads are presented schematically in Figure 2.5.

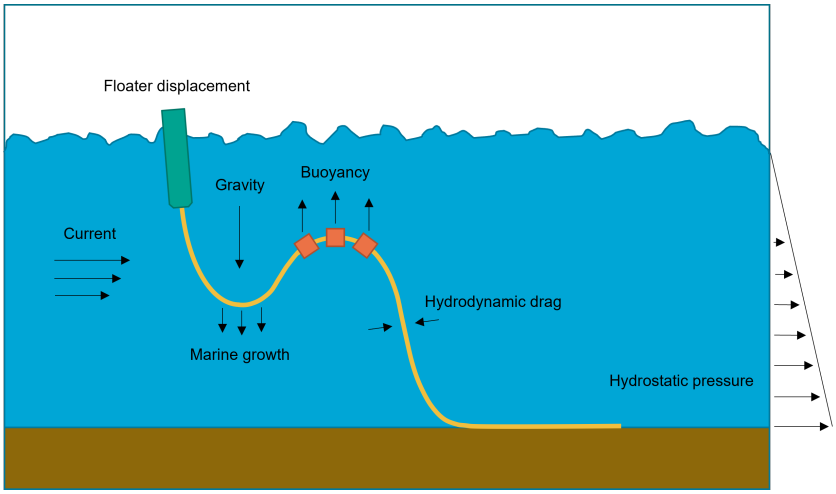


Figure 2.5: Loads on the DPC configuration [32]

### 2.2.1. Waves

Wave loads play a role on a DPC's dynamic behaviour near the water surface. They make a predominant contribution to the total dynamic load in shallow waters in particular [29]. The wave load on a DPC at a specific location is made up from a number of load combinations representing different sea states. Sea states are characterised by the following parameters:

- Significant wave height
- Wave period
- Wave direction

Ocean waves can be modelled to have a simplified sinusoidal shape (linear wave theory). However, this is not a realistic representation of a sea state in practice. Because of the random nature of wind-generated gravity waves, a stochastic approach to modelling waves is common. The spectral density function of the waves is of particular interest, for which good spectral density estimators are needed [33]. Therefore, several different parametric ocean wave spectra have been developed. The following spectra are most commonly found in literature:

- Bretschneider/ISSC
- Pierson-Moskowitz
- Torsethaugen
- Wallops
- TMA
- JONSWAP
- Ochi-Hubble

The wave spectrum that is considered to be most suitable for engineering applications is the Joint North Sea Wave Observation Project (JONSWAP) spectrum [34]. JONSWAP was developed from experimental measurements in the North Sea.

### 2.2.2. Currents

Sea currents are responsible for causing hydrodynamic drag forces (Section 2.2.3) and Vortex-Induced Vibrations (VIV) (Section 2.2.9), both of which play an important role in the fatigue of the DPC [32]. Where waves have influence on the top section of the cable, in deeper waters currents tend to influence the dynamic behaviour of the lower section [29]. The current is often expressed as a velocity pattern varying with water depth [35]. This relationship can be modelled as linear, exponential or constant. The current data can also be obtained from real-life measurements.

### 2.2.3. Hydrodynamic Drag and Added Mass

The hydrodynamic forces on a slender cylinder in an oscillatory flow in water can be described using the Morison equation [36]:

$$F_h(t) = \rho_w V \dot{u}(t) + \rho_w C_a V(\dot{u}(t) - \dot{v}(t)) + \frac{1}{2}\rho_w C_d A(u(t) - v(t))|u(t) - v(t)| \tag{2.1}$$

where:

- $\rho_w$ is the density of the water
- $V$ is the cylinder volume per unit length
- $u$ is the flow velocity
- $v$ is the velocity of the moving body
- $C_a$ is the added mass coefficient
- $C_d$ is the drag coefficient
- $A$ is the reference area

The first term of the Morison equation represents the Froude-Krylov force. This force is caused by the pressure gradient generated by the acceleration of the fluid in the outer flow region. The second term is the hydrodynamic mass force. The hydrodynamic mass is defined as the mass of the fluid surrounding the body, which is accelerated when pressure is exerted on it by the moving body. The added mass coefficient $C_a$ depends on the body's shape and orientation with respect to the flow direction. Finally, the third term contains the hydrodynamic drag force, where $C_d$ is the hydrodynamic drag coefficient [37]. These hydrodynamic coefficients can be determined with experiments. They are considered to be functions of the Reynolds number, the Keulegan-Carpenter number, the phase angle of the periodic motion and the relative roughness of the cylinder [38].

### 2.2.4. Hydrostatic Pressure

Hydrostatic pressure loads are exerted on the cable. The pressure $p_h$ increases with water depth according to the following equation:

$$p_h = p_0 + \rho_w g D \tag{2.2}$$

where $p_0$ is the ambient air pressure, the sea water density, $g$ the gravitational acceleration and $D$ the water depth. The hydrostatic pressure in deep waters might cause large compression forces on the circumference of the cable and on the auxiliary components.

### 2.2.5. Gravity

Gravitational forces on the cable play an important role for long cables with a large mass. A portion of the weight, or even all of the weight in case of a catenary shape configuration, is suspended from the HOP, causing large axial stresses at this point. These stresses can increase fatigue or even cause ultimate failure. The total gravitational force at the HOP is expressed by:

$$F_{g,HOP} = w_{dry} g L \tag{2.3}$$

where $w_{dry}$ is the mass of the cable per metre in air and $L$ is the total cable length.
Gravity also acts on the auxiliary components, in which case the gravitational force is gives as:

$$F_{g,aux} = m_{aux} g \tag{2.4}$$

where $m_{aux}$ is the mass of the auxiliary component in question.

### 2.2.6. Buoyancy

The buoyancy force generated by the attached buoyancy modules counters the gravitational force and allows for configurations such as the lazy wave. The buoyancy force on an object is equal to the weight of the displaced fluid and is therefore given by:

$$F_b = \rho_w g V \tag{2.5}$$

where V stands for the volume of displaced sea water, which is given by the dimensions of the buoyancy module. Buoyancy forces do not exclusively act on the buoyancy modules, but also on the DPC itself. Therefore, along with a specific mass (Section 2.2.5) an equivalent specific mass in water $w_{wet}$ of the cable can be calculated. Essentially, the cable becomes 'lighter' when it is submerged, because part of the gravitational force is countered by a buoyancy force. This wet cable weight is expressed as:

$$F_{wet} = -F_{g,cbl} + F_{b,cbl} = (-\rho_{cbl} + \rho_w) g V = -w_{wet} g L \tag{2.6}$$

where $\rho_{cbl}$ is the density of the DPC.

### 2.2.7. Marine Growth

As a DPC is submerged in the sea over many years, marine growth will accumulate on the cable. This marine growth is from plants, animals and bacteria forming a layer around the cable and buoyancy modules. This over time increasingly thick layer alters the weight and buoyancy properties of the system. Thus, marine growth can have considerable influence on the dynamic behaviour of the DPC. The type and rate of marine growth depends on the environmental conditions at the operational site [35].

### 2.2.8. Floater Motions

The motion of a floating platform can be describes in 6DoF. The marine terms are surge, sway and heave for translations and roll, pitch and yaw for rotations. A floating platform's motion behaviour is dictated by the hydrodynamic loads on the structure caused by waves and currents and the aerodynamic loads on the top of the structure. The motions characteristics of the floater can be influenced by the tension in the mooring lines or DPC. Whether or not these effects are taken into account when modelling the motion of the floater depends on if a coupled or decoupled approach is taken (see Section 3.1). For motion analysis of the floater, several approaches are possible:

- *Simulation:* Modelling and simulation of a floating platform are possible with dedicated software packages. The simulations can involve all kinds of environmental effects including wind, waves and currents. Well-documented and validated FOWT floater models, such as the NREL 5MW turbine mounted on the OC3 Hywind spar buoy [39], are available.
- *Experiments:* Wave tank experiments with a scale model of the floating platform are possible to estimate the motion behaviour at full scale. This approach was used to gain insight on the motion characteristics of a 10MW FOWT by Yu et al. [40].

After having analysed the floater's motion characteristics, they can be given as input parameters to a numerical DPC model as a 6DoF motion time history applied to the HOP of the cable. When taking a coupled approach to the motion analysis of the system, all components (floater, DPC, mooring) are simulated in time-domain simultaneously.

### 2.2.9. Vortex-Induced Vibrations

VIV are a phenomenon that can occur if a bluff body is placed in an external flow. At Reynolds numbers > 50, the boundary layer around a cylinder, which is an analogy for a globally modelled DPC, separates. This creates a downstream wake in which regular vertices are formed, also referred to as a Karman street [41]. The vertices are shedded alternately from opposite sides of the cylinder, creating an oscillating force perpendicular to the direction of the flow. This force then causes vibrations of the cable, referred to as VIV [42]. The Reynolds number for flow around a cylindrical shaped body is calculated as:

$$Re = \frac{\rho u O D}{\mu} \tag{2.7}$$

It is therefore a function of the fluid density $\rho$, velocity of the flow $u$, outer diameter of the object $OD$ and dynamic viscosity of the fluid $\mu$. The lift force generated as a result of VIV is defined as [43]:

$$F_L = \rho u^2 OD C_L \sin(2\pi f_v t + ps) \tag{2.8}$$

where $C_L$ is the dimensionless lift coefficient, $f_v$ is the frequency of the vortex shedding, $t$ is time and $ps$ is the phase shift. The lift force is what generates the VIV and is illustrated in Figure 2.6.

When $f_v$ approaches the natural frequency of the DPC, resonance will occur. This phenomenon is called lock-in. In case of lock-in conditions, the vortex shedding frequency adapts itself to the oscillation frequency of the cable, which means that resonance due to VIV can occur across a fairly large frequency range. During lock-in the size of the vertices, and therefore the strength of the oscillating force, increase. The maximum amplitude that VIV can achieve is limited to one times the cable diameter [42]. Naturally, if the amplitude of the vibrations vastly increases, this can have a tremendous impact on the fatigue life of the DPC.

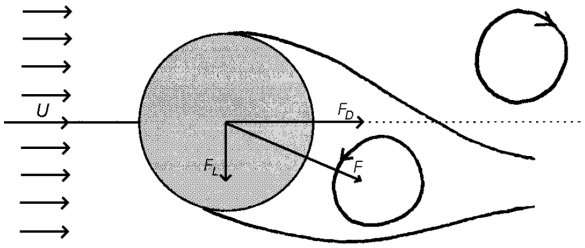


Figure 2.6: Lift force generated by vortex shedding [43]

## 2.3. Failure Mechanisms

This section explains the most important failure mechanisms of DPCs. The failure of a DPC is the consequence of damage to the cable that is severe enough to stop the cable from functioning properly, in which case repairs or replacements are required. Failure mechanisms of submarine power cables can be classified according to their nature [21]:

- Mechanical, e.g. over-elongation or over-compression
- Thermal, e.g. overheating
- Electrical, e.g. insulation breakdown
- Chemical, e.g. armour corrosion

These failures can occur during the following life phases of a cable [22]:

- Design
- Manufacturing
- Transportation/installation
- Operation
- Decommissioning

Keeping in mind the scope of this thesis, the remainder of this section will focus on mechanical failures of the cable during its operational life phase. The following failure mechanisms are of particular concern for DPCs [15]:

- Exceedance of axial tension limits
- Over bending
- Fatigue damage due to extreme dynamic and cyclic loading

- Axial compression leading to ‘birdcaging’, meaning spreading wire strands
- Loop formation and kinking
- Layer separation and instability

In short, most mechanical failures that apply to static power cables also apply to DPCs, while the ones mentioned above are potentially even more hazardous in dynamic applications. Accidental damages by human activities, e.g. fishing and anchoring, seem to be of lesser threat to DPCs. Offshore wind farms have safety zones in which fishing activity and anchoring is prohibited. Therefore, the dynamic cable sections do not cross any shipping routes and are unlikely to experience human interference [32].

## 2.4. Design Requirements

Failures on DPCs can occur if one of the limit states is exceeded. If this happens to be the case, then the structure can no longer fulfil its relevant design criteria. Limit state design must verify that none of the limit states is exceeded for all relevant situations [44]. The following limit states can be defined for subsea power cables [21]:

- *Serviceability Limit State (SLS):* A condition that renders the cable unsuitable for normal operation, e.g. extreme environmental conditions or damage.
- *Ultimate Limit State (ULS):* Exceedance of ultimate stress levels, e.g. maximum core temperature or minimum bending radius.
- *Fatigue Limit State (FLS):* Damage caused by repeated motion, e.g. vibrations or cyclic loading.
- *Accidental Limit State (ALS):* Accidents, e.g. anchor collisions.

In order to prevent failures, DPCs design must meet a number of established design requirements. These requirements are documented in standards. In the following subsections, the relevant standards are listed and the important design criteria for DPCs are given.

### 2.4.1. Standards

A complete summarized overview of the methodologies for design, manufacturing, transportation, installation, operation and decommissioning of subsea power cables for offshore wind farms is given by the standard DNVGL-ST-0359 [45]. The standard therefore covers the complete life cycle of a submarine power cable and many of the given design, analysis and operation recommendations also apply to dynamic cables.

The standard DNV-OS-J103 [46] about the design of floating wind turbine structures has a full section (section 16 of the standard) dedicated to more detailed design and analysis procedures for DPCs. This document specifies the following aspects:

- Design principles
- Functional requirements
- Analysis methodology
- Loads and load effects
- Material strength
- Design resistance and design criteria
- Other

This standard commonly refers to other standards and recommended practices for specific design or analysis aspects. For example, the methodology for load and fatigue analysis during operation is described by DVN-OS-F201 [47]. An overview of all the standards referred to is listed in Appendix B.

### 2.4.2. Design Requirements and Criteria

DNV-OS-J103 section 16 [46] prescribes several design resistance and criteria that are to be taken into account for the design of DPCs. The parameters that are relevant to the global design and analysis of the DPC configuration are explained in this section.

**Characteristic Resistance**

Characteristic strength of steel must be taken as the smaller of:

- Specified minimum yield stress
- 90% of specified minimum tensile stress

**Resistance Factors**

The utilization factor of load-carrying DPC elements during normal operation must not be taken greater than $\eta$=0.62. The material factor for cable ancillaries (auxiliary cable components) during operational conditions must not be taken smaller than $\gamma_m$=1.10.

**Design Criteria for ULS and ALS**

The general design criterion for load bearing steel components is defined as:

$$S_d \leq \eta R_k \tag{2.9}$$

Where $S_d$ is the design load effect and $R_k$ the characteristic resistance. The design criterion for cable terminations and other cable ancillaries is defined as:

$$S_d \leq \frac{R_k}{\gamma_m} \tag{2.10}$$

where

$$S_d = \gamma_F S_{eF} + \gamma_E S_{eE} + \gamma_A S_{eA} \tag{2.11}$$

Here $S_{eF}$, $S_{eE}$ and $S_{eA}$ represent the characteristic stresses from functional, environmental and accidental loads respectively.

**Design Criteria for FLS**

The design cumulative fatigue damage is defined as:

$$D_D = (DFF)D_C \tag{2.12}$$

where $DFF$ is the design fatigue factor, which must not be taken smaller than 10. $D_c$ represents the characteristic culmulative fatigue damage, which is calculated from fatigue analysis. The fatigue design criterion is defined as:

$$D_D \leq 1.0 \tag{2.13}$$

## 2.5. Design Parameters

Having gained insight on the DPC configuration and all its individual aspects, it is important to understand the influence of the individual parameters on the behaviour of the cable. Choosing the correct parameter values for the environment in which the DPC is operating is crucial to obtain a configuration that will operate safely without failure. This section first lists all the relevant environmental parameters that need to be taken into account when making the design. It then gives the configuration related parameters and explains their predicted influence on the DPC behaviour. Note that the structural parameters of the cable, e.g. cable mass and stiffness, are not mentioned here. These properties are prescribed by the cable manufacturers and are deemed to be difficult to change individually due to their interdependence.

### 2.5.1. Environmental Parameters

The environmental parameters are given by the location in which the FOWT is operating. They determine for a large part the loads that act on the DPC, which were previously described in Section 2.2. The motion of the floater is also dependent on the environmental conditions. Of course, environmental conditions at the operating site cannot be influenced by the designer of the DPC, but they play an important role in site choice and cable configuration design.

**Wave Characteristics**
Realistic ocean waves cannot be expressed as regular waves. Instead, irregular waves are presented using linear superposition of a number of different regular wave components with different amplitudes, frequencies and phases. These waves are defined by the following wave parameters [48]:

- *Height:* The wave height is defined as the vertical distance between the highest and lowest surface elevation in an wave. The significant wave height, which is defined as the mean of the highest one-third of waves that were recorded, is often used to characterize the wave height of a sea state:

$$H_s = H_{1/3} = \frac{1}{N/3}\sum_{j=1}^{N/3} H_j \tag{2.14}$$

  where $j$ is the rank number of the wave ($j = 1$ is the highest wave, $j = 2$ is the second highest wave, and so on).

- *Wave period:* The wave period is defined as the time interval between start and the end of the wave. It is sometimes also referred to as the zero-crossing period $T_z$. A significant wave period can be defined as the mean period of the highest one-third of all waves on record:

$$T_s = T_{1/3} = \frac{1}{N/3}\sum_{j=1}^{N/3} T_{z,j} \tag{2.15}$$

Another parameter that plays an important role is the wave direction. Wave rose diagrams are a tool that express the directionality of waves with respects to one central location. They show the percentile occurrence of different wave heights and periods from different directions towards the central target [49]. An example of a wave rose diagram is displayed in Figure 2.7.

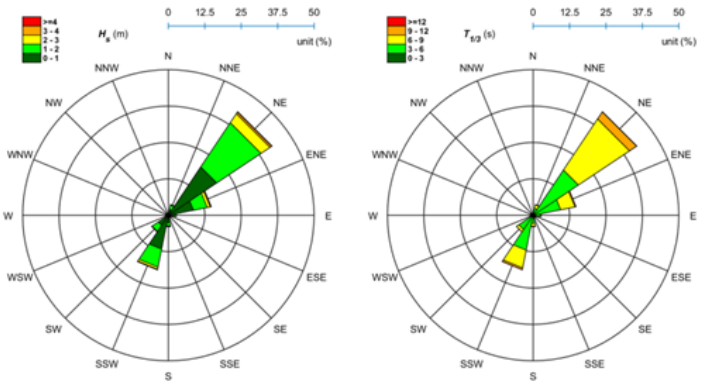


Figure 2.7: Example of wave rose diagrams for $H_s$ and $T_s$ [50]

As mentioned in Section 2.2.1, the sea elevation can be estimated using an ocean wave spectrum. A commonly used spectrum is the JONSWAP spectrum, which is defined as follows [51]:

$$S(f_W) = \frac{\alpha g^2}{(2\pi)^4} f_W^{-5} \exp[-\frac{5}{4}(\frac{f_W}{f_p})^{-4}]\gamma^{p*} \tag{2.16}$$

where

$$p* = \exp[-\frac{(T_p f_W - 1)^2}{2\sigma^2}] \tag{2.17}$$

and

- $\alpha = 0.0081$ is the Phillips parameter
- $g$ is the gravitational acceleration

- $f_W$ is the wave frequency
- $f_p$ is the spectral peak frequency
- $\gamma$ is the peak enhancement factor
- $\sigma = \sigma_a = 0.07$ for $f \leq f_p$, $\sigma = \sigma_a = 0.09$ for $f > f_p$

Alternatively, the JONSWAP spectrum can be expressed in terms of the significant wave height $H_s$ and the peak wave period $T_p$ [1] [52]:

$$S(f_W) = B_J H_s^2 T_p^{-4} f_W^{-5} \exp[-\frac{5}{4}(T_p f_W)^{-4}]\gamma^{p*} \tag{2.18}$$

where

$$B_J = \frac{0.0624(1.094 - 0.01915 \ln \gamma)}{0.230 + 0.033\gamma - 0.185(1.9 + \gamma)^{-1}} \tag{2.19}$$

and

$$T_p \approx \frac{T_s}{1 - 0.132(\gamma + 0.2)^{-0.559}} \tag{2.20}$$

**Currents**
Ocean currents can influence the hydrodynamic behaviour of the cable by causing hydrodynamic drag and added mass forces (Section 2.2.3) and VIV (Section 2.2.9). Current data can be gathered through field measurements. When these measurements are not available, which is likely when investigating a new site, the current can be modelled. The method for this is described in the standard DNVGL-ST-0437 [35], in which the current velocity with respect to the distance from the seabed is expressed as:

$$U(z) = U_{tide}(z) + U_{wind}(z) \tag{2.21}$$

where

$$U_{tide}(z) = U_{tide0}(\frac{D + z}{D})^{\frac{1}{7}} \quad \text{for} \quad z \leq 0 \tag{2.22}$$

and

$$U_{wind}(z) = U_{wind0}(\frac{D_0 + z}{D_0}) \quad \text{for} \quad -D_0 \leq z \leq 0 \tag{2.23}$$

in which

- $U(z)$ is the total current velocity at level $z$
- $z$ is the vertical coordinate from still water level
- $U_{tide0}$ is the tidal current at still water level
- $U_{wind0}$ is the wind-generated current at still water level
- $D$ is the water depth from still water level
- $D_0$ = 50 m is the reference depth for wind-generated current

[1] The peak wave period or dominant wave period is associated with the highest energy waves within the spectrum.

**Sea Depth**
The sea depth plays an important role in configuration choice. In shallower waters the catenary configuration without buoyancy modules is likely to be possible. With a limited mass, HOP axial stresses may stay within limits and the short cable length and absence of buoyancy elements makes for a cost-effective solution. FOWTs however are only financially feasible in deep waters, upwards of 50 m and will therefore almost certainly require a configuration with buoyancy modules. Within the scope of this research, water depths between 50 m and 220 m are considered, because this is where most of the European wind energy potential lies [10].

**Other Water properties**
The following parameters need to be taken into consideration when making calculations or calibrating simulations:

- *Water density:* has influence of the behaviour of the cable underwater
- *Water temperature:* has influence on the strength of the materials

## 2.5.2. Configuration Parameters

Configuration parameters can be adjusted to change the shape of the configuration. They can have different impacts on the behaviour of the cable, such an a decrease in tension a the HOP or a decrease in fatigue stress at a fatigue critical point. Therefore, they need to be chosen carefully, depending on the application of the DPC and the environmental conditions at the operation site. Parametric studies can be performed to test the influence that different parameters have on the behaviour of the cable.

**Length**
Changing the length of the DPC can have a considerable effect on the maximum curvature and tension in the cable. When considering a cable that is suspended between a floating platform and a fixed platform without making contact with the seabed, an increased cable length was calculated to decrease the amount of curvature at the suspension points [53]. While the cable configuration in this example did not contain any buoyancy modules, the application is similar to that of the W-shape configuration. Note that, even though [53] did not investigate the matter, an increased cable length will almost certainly lead to an increase of tension at the HOP, due to the additional mass of the cable.

Rentschler et al. [54] performed a parametric study of the catenary and LWS configuration for a FOWT application, by varying the total DPC length. In the case of the lazy wave, the ratio between the non-buoyant and buoyant cable sections was also investigated. The results from this study were somewhat different than from those with the cable that was suspended from both ends in [53]. A longer cable length of the catenary configuration resulted in lower HOP tension and higher maximum curvature towards the TDP. A shorter length resulted in higher tension at the HOP and lower maximum curvature. The reason for this is because a longer cable descends to the seabed more steeply, therefore touching down closer to the floater and resulting in a shorter section of cable being suspended through the water column. The best performing for a catenary shapes were found to have a cable length to water depth ratio between 2.7 and 2.8, but HOP tensions for water depths over 100 metres were too great for the catenary shape. The LWS was able to perform much better at water depths up to 200 metres. The best performing solutions had a cable length to water depth ratio of approximately 2.8 and a non-buoyant to buoyant to non-buoyant length ratio of approximately 1:1:2.

**Buoyancy Module Properties**
The BMs contribute to creating the shape of the DPC configuration. As previously explained in Sections 2.2.5 and 2.2.6, a gravitational and a buoyant force act on all submerged components of a DPC. The resulting vertical force on a buoyancy module can therefore be expressed as:

$$F_{BM} = -F_{g,BM} + F_{b,BM} = -m_{BM}g + \rho_W g V_{BM} = (\rho_w - \rho_{BM})gV_{BM} \tag{2.24}$$

Therefore, the parameters that determine the resulting upward force on a single buoyancy force are the density of the foam and the volume of the BM. Being roughly shaped as a hollow cylinder, a BM's volume can be approximated as:

$$V_{BM} = \frac{\pi}{4}(D_{BM,o}^2 - D_{BM,i}^2)L_{BM} \tag{2.25}$$

Figure 5.7 shows an illustration of two BMs clamped to a DPC. The overall length of the buoyancy cable section is determined by the number of buoyancy modules $n_{BM}$ and the length interval between each module $d_{BM}$.

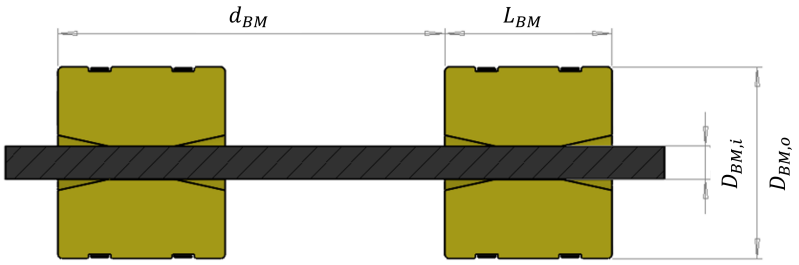


Figure 2.8: Two BMs and their dimensional parameters

It is also possible to model the buoyant cable section continuously, rather than discretely. This means that the buoyant section is modelled as a normal cable without attachments but with a different mass and volume. In this case the vertical force on the buoyant cable section is expressed as:

$$F_z = -m_{C,b}g + \rho_W V_{C,b}g \tag{2.26}$$

where $m_{C,b}$ and $V_{C,b}$ are the total mass and volume of the buoyant cable section respectively.

**Bend Stiffener Properties**

Bend stiffeners or cable stiffeners prevent excessive curvature at critical points, in particular at the HOP. The additional bending stiffness that they provide is given by their dimensions and material properties. This stiffness can be expressed as [30]:

$$EI_{BS}(s) = EI_C + \frac{\pi}{4}E_{BS}(R_o^4(s) - R_i^4), \quad 0 \leq s \leq L_{BS} \tag{2.27}$$

where

- $s$ is the longitudinal position along the BS
- $EI_C$ is the bending stiffness of the DPC
- $E_{BS}$ is the Young's modulus of the BS
- $R_o$ is the outer radius of the BS
- $R_i$ is the inner radius of the BS
- $L_{BS}$ is the length of the BS

Given a conical shape of the bend stiffener, the dimensional parameters of a bend stiffener are shown in Figure 2.9. Note that $D_o(s) = 2R_o(s)$ and $D_i = 2R_i$.

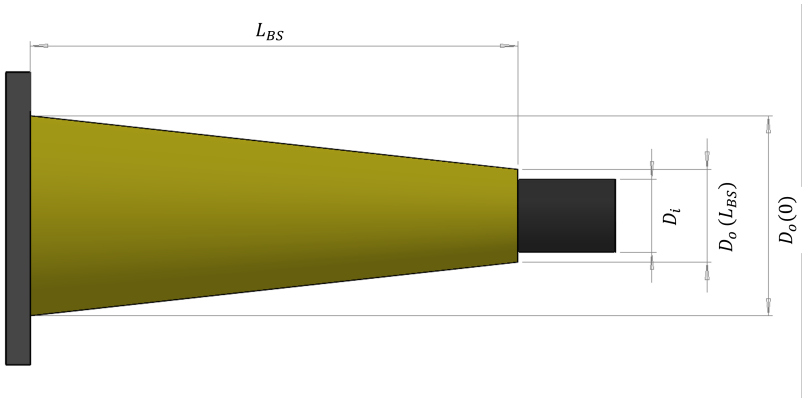


Figure 2.9: BS and its dimensional parameters (not to scale)

## 2.6. Conclusion

A good design for the DPC configuration is crucial to ensure the structural integrity of the umbilical throughout its intended life time. From the many configuration types that are available, the LWS and W-shape appear to be the most suitable for the application with FOWTs. The LWS has already been researched and tested, while the more particular W-shape in still in its conceptual design phase and requires analysis. Buoyancy modules and bend stiffeners are important auxiliary components, contributing to achieving the correct shape of the DPC configuration and limiting stresses on the cable.

The dynamic environmental loading on the DPC must be taken into careful consideration. Waves and currents cause hydrodynamic loads and 6DoF motion excitement at the HOP due to motion of the floater. Additional loading on the configuration is from gravity and buoyancy on cable and auxiliary components. The mass increase due to marine growth can also have an influence over time. VIV, caused by flow across the cable, can contribute to fatigue damage.

Failures can occur under the harsh dynamic loading conditions of DPCs. During its operational life phase, a DPC is susceptible to a number of mechanical failure mechanisms. These are primarily related to over stretching, compression or over bending of the cable. Fatigue damage is of particular concern, due to the cyclic loading.

A number of standards has been composed that describe the correct design steps for DPCs and their configuration. Limit state design prevents exceeding of any of the limit states, which would result in failures. Several design criteria must be met to ensure safe operation of the DPC.

The DPC configuration is defined by a number of parameters. Environmental parameters define the location and environmental loads that act on the DPC and the floater. Configuration parameters directly influence the shape and the properties of the configuration. Cable length and properties of BMs and BSs are considered important configuration parameters. Given certain environmental conditions, the configuration parameters must be chosen so that the stresses on the cable are kept within limits.

# 3

# Analysis of Dynamic Power Cables

Before it is possible to make any decisions about the design of DPCs, it is necessary to understand their behaviour. In the past, a number of analysis methods have been applied to estimate the motions, loads and fatigue damage experienced by DPCs in order to be able to verify or make design decisions.

This chapter provides an overview of the analysis methods used in previous research and answers the sub-question *'How can the global motions, loads and fatigue on DPCs be calculated?'*. As the formulation of this question suggests, only global DPC analysis will be taken into account. This approach calculates the global motions, loads and fatigue stresses along the entire length of the cable.

Using a global rather than local approach, the cable is modelled as a umbilical with a uniform, solid cross-section. Therefore, loads and fatigue on the individual internal components of the DPC cross-section cannot be directly accurately calculated. A number of physical effects is not included in global analysis, such as movement and friction between the internal components. However, the global stresses that contribute to fatigue damage at different locations along the cable can be estimated. Given the time savings that global analysis offers, the global approach is deemed appropriate for this research. No deeper research into the differences between global and local analysis will be conducted in this research, but it is important to take note of the physical limitations of the cable model.

There is a distinct difference between coupled and decoupled analysis methods. The first section in this chapter will explain the differences between both approaches and their advantages and disadvantages with regards to the DPC application. Following that, the methodologies for structural response analysis and fatigue analysis will be explained. Finally, the findings from this chapter are concluded.

## 3.1. Coupled and Decoupled Analysis

Coupled analysis couples the motion of the floating platform to those of the DPC and mooring system. Rather than simulating the components individually, the whole system is modelled as one. The influence of the slender components on the static and dynamic response of the floater can be attributed to the following forces (coupling effects) [55]:

**Restoring**

- Static restoring force from the mooring and DPC system as a function of floater offset
- Current loading and its effects on the restoring force of the mooring and DPC system
- Seafloor friction (if mooring lines and/or DPC have bottom contact)

**Damping**

- Damping from mooring and DPC system due to dynamics, current, etc.
- Friction force due to floater/DPC contact

**Inertia**

- Additional inertia forces due to the mooring and DPC system

Decoupled analysis considers individual components of the system separately. It therefore does not take any coupling effects into account. Generally, the motion of the floating platform is analysed first, either through numerical modelling of an experimental setup (e.g. [13]). This 6DoF motion time history is then used as input data for the simulation of the DPC. It is also possible to do frequency domain simulation of the floater to obtain its Response Amplitude Operator (RAO) values, which can later be used as input parameters for time-domain solutions of the other components [56].

The work by Yang et al. [56] compared the coupled and decoupled analysis of the mooring lines of a FWEC system. The decoupled approach started by performing hydrodynamic analysis of the FWEC in frequency-domain and finding its RAOs. After that, time-domain simulations of the mooring system were done, using the floater's motion response to the modelled sea state as an input motion at the connection points of the mooring lines. In contrary, the coupled analysis used the results from time-domain simulations of the entire system, thus modelling the FWEC and its mooring system together within the same software package. Both approaches produced stress and fatigue response results in the mooring lines. The results in terms of motion response of the mooring system near the HOP point were comparable between both methods. Discrepancies occurred at points further down the lines, which were believed to be caused by the coupling effects described earlier on in this section. Stress cycle amplitude results from the coupled analysis were higher, especially near the HOP, as were accumulated fatigue damages. These fatigue results motivated the authors' preference for the coupled analysis.

Whether or not the conclusions from [56] are directly applicable to the analysis of DPCs is questionable. While mooring lines are configured in a catenary shape, common practice with DPCs is the LWS. The buoyancy modules used in this configuration decouple the motions of the floating platform from the touchdown point and also reduce the tension at the HOP [57]. Other configurations that use buoyant cable sections have similar effects [25]. One can therefore assume that, in the case of a DPC, the motions of the floater have lesser influence on the cable's behaviour, thus making decoupled analysis a viable alternative to the fully coupled approach.

There are pros and cons for both approaches. Coupled analysis produces more realistic results, due to the inclusion of the coupling effects. It is however more computationally expensive and requires extensive modelling efforts. Decoupled analysis is faster and more flexible, because different floater types are more easily implemented. Decoupled analysis can even be performed with RAOs or motion time history data from previous research. It does however suffer from inaccuracies because the coupling effects are (partially) disregarded. As mentioned before, the effects of these inaccuracies on a DPC configuration with buoyant elements are expected to be somewhat less than on a catenary shape umbilical, such as a mooring line.

## 3.2. Structural Response Analysis

Structural response analysis seeks to calculate the motions and loads on a DPC given a certain excitation by external loads. This type of analysis is used to assess whether or not any of the ultimate failure mechanisms, such as over tensioning of the cable, is likely to occur.

### 3.2.1. Environmental Analysis

In order to estimate the external loads that act on the DPC, an environmental analysis of the location in which the DPC will operate is necessary. Metocean data is generally used to estimate the wave, wind and current conditions at the site.

For the ULS analysis, extreme weather conditions are usually used. Different load cases are constructed, in which the environmental input parameters for the simulations are defined. Kim et al. [58] used the metocean data for 10-year return period winter storms and 100-year return period hurricanes as loading conditions for their analysis of free-standing hybrid risers. The data consists of significant wave height, peak spectral period, peak enhancement factor, wind speeds and current speeds at different depths. Similarly, Poirette et al. [18] combined several 50-year return period conditions for waves, currents and winds to create load cases for their analysis of a DPC under extreme environmental conditions. The waves were modelled using the JONSWAP spectrum. The metocean conditions can also be expressed by a wave scatter diagram, as was done by Yang et al. [53]. A wave scatter diagram

displays the occurrence probability of sea states, which are defined as combinations of specific wave heights and periods. In some examples of previous research, e.g. the paper on failure prediction of DPCs by Young et al. [59], a single sea state from different directions was deemed sufficient to identify the critical loading points of the DPC configuration. The recommended practice DNV-RP-C205 [60], recommends a 50-year return period on environmental conditions and environmental loads.

### 3.2.2. Modelling and Simulation

Several commercial software programs are available for the modelling of subsea umbilicals such as DPCs. The following steps are required to create an accurate model of a DPC and its environment:

- *Correct implementation of the environmental parameters* as established from the environmental analysis. Create the load cases that represent the most common environmental conditions and verify if they behave as expected. Make sure that other environmental parameters (e.g. water depth) are correct too.

- *Accurate representation of the floater motions*. Whether the floater is fully modelled or the motion is governed by previously obtained motion time histories, verify that the motion response of the floater to an input sea state is as expected.

- *The parameters for the DPC and for the auxiliary components* need to be realistic and implemented correctly. Examples of such parameters are the cable stiffness, density of buoyancy modules or the hydrodynamic drag coefficients. For validation of the model, parameter values from previous literature (e.g. [19], [61]) can be used as input.

Simulation parameters need to be adjusted in order to get accurate results without sacrificing too much computational efficiency. The following aspects need to be taken into consideration:

- *Duration:* The length of the time-domain simulation needs to be sufficiently long to capture all the dynamic loading and get a good picture of the behaviour of the system. In some cases the early stage of the simulations is not included in the results, because the system response has not fully developed yet.

- *Time step:* Small time steps might produce accurate results, but can cause long computation times. Sensitivity studies are required to find the right balance between accurate results and computational efficiency.

- *Mesh size of the cable model:* Choosing a suitable mesh size or segment length for the DPC model is crucial to obtain accurate results. It is possible to have a variable segment length for different sections of the DPC. Especially critical points under bending require a small segment length, while sections that are not critically loaded and therefore require no accurate analysis can have longer segment lengths. Again, sensitivity studies to find the correct values are required.

### 3.2.3. Results

As mentioned earlier, structural response analysis describes the motion and load behaviour of a DPC under (extreme) environmental loading conditions. Possible outcomes of such an analysis can be:

- *Range graph:* description of the minimum/mean/maximum values of a load/displacement of the DPC, along its entire length (example in Figure 3.1a).

- *Time history:* description of the load acting on a specific point along the DPC over time (example in Figure 3.1b).

The range graph data is useful to identify critical points where loads on the cable are high. Time histories can be used to inspect cyclic loading on the cable. Versions of either, where the load/motion is normalized against its ultimate limit, are used to visualize failures and in case of confidential cable specifications.

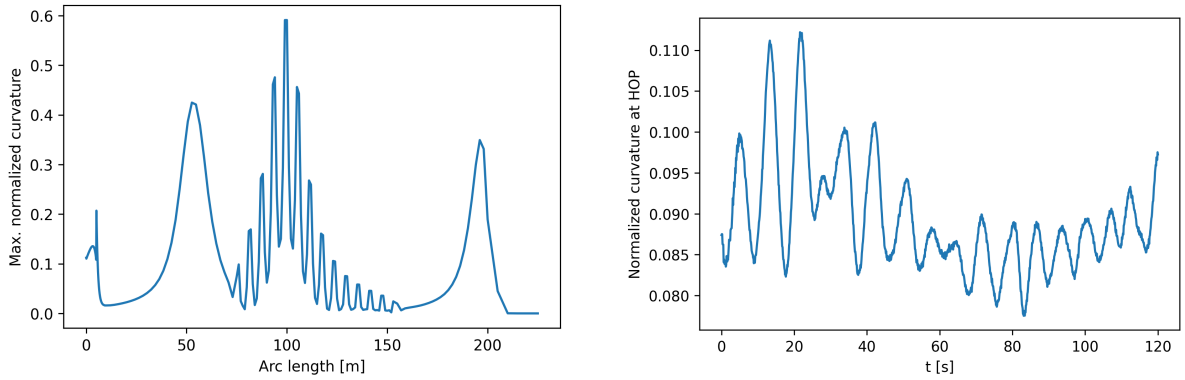


(a) Range graph of maximum normalized curvature

(b) Time history of normalized curvature at HOP

Figure 3.1: Example of the output from structural response analysis

## 3.3. Fatigue Analysis

Fatigue analysis uses the stress time history output from a structural response assessment to make an estimate on the amplitude and quantity of load cycles that the DPC experiences during its life time. The contribution of each stress cycle to the total fatigue damage can then be calculated using appropriate S-N curves. The following subsections explain all the aspects of fatigue analysis in detail.

### 3.3.1. Environmental Loading

Similarly to ULS analysis, FLS analysis requires appropriate modelling of the environment to begin with. Short-term sea states are used, rather than extreme weather conditions, to reproduce normal operating conditions [24]. Wave scatter tables with (annual) occurrence probabilities can be used to compose load cases for the simulations.

### 3.3.2. Stress and Strain Calculation

It is necessary to calculate the stresses or strains within the DPC to make approximations of the fatigue damage. Fatigue on offshore structures is mainly induced by action from waves and environment. The corresponding number of stress cycles can be in the order of millions per year [62]. Low-cycle fatigue is characterized by large strains within the plastic domain. Therefore, low-cycle fatigue failure occurs for up to as little as 1e4 stress cycles. This means that for DPCs predominantly high-cycle fatigue is expected to be of significance. High-cycle fatigue is characterized by stresses and strains within the elastic domain [63].

Based on the loads and motions that result from the structural response analysis, the stresses and strains can be calculated using the geometrical and structural properties of the cable. The stress and strain due to axial tension in a solid cylinder are calculated as:

$$\sigma_a = \frac{F_a}{A} = \frac{4F_a}{\pi OD^2} \tag{3.1}$$

$$\epsilon_a = \frac{\sigma_a}{E} \tag{3.2}$$

where $F_a$ is the axial force, $OD$ is the outer diameter of the cable and $E$ is the Young's modulus of the cable. Considering that the DPC is considered to be homogeneous in this research, the axial stress is constant across the cross-section.

The stress and strain due to bending in a solid cylinder are calculated as:

$$\sigma_b = Ey\kappa \tag{3.3}$$

$$\epsilon_b = \frac{\sigma_b}{E} \tag{3.4}$$

where $y$ is the distance from the centre line of the cable and $\kappa$ is the curvature. With a homogeneous cross-section in mind, the maximum bending stress occurs at the outer edge of the cable. This yields the following equation for the bending stress:

$$\sigma_{b,max} = \frac{E(OD)\kappa}{2} \tag{3.5}$$

Note that the equations above only hold when the stresses in the material remain below the maximum yield stress $\sigma_y$, in which case only elastic deformation occurs. This corresponds with the previously introduced statements that fatigue damage is most likely to take place in the high-frequency, low-stress domain.

### 3.3.3. Fatigue Curves

Fatigue properties of materials can be described using Stress-Life (S-N) curves. They describe the relation between applied stress amplitude and number of stress cycles of that amplitude until fatigue failure occurs. S-N curves are derived from fatigue experiments and are unique for each material. A fatigue level or endurance level can be defined, which is the stress level below which an infinite number of stress cycles can be applied without causing fatigue failure [64]. Figure 3.2 shows the characteristic features of a S-N curve.

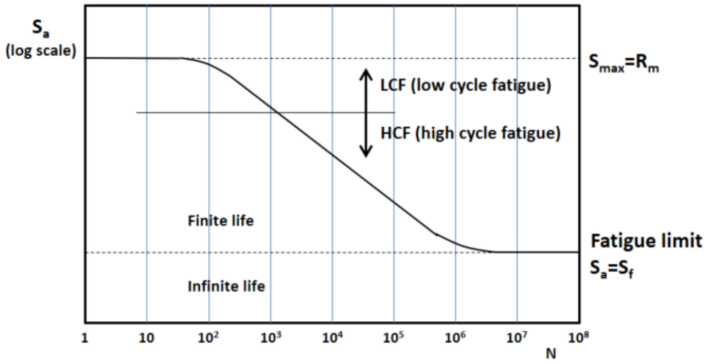


Figure 3.2: Example of S-N curve with characteristic features [64]

When conducting global fatigue analysis, the fatigue properties of the copper conductor cores are often taken used to calculate the fatigue damage on a DPC (e.g. [13], [61]), because this component is considered to be fatigue sensitive. The S-N curve of the copper conductor strands of a dynamic power cable for FOWT applications has been approximated by Nasution et al. [65]. Single wire fatigue tests were conducted after which a fatigue curve was fitted to the test results. The mathematical formulation of the fatigue curve is:

$$N(\Delta\sigma)^m = A \tag{3.6}$$

where $N$ represents the number of cycles to failure, $\Delta\sigma$ is the applied stress range and $m$ and $A$ are constant coefficients. The best fit, found for $m$ = 6.238 and $A$ = 6.098e19, is shown in Figure 3.3a.

In some instances, authors of previous research make use of strain-life or $\epsilon$-N curves, rather than S-N curves. The reason for this is that the Electrolytic Tough Pitch Copper (ETPC), which is commonly used on DPC conductors because of its excellent conductivity, has poor mechanical properties. The stress-strain relationship of ETPC is non-linear and the material suffers from creeping, both of which need to be taken into account for the fatigue analysis of the conductor [66].

While S-N curves only take elastic strain into consideration, $\epsilon$-N curves also include plastic deformation. The $\epsilon$-N curve can be expressed by the Coffin-Manson relationship [67]:

$$\epsilon_{tot} = \epsilon_{pl} + \epsilon_{el} = C_1 N^{-\beta_1} + C_2 N^{-\beta_2} \tag{3.7}$$

where $C_1$, $C_2$, $\beta_1$ and $\beta_2$ are material specific coefficients that describe the shape of the $\epsilon$-N curve. The values for these coefficients for ETPC were found to be [65]:

- $C_1$ = 0.7692
- $C_2$ = 0.0219

- $\beta_1$ = 0.5879
- $\beta_2$ = 0.1745

The resulting $\epsilon$-N curve for ETPC is shown in Figure 3.3b. Note that the plastic strain contribution is only taken into account if in the case of low-cycle fatigue when the total stress on the conductor exceeds the yield stress of the copper material, which only occurs under extreme loading of the cable. Similarly to earlier statements from [63], the transition from low-cycle to high-cycle fatigue occurs at about 1e4 stress cycles. The slope of the $\epsilon$-N curve changes, indicating a change in the relationship between stress and strain.

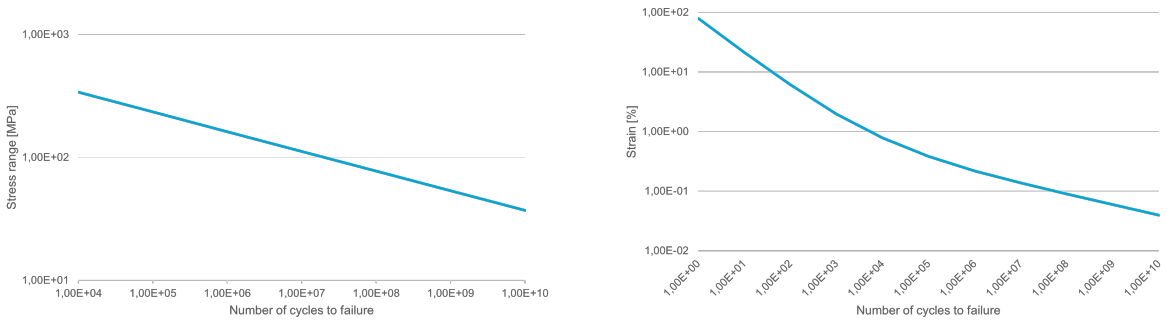


(a) S-N curve

(b) $\epsilon$-N curve

Figure 3.3: Fatigue curves for copper.

### 3.3.4. Load Cycle Counting

Figure 3.4 shows the calculated stress time history at a critical location of a DPC, which was a result from structural response analysis. It is evident that the cyclic loading is highly irregular. This type of loading is to be expected for marine structures in irregular seas. In order to be able to perform fatigue analysis using the S-N/$\epsilon$-N curves, these irregular stress cycles need to be organised into a number of regular stress cycles with different amplitudes.

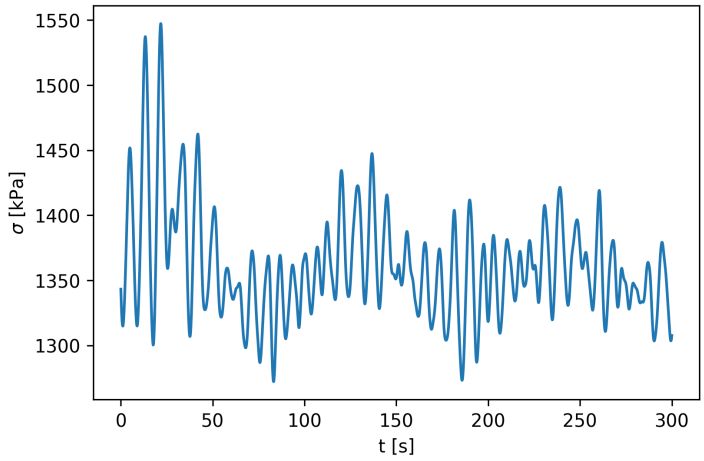


Figure 3.4: Stress time history at a critical location

**Rainflow Counting**

The stress cycle counting method that is most commonly used in literature is the rainflow counting algorithm. This method identifies the stress-strain response (hysteresis loops) of the tested material by identifying individual stress cycles from the calculated stress/strain time history. Rainflow counting was inspired by rain dripping down a pagoda roof. An example is shown in Figure 3.5. A stress/strain half cycle is counted each time a stream of water [68]:

- Reaches a maximum that is larger than the previous maximum (e.g. stream A-D)
- Reaches a minimum that is smaller than the previous minimum (e.g. stream B-C)
- Hits another stream falling from above (e.g. stream C-B)
- Reaches the end of the time history (e.g. D-A)

The counted half cycles that have the same range can be added up to form a number of full stress cycles with specific amplitudes. The contribution of each stress cycle to the fatigue of the material can then be evaluated, using the S-N curves. The stress cycles counted from the example stress time history in Figure 3.5 are listed in Table 3.1.

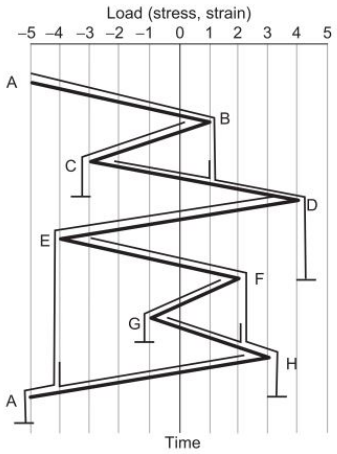


Figure 3.5: Graphic representation of the rainflow counting method [68]

| No. of full cycles | Points | Range | Mean |
|---|---|---|---|
| 1 | A-D | 9 | -0.5 |
| 1 | B-C | 4 | -1 |
| 1 | E-H | 7 | -0.5 |
| 1 | F-G | 3 | 0.5 |

Table 3.1: Counted stress/strain cycles from Figure 3.5

### 3.3.5. Damage Calculation

Accumulated fatigue damage can be calculated using an S-N curve and the Palmgren-Miner rule [69]:

$$D_{ftg} = \sum_{i=1}^{k} \frac{n_i}{N_i} \tag{3.8}$$

where:

- $k$ stands for the different stress levels from the rainflow analysis
- $N_i$ is the average number of cycles to failure at stress level $S_i$
- $n_i$ is the number of stress cycles at stress level $S_i$

Fatigue failure occurs when design $D_D > 1$. However, considering that the safety factor for fatigue $DFF$ must be taken at least 10, the calculated fatigue damage must be [46]:

$$D_c \leq \frac{D_D}{DFF} = 0.1 \tag{3.9}$$

This design criterium was previously explained in Section 2.4.2.

## 3.4. Conclusion

Global analysis of the DPC configuration can be conducted using a coupled or decoupled approach. The coupled method takes the coupling effects that arise from interaction between the floater and the DPC into account, which can give more accurate results. It is however computationally expensive, due to the need to fully model the entire system. The decoupled method only requires detailed modelling of the DPC, while floater behaviour is represented as a 6DoF motion input. It is therefore less computationally expensive, but can potentially be inaccurate due to the lack of coupling forces. However, given that the buoyant part of a DPC configuration decouples the motions of floater and DPC for a large part, these coupling effects become less important. Therefore, decoupled analysis is a viable option for the analysis of DPCs.

The response behaviour of the cable is approximated using structural response analysis methods. A good representation of suitable environmental conditions stands at the base of the analysis operation. Extreme weather conditions need to be modelled to test the ULS design of the DPC configuration. Correct implementation in the modelling and simulation software is crucial to get reliable results. These results can be used to assess whether or not any of the ULS design criteria is exceeded during the operational conditions to which the cable is exposed.

Fatigue analysis uses the outcome of a structural response analysis with environmental load cases representing normal operational conditions as an input. From the gathered stress-time histories at critical points, the stress cycles that contribute to fatigue damage are counted. Total fatigue damage is calculated by summating all the contributions from individual stress cycles. For the fatigue analysis of the conductors, it is common practice to use strain-life based fatigue curves, due to the nonlinear stress-strain relationship of the copper material.

# 4

# Optimization of Dynamic Power Cables

Mathematical optimization can be a useful tool to accelerate the design of DPCs and the DPC configuration. Without requiring extensive experience or expert knowledge on a fairly unexplored topic, optimization can give the designers a preliminary design specification of the DPC configuration, based on which a more detailed design of the system can be made. This chapter answers the research subquestion “What are the available methods for optimization of the DPC configuration?”. It begins by giving an overview of blackbox optimization methods, which are required for the optimization of computer simulation-based optimization, for which the exact correlation between the input and output of the system is unknown. The following section contains a state-of-the-art review on global subsea umbilical optimization. Finally, conclusions on the research topic of this chapter are given.

## 4.1. Blackbox Optimization

The complex dynamic loads that act on DPCs make it difficult to do an analytical assessment of the cable’s structural response. To overcome this, several commercial hydrodynamic analysis software packages are available for the numerical simulation of DPCs and other subsea umbilicals. Examples that were used in previous literature are OrcaFlex (e.g. [19]) and Ansys AQWA (e.g. [61]). While software programs offer great opportunity for the global structural analysis of DPCs, their application within optimization problems can be somewhat troublesome. Usually, the analytical forms of the underlying algebraic equations are not available, which makes it impossible to apply classical gradient-based optimization methods [70].

Blackbox Optimization (BBO), in literature also referred to as simulation-based optimization, attempts to find a solution to optimization problems where the algebraic equations are not available. The objective and constraint function values are the result of computer simulations, legacy codes or physical experiments [70]. Given that the global analysis of the DPC configuration requires the use of a ‘blackbox’ software package, the optimization can only be performed using some kind of BBO method. BBO methods can be divided into the following categories [71]:

- Direct search methods
- Heuristic methods
- Model-based methods

In the remainder of this section, these categories will be further explained, along with their suitability for the optimization of the DPC configuration. Given that function evaluations can be extremely computationally expensive, using an efficient BBO method is very important for the feasibility of the overall optimization strategy.

### 4.1.1. Direct Search Methods

Direct Search (DS) methods seek to find the optimum value for functions for which explicit information about their derivatives is unknown or untrustworthy [72]. Simple approaches to DS are the exhaustive search, grid search and coordinate search methods [71]:

- *Exhaustive search* explores all the possible solutions to find an optimum. While theoretically this method is guaranteed to converge this also requires an infinite amount of function evaluations.
- *Grid Search (GS)* requires a bounded set of constraints. The function is then evaluated for a finite number of points that are located on a grid on the space of variables. GS is still extremely inefficient due to the exponential growth of required function evaluations with each dimension added to the problem.
- *Coordinate search* iteratively evaluates candidate solutions located at a fixed step length from the current best solution. If an improvement is found, this becomes the new best solution. If not, then the step length is deceased. The algorithm is terminated after the step length drops below a pre-defined threshold, a pre-defined number of function evaluations is reached, a specified amount of time has passed or the objective function has reached a small enough value. Coordinate search is considerably more effective than GS, but the number of function evaluations still increases linearly with the number of variables.

The methods listed above can converge to an optimum, given enough time and a simple enough problem. In order to accelerate convergence and be able to increase dimensionality, advancements on the aforementioned methods have been developed [70], [71], [73]:

- The *generalised pattern search* algorithm adds flexibility to the coordinate search algorithm by not limiting the search for improved solutions to fixed coordinate directions and step lengths. Instead, the candidate solutions are represented by a collection of vectors that changes with each iteration. The algorithm begins with a search step, in which the variable search space is discretized by a mesh. A subset of candidates on the mesh is then evaluated. If an improved solution is found, the mesh coarseness is increased for the next iteration. Otherwise, the so-called poll step is executed, in which an improvement is sought after more locally around the current optimum. If the poll step does not yield an improved objective value, the mesh coarseness is decreased. When compared to coordinate search, generalised pattern search is less likely to get stuck at a local optimum, due to the inclusion of the global search step.
- *Mesh adaptive search* is an extension of the generalised pattern search method. Mesh adaptive search does not limit the poll step candidates to be within the mesh of the search step, but introduces a frame. Any poll candidate solution that lies within the frame is acceptable. This further improves the convergence of the method.

While convergence can be mathematically proven for most DS methods, convergence rate can be very slow. On top of that, most methods require a steeply increasing amount of function evaluations with increasing dimensionality of the search space [72]. Therefore, applying a DS method to a complex optimization problem with an expensive objective function evaluation might well result in unacceptably high computational costs. With respect to the optimization the DPC configuration, this means that the execution of the hydrodynamic simulations will need to be quick and the number of decision variables needs to be chosen wisely.

### 4.1.2. Heuristic Methods

The designation heuristic optimization is given to optimization methods that iteratively search for a good but not necessarily optimal solution to an optimization problem [74]. These types of optimization can be applied to a wide range of optimization problems. Amongst these can be BBO problems as well as cases where the underlying algebraic structure is known, but a large problem size makes efficient calculation with gradient-based optimization methods difficult [75]. Some of the most common heuristic optimization methods are explained below [71], [76], [77]:

- A *Genetic Algorithm (GA)* is modelled after the principles of evolution and ‘survival of the fittest’. The process begins with an initial population of individuals, all of which are encoded as chromosomes. A fitness value is then assigned to each individual based on an evaluation of the objective function. Now the reproduction phase begins, which consists of a selection, crossover and mutation step, after which an updated next generation is formed. This process is repeated until some stopping criterion is reached. The GA method is very flexible and multiple implementations of the different steps are possible. Careful encoding and selection of simulation parameters (e.g. population size) are key to achieving a successfully functioning GA.

- *Particle swarm optimization* is based on the behaviour of swarms in nature (e.g. a flock of birds). A swarm of particles is initialized with random position and velocity, within a bound search space. With every iteration, the velocity and position of each particle are updated based on the particle's previous velocity, the particle's best previous position and swarm's overall best position. One can say that a particle's next state is determined by an inertia component, a cognitive component and a social component. In previous literature (e.g. [78]), particle swarm optimization based methods have been proven superior over GA based methods, both in terms of speed and quality of the found solution.
- The *Nelder-Mead* method optimizes a function of $n$ variables by evaluating the values at the vertices of a $(n+1)$-sized simplex and replacing the worst vertex by another vertex, creating a new simplex. The algorithm executes reflection, expansion, contraction and shrink steps, all based on the performance of new found vertices compared to the existing vertices, to iteratively change the simplex's shape and improve its overall performance. While the Nelder-Mead algorithm is widely used and performs well on practical problems, its convergence to a stationary point is not guaranteed. There can also be a tendency to converge towards local optima.

In general, heuristic optimization methods are easy to understand and implement and are widely applicable. Therefore they are well-suited for individual problems with computationally inexpensive objective functions. Due to their slow convergence, heuristic algorithms are not particularly suitable for problems with more expensive objective functions. The large number of function evaluations that is needed might cause unacceptably high computational costs. On top of that, heuristic optimization methods provide no mathematically proven stopping criteria that assure optimality [71]. This leads to believe that a heuristic optimization method is not the best choice for optimization of the DPC configuration.

### 4.1.3. Model-based Methods

Even though the objective function of BBO models is unknown, in many cases it is reasonable to assume that this function is smooth. Model based optimization attempts to approximate this unknown objective function with a fully defined model function. The derivatives of this model function can then be used for the optimization of the model with the use of efficient, derivative-based optimization methods [71]. These approximation models are often referred to as surrogate models or metamodels. The formulation of a model-based optimization method can be seen as a three-phase operation, which is explained in this section.

**Phase 1: Design of Experiment**

The process of Surrogate Model Optimization (SMO) begins with the experimental design phase. This phase involves taking samples and performing experiments or simulations. The gathered training data is later used to construct the surrogate model function. To be able to construct an accurate enough surrogate model, a careful Design of Experiment (DoE) method choice is important. In short, the most important requirements for good experimental design are [79]:

- Uniform distribution across the design space *(space-filling)*
- No two design points should share the same coordinate value *(non-collapsing)*
- The design points have to satisfy the constraints *(constraint-filling)*

One could use a pseudo-random DOE method, such as Monte-Carlo Sampling (MCS), to obtain the required samples. The problem with this is the extremely large number of samples needed. Therefore, more efficient sampling techniques are desired when working with computationally expensive simulations.

The most popular DoE method for engineering applications is Latin Hypercube Sampling (LHS). This method divides the range of each input variable into $p$ intervals of equal probability. For a problem with $k$ variables, this results in a division of the design space into $p^k$ bins. Samples are taken randomly from within each interval of each variable, but in such a manner that all bins that are within each one-dimensional projection of a 'filled' bin are empty. The advantage that LHS offers over pseudo-random MCS is that the number of samples needed scales as $\mathcal{O}(k)$ rather than $\mathcal{O}(2^k)$, while providing more precise results given an equal number of samples [80]. LHS can therefore be used to reduce the number of required samples, without sacrificing performance.

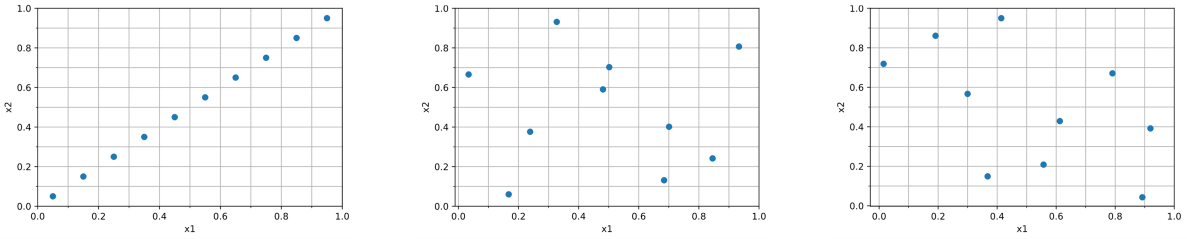


(a) LHS design A (b) LHS design B (c) LHS design C

Figure 4.1: Three cases of LHS from worst to best performing. The samples in example C are more uniformly distributed across the design space and less clustered than in example B.

While the most basic form of LHS ensures the non-collapsing design requirement, the space-filling requirement is not guaranteed. For example, a two-dimensional LHS design where all samples are located on the diagonal of the search space does not give an accurate representation of the system's behaviour. In order to achieve a sufficiently space-filling DoE, many improvements have been made to the method since its introduction. Researchers focused on the optimization of the sample point locations, by means of different optimization algorithms and objective functions. While LHS optimization is computationally challenging (the number of possible LHS designs scales as $O((p!)^k)$, on modern computers it is possible to generate good LHS designs for moderate amounts of variables and sample points within seconds [81]. Figure 4.1 shows three LHS designs, from worst to best performing. Improvements to the space-filling properties of design C have been made by applying 'maximin' optimization to the LHS design, similar to the research in [82].

Another family of DoE methods that is often referred to is quasi-MCS. Where random sampling can result in clustering of samples or large gaps in the design space, quasi-MCS applies low-discrepancy sequences to achieve a more evenly filled design space. Amongst these sequences are the Halton, Sobol and Faure sequence [83]. Quasi-MCS tends to outperform traditional MCS and non-optimized LHS, both in terms of accuracy and space-filling capacity. That being said, for lower dimensionality problems, where LHS optimization is possible, LHS provides excellent space-filling properties without requiring a large number of samples [84].

**Phase 2: Surrogate Model Selection**

The next phase involves selecting an appropriate surrogate model to fit to the earlier obtained set of training data. Polynomial regression is one of the most simple forms of constructing a usable surrogate model. This method is however not particularly well-suited to globally estimate highly nonlinear, multi-dimensional functions [79]. Therefore other, more appropriate surrogate model types are presented in this section.

A common method to construct surrogate model is through the use of *radial basis functions*. A radial function is a function whose value only depends on the Euclidian distance between the point at which it is evaluated and the origin and therefore has the form $\phi(x) = \varphi(\| x \|)$, where $\varphi$ is a real function. Examples of radial basis functions are linear, cubic, multiquadric or Gaussian functions [79]. The output of the system as estimated by the Radial Basis Function (RBF) surrogate model is then formulated as follows [85]:

$$\hat{f}(x) = \sum_{i-1}^{n} \theta_i \phi(||x - x_i||) \tag{4.1}$$

where the weights $\theta_i$ are determined by solving:

$$\theta = \Phi^{-1} f \tag{4.2}$$

Herein $n$ is the number of samples, $\Phi \in \mathbb{R}^{nxn} : \Phi_{i,j} = \varphi(||x - x_i||), i, j = 1, ..., n$ represents the RBFs and $f = f_1, ..., f_n$ is the vector of sampled function evaluations.

Another popular surrogate modelling method is *kriging*. Originally developed for use in geostatistics, kriging interpolation is now widely applied in computer aided engineering. In kriging the predicted output for a 'new', not yet simulated input $\hat{Y}(x_{n+1})$ is given as a weighted linear combination of the 'old', already

simulated inputs $Y(x_i)$. The general formulation of the kriging model is then [86]:

$$\hat{Y}(x_{n+1}) = \sum_{i=1}^{n} \lambda_i Y(x_i) = \lambda Y \tag{4.3}$$

Where the set of weights is represented as $\sum_{i=1}^{n} \lambda_i = 1, \lambda = \{\lambda_1, ..., \lambda_n\}$ and the vector of input variables is $Y = \{Y(x_1), ..., Y(x_n)\}$. Previous research has been conducted, in which the performance of RBF and kriging surrogates was compared to other surrogate models. While exact comparison of all methods is difficult, following findings can be summarized:

- Kriging is able to give more accurate predictions of the blackbox function values than polynomial regression [86].
- RBF models offer a higher modelling accuracy and more robustness (less susceptible to crashing) than kriging models [85].
- RBF models are easier to construct and give more accurate results than kriging models [87].

Overall, RBF surrogate models seem to perform better than kriging surrogate models. Their application in optimization of subsea umbilicals is not unheard of, more of which will be explained in Section 4.2. Other SMO techniques than the ones listed in the current section are available (e.g. support vector machines), but are not included in this research.

**Phase 3: Solving the Optimization Problem**
Once the surrogate model has been constructed, the next phase of SMO involves finding the optimal solution to the problem. However, simply finding the optimum of the surrogate model might not be enough, because the optimum of the surrogate might not accurately represent the optimum of the real model due to errors in the surrogate model. Therefore, new candidate points at which to evaluate the model must be chosen carefully and added to the training data set to improve the surrogate. In search for improvement, a search around the current best point must be conducted. However, points further away must also be taken into account in order to avoid ending up in a local optimum. A balance between local search (exploitation) and global search (exploration) must be found [79].

## 4.2. Optimization of Subsea Umbilicals: State-of-the-Art

Previous efforts to incorporate optimization into the design of the DPC configuration have been made by various authors. All of their approaches differ in terms of the optimization method, decision variables, objectives or constraints that were used. This section contains the most important work on optimization of the DPC configuration. For a more complete overview of available methods, previous work on the global optimization of other subsea umbilicals is included too.

### 4.2.1. Optimization of the DPC configuration

An early investigation into optimization of the FOWT system was done by Fylling and Berthelsen [88]. Their model included optimization of the floating spar buoy platform, mooring lines and lazy-wave power cable, with the objective to minimize the total cost of the system. Cost was calculated as a function of the type and amount of material used. The decision variables for the DPC in particular were the weight and length of the buoyant cable section, while constraints limited the maximum tension, curvature and horizontal offset. The structural response analysis was performed using both normal operation conditions and extreme survival conditions. A sequential quadratic programming approach, which is a classical method for nonlinear constrained optimization, was used to solve the optimization problem.

Research that focused specifically on optimising the inter-array DPC configuration was conducted by Poirette et al. [18]. After formulating 28 ULS load cases based on analysis of the metocean conditions, the configuration was optimised for overall costs, which were a combination of cable costs, buoyancy section costs and bend stiffener costs. Constraints assured that none of the mechanical ultimate limits of the cable were exceeded. Chosen as design parameters were cable section lengths, total cable length, cable and buoyancy module diameter, bend stiffener length and bend stiffener base diameter. Using these design parameters, initial cable configurations were generated through LHS

and surface fitting (SMO). Accurate optimization using more computationally expensive Finite Element Modelling (FEM) simulations was then conducted using an in-house optimization method based on sequential quadratic approximation.

Rentschler et al. [19] conducted an extensive research on the optimization of the DPC configuration in an FOWT application. In other research [54] they performed static analysis on the LWS, from which they found a dimensional relation between water depth and cable section length. They then used this rule of thumb as a starting point for optimization in a dynamic scenario. The optimization model included a LWS cable model with fully discretized BMs and a bend stiffener at the HOP. The environmental conditions were simplified into an energy equivalent sea state with irregular wave loading. An important aspect of this research was the inclusion of fatigue analysis of the DPC. This fatigue was analysed for the conductor of the cable, assuming that this is the most fatigue sensitive component. A multi-objective optimization approach without constraints was used to minimize ultimate loads, cable length and fatigue damage of the cable. The only decision variable that was taken into consideration was the placement of the BMs along the length of the cable. A heuristic optimizer, in the form of a GA with a population size of 20, was used to solve the optimization problem.

### 4.2.2. Optimization of Other Subsea Umbilicals

With limited work on the optimization of the DPC configuration available, previous research on other subsea umbilicals must also be considered. Flexible risers and mooring lines have in the past been modelled similarly to DPCs and are applicable to scenarios with dynamic loading in deep waters. While having to fulfil totally different functions, when modelled globally these structures also have comparable dimensions and dynamic behaviour. The findings about optimization of subsea umbilical configurations can potentially be used to further expand the optimization techniques for DPCs.

The optimization of a steep wave shape (see Section 2.1) riser was investigated by Chen et al. [87]. They utilised SMO, in order to reduce the amount of computationally expensive time-domain simulations. Samples from LHS provided a basis on which to construct kriging and RBF models. After having determined that the RBF model performed better, the authors performed global optimization with a multi-island genetic algorithm and further improved the result using a method named nonlinear programming by quadratic Lagrangian. The objective of this research was to minimize the curvature at the hog bend of the riser. Design constraints included maximum tension, maximum hang-off angle, minimum clearance between the sag bend and seabed and a length redundancy to ensure sufficient length of the riser. The design variables used were the riser section lengths and the horizontal distance between HOP and TDP.

A comparison between two riser design optimization methods was presented by Bhowmik et al. [89], both of which took a SMO approach in combination with an evolutionary algorithm. The steel LWS configuration's design variables consisted of riser segment lengths, BM diameter, BM spacing and hang-off angle, while the objective was to minimize both cost and accumulated fatigue damage, though not simultaneously.

An optimization framework for a mooring system can be found in the work of Pillai et al. [90]. The design of the three mooing lines was formulated by varying the horizontal distance between HOP and anchor point, angle between floating body and anchor, mooring line section lengths and mooring line section types. Just like in some of the previously given examples involving DPCs and risers, the objective here was to minimize the overall costs. A multi-objective problem was formulated by also attempting to minimize the maximum tension in the mooring lines. This resulted in a trade-off between both objectives, which was visualized by a Pareto front. The optimization problem was solved with a GA.

## 4.3. Conclusion

For optimization problems that involve computer simulations, it is common practice to apply a BBO method. Many different BBO methods have been developed, all of which are suitable for different types of optimization problems. The hydrodynamic simulations of DPCs are computationally expensive, which is why an efficient optimizer that requires only a small number of function evaluations is needed for the optimization of the DPC configuration.

The convergence rate of direct search BBO methods can be slow. The required number of function evaluations is greatly increased for higher dimensionality problems. Heuristic methods are easily

implemented, but they too can be inefficient. They also lack proof of convergence and good stopping criteria. BBO methods from the direct search and heuristic categories are therefore considered insufficiently compatible with the optimization problem at hand.

Model-based BBO methods make use of a surrogate model, which is an approximation of the 'real' model. The surrogate model can be optimized easily with a classical derivative-based optimization method, because its algebraic form is known. After obtaining training data using a carefully formulated DoE, a surrogate model is fitted to the data by means of some type of interpolation. Kriging and RBF interpolation are popular, where RBF models tend to be more accurate. The surrogate model is then updated with new function evaluations until an optimum is found. A well formulated SMO method does not require an excessive number of function evaluations, even when multiple decision variables are involved.

Some research on the global optimization of DPCs and similar subsea umbilicals has been conducted in the past. A wide variety of BBO methods was used including GA (heuristic) and kriging SMO (model-based). The objective functions involved minimization of costs, cable length, maximum loads and fatigue damage. Decision variables could be either focused on the cable (e.g. length, weight, distance to TDP) or on the auxiliary components (e.g. spacing between the BMs).

The research conducted in this chapter leads to believe that model-based BBO methods are most suitable for the optimization of the DPC configuration. A SMO approach using a RBF interpolant to construct the approximation model promises the highest accuracy, which is important to achieve efficient convergence to a high quality optimal solution.

# 5

# Dynamic Power Cable Model

Global analysis of the DPC configuration requires accurate representations of the DPC system with numerical computer models. The characteristics of the models are defined by parametric settings, hence the term parametric model is used in this report. Within this chapter, the different modelling choices are explained and the influence and relevance of the physical parameters is reviewed. The sub-question *"How can a parametric model of the DPC configuration be developed?"* is to be answered. First, the development of models for the floating platform, DPC and fatigue analysis is explained. To ensure that these models work as expected, some model verifications are presented subsequently. Following that, a convergence study is conducted to find the desired simulation parameter values. In order to gain insight on the influence of the physical parameters on the behaviour of the DPC configuration, sensitivity studies are conducted the relevant configuration parameters. Finally, concluding remarks are given.

## 5.1. Model Description

The software package OrcaFlex [91] was used to model the DPC system's components. This software package offers all the important features required for the analysis of the DPC, including time-domain aerodynamic and hydrodynamic simulations and rainflow counting for fatigue analysis. The complete response of the DPC configuration to externally applied loads was calculated in a three-stage progress, in which the following three models were used:

- Floating platform model
- Global DPC model
- Fatigue model

The inputs, outputs and interactions between the models are described by Figure 5.1. The remainder of this section will explain the individual models in more detail.

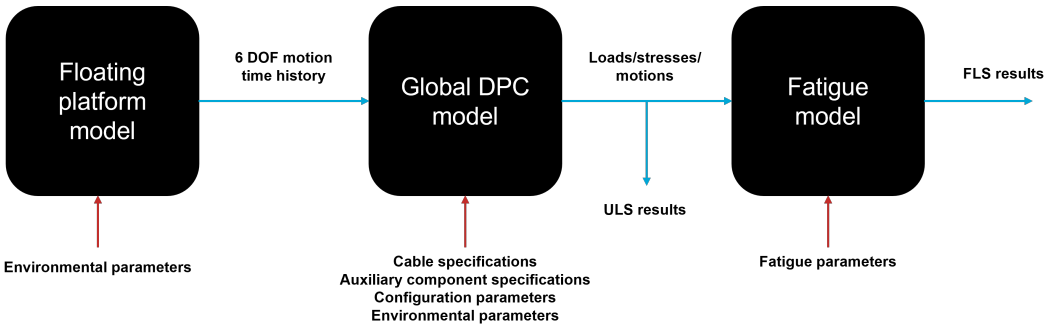


Figure 5.1: DPC system modelling flowchart

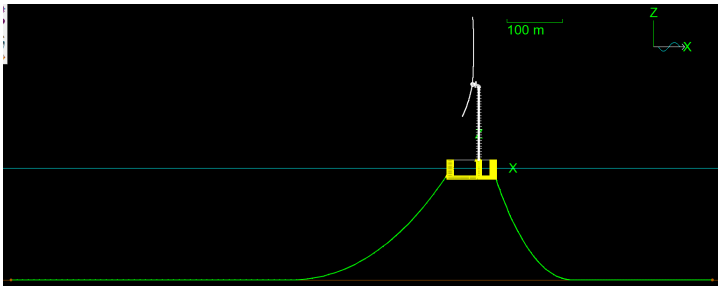


Figure 5.2: OrcaFlex model of the turbine, floater and mooring lines

### 5.1.1. Floating Platform Model

Due to the limitations dictated by the scope of this research, no explicit efforts are made in modelling of the floating platform. Instead, a fully developed readily available OrcaFlex model of a FOWT is used to calculate the floater motions and gather the required inputs for the simulations of the cable. This model is based on a semi-submersible platform for a 15MW FOWT developed by the University of Maine in collaboration with the National Renewable Energy Laboratory. The OrcaFlex model contains the turbine, floating platform and three mooring lines, see Figure 5.2. Descriptions of the turbine and platform design are available online [92], as well a description of the OrcaFlex model in question [93].

The environmental conditions are used as input parameters for the floater model. These include wind, wave and current properties, all of which are further described in Table 5.1. The aero- and hydrodynamic loads caused by these environmental conditions are translated into a 6DoF floater motion response over time by performing time-domain simulations in OrcaFlex. Note that in this research a JONSWAP spectrum is used to estimate the sea elevation over time, representing a fully developed irregular sea state. For more detailed description of the environmental parameters, see Section 2.5.1.

| Parameter | Symbol | Unit |
|---|---|---|
| Sea bed depth | $D$ | m |
| Wind velocity | $v_{wind}$ | m s$^{-1}$ |
| Wind direction | $d_{wind}$ | ° |
| Significant wave height | $H_s$ | m |
| Peak wave period | $T_p$ | s |
| Wave direction | $d_{wave}$ | ° |
| Surface current velocity | $U_0$ | m s$^{-1}$ |
| Current direction | $d_{cur}$ | ° |

Table 5.1: Environmental input parameters

### 5.1.2. Global DPC Model

The global cable model is explicitly modelled in OrcaFlex. Accurate recreation of a LWS DPC configuration requires modelling of the regular cable, a bend stiffener and some kind of buoyant cable section. The overall shape of the configuration is determined by the global configuration parameters (Table 5.2) and the structural parameters of cable and auxiliary components, which are explained later on in this section. An overview of the global DPC model is shown in Figure 5.3.

| Parameter | Symbol | Unit |
|---|---|---|
| Hang-off point height | $H$ | m |
| Length of first dynamic section | $L_1$ | m |
| Length of buoyant section | $L_2$ | m |
| Length of second dynamic section | $L_3$ | m |
| Length of static section | $L_{st}$ | m |
| Horizontal distance to the termination point | $x_{TP}$ | m |

Table 5.2: Global configuration parameters

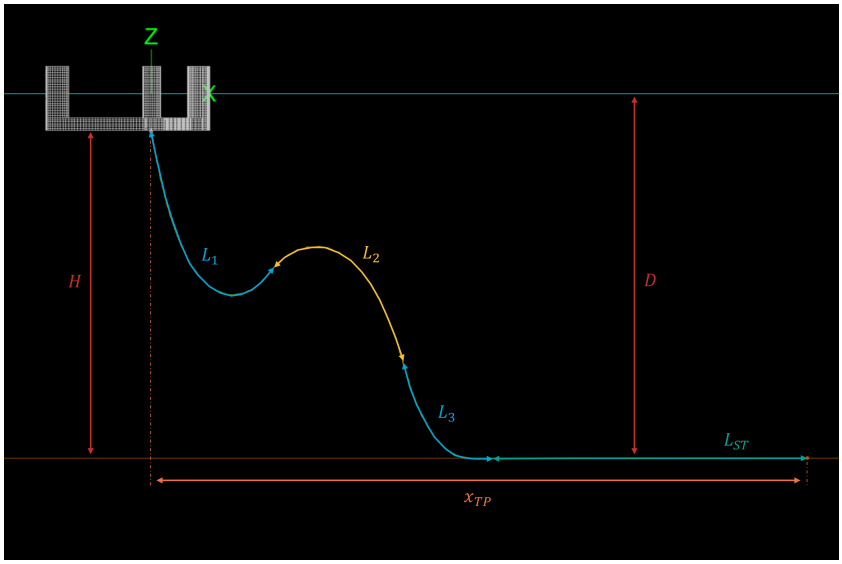


Figure 5.3: Global DPC model and parameters

**Regular Cable**

The power cable is modelled as a solid homogeneous cylinder. Its structural parameters are therefore constant across its length and cross-section. Table 5.3 shows the structural parameters involved in the modelling of the cable. The cable specifications are provided by a cable manufacturer and are confidential.

Within OrcaFlex, the regular cable is modelled as a flexible line. Lines are represented in OrcaFlex by a lumped mass model, made up from nodes which are connected by short segments [94]. An illustration of a lumped mass model line is shown in Figure 5.4. Herein, the nodes are represented by points with mass, drag and buoyancy properties. The segments on the other hand are weightless springs which provide the correct cable stiffness properties. Towards the TDP, dampening by the seabed is modelled by additional springs and dampers.

| Parameter | Symbol | Unit |
|---|---|---|
| Outer diameter | $OD$ | m |
| Mass per unit length | $w_{dry}$ | kg m$^{-1}$ |
| Axial stiffness | $EA$ | N |
| Bending stiffness | $EI$ | N m$^2$ |
| Minimum break load | $MBL$ | N |
| Minimum bend radius | $MBR$ | m |

Table 5.3: DPC structural parameters

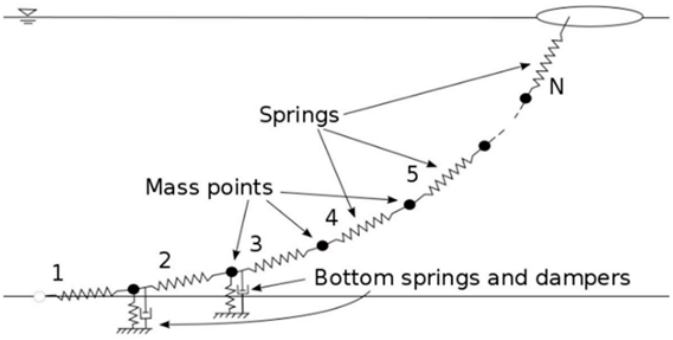


Figure 5.4: Line represented as lumped mass model [95]

**Bend Stiffener**

A BS is added at the HOP to prevent over bending and excessive fatigue near the HOP. The dimensional and material parameters that define the BS are listed in Table 5.4 and the bend stiffener's design is illustrated in Figure 5.6. Due to lack of accurate data on real-life BSs, a simplified conically shaped BS is used in this research with estimated material properties from reference studies ([19], [36]).

The BS is made from a polyurethane material with a density $\rho_{BS} = 1200\ kg/m_3$. The stress-strain relationship of the material is shown in Figure 5.5.

| Parameter | Symbol | Value | Unit |
|---|---|---|---|
| Length | $L_{BS}$ | 5 | m |
| Outer diameter at base | $D_o(0)$ | 0.41 | m |
| Outer diameter at tip | $D_o(L_{BS})$ | 0.19 | m |
| Inner diameter | $D_i$ | 0.15 | m |
| Density | $\rho_{BS}$ | 1200 | kg m$^{-3}$ |

Table 5.4: Bend stiffener design parameters

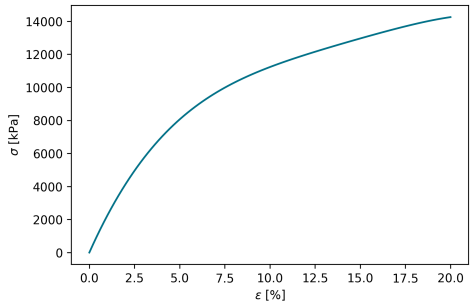


Figure 5.5: Stress-strain relationship for BS material

The BS is modelled in OrcaFlex using the stiffener modelling feature. A dedicated line type is formulated for the BS which is hollow and has an outer diameter that decreases linearly from the base towards the tip of the BS. The BS is connected to the HOP rigidly.

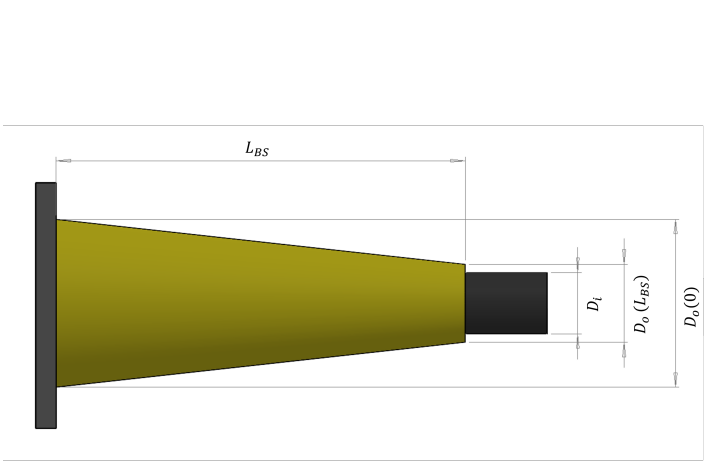


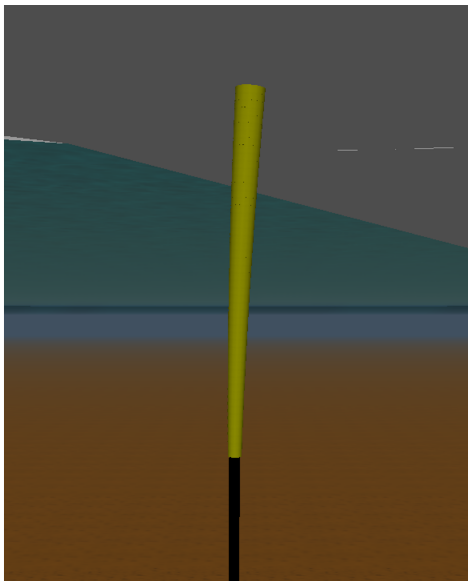

Figure 5.6: Bend stiffener model

**Buoyant Cable Section**

The buoyant cable section can be modelled as a continuous cable with different properties as the regular cable section. Altering the diameter and weight of this section will change its buoyancy properties, thus allowing the creation of buoyant cable configurations such as the LWS. However, this method does not clearly define the number of BMs that are attached to the cable, nor does the analysis provide any information about the behaviour of the cable in between the individual BMs. Therefore, the decision was made to model the buoyant cable section with the same properties as the regular cable section but with a number of BMs attached to it at regular intervals. The parameters involved in this 'discrete' modelling of the buoyant cable section are given in Table 5.5. An illustration of two BMs attached to a piece of cable is shown in Figure 5.7.

| Parameter | Symbol | Value | Unit |
|---|---|---|---|
| Length | $L_{BM}$ | 0.87 | m |
| Outer diameter | $D_{BM,o}$ | 0.76 | m |
| Inner diameter | $D_{BM,i}$ | 0.15 | m |
| Volume | $V_{BM}$ | 0.38 | kg m$^{-3}$ |
| Mass | $m_{BM}$ | 140 | kg |

Table 5.5: Buoyancy module design parameters

OrcaFlex offers a feature in which BMs can be modelled as spherical attachments to the cable. The BMs are defined by their mass, volume, height and offset from the centre of the cable. Note that, as shown in Figure 5.7, the parametric model of the BMs describes them as cylindrical shaped, rather than spherical. Within this research, the influence of the shape of the BM on the hydrodynamic response is considered negligible.

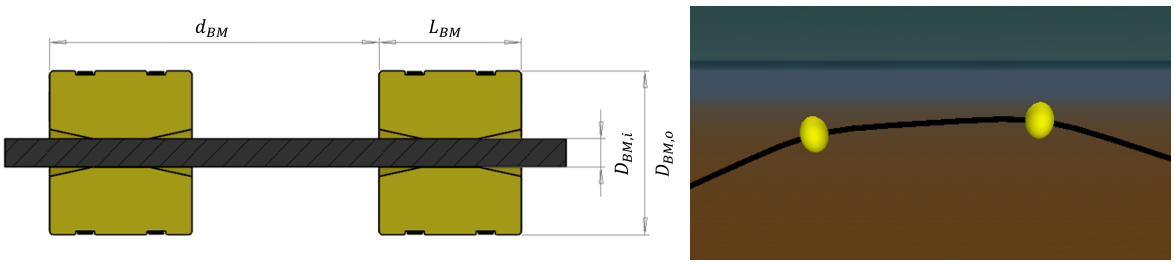


Figure 5.7: Buoyancy module model

## 5.1.3. Fatigue Calculation Model

The different aspects involved in calculating the fatigue damage on a DPC were previously explained in Section 3.3. In short, the total fatigue damage is estimated by counting the individual stress cycles obtained from the structural response analysis using rainflow counting, calculating each stress cycle's damage contribution using a S-N curve and finally summing up the individual damage contributions using Miner's rule. OrcaFlex offers a fatigue analysis tool that can perform these calculations and requires a number of input parameters to obtain correct results.

**Tension and Curvature Stresses on the Conductor**

Since the most fatigue sensitive component within the DPC is the copper conductor, it is necessary to estimate the fatigue on this specific component, rather than for the cable as a whole. This is not a straight forward calculation, due to the fact that the cable is modelled as a uniform cylinder. Estimations of the stresses and strains on the conductor as a function of the global loads and motions of the cable need to be made. Figure 5.8 shows a cross-section of the reference DPC that was used in this research.

Because of the difference in material properties and cross-sectional area of the three conductor cores when compared to the rest of the cable, a Tension Stress Factor (TSF) and Curvature Stress Factor (CSF) are introduced. These convert the global loads on the cable as calculated with the global cable model into stresses on the conductor. This expression of the stresses on the conductor is a required input parameter for the OrcaFlex fatigue analysis tool.

For the axial contribution, we can assume that the axial strain is constant across the entire cross-section. Therefore the axial strain on the conductor is equal to the axial strain on the cable:

$$\epsilon_{a,c} = \epsilon_a \tag{5.1}$$

where the subscript $c$ denotes the conductor properties. Global cable properties are not additionally subscripted. This translates to the following equalities:

$$\frac{\sigma_{a,c}}{E_c} = \frac{\sigma_a}{E} \tag{5.2}$$

$$\frac{F_{a,c}}{E_c A_c} = \frac{F_a}{EA} \tag{5.3}$$

These equations can be rearranged into the TSF, which relates the axial stress in the conductor to the global axial force in the cable:

$$TSF = \frac{\sigma_{a,c}}{F_a} = \frac{E_c}{EA} \tag{5.4}$$

A similar approach is used to estimate the curvature stresses on the conductor. The assumption here is that the maximum bending stress on the conductor occurs at the conductor's outermost strand. This location is represented by the conductor diameter $D_c$. Referring back to the equations in Section 3.3.2, the maximum bending stress on the conductor can thus be expressed as:

$$\sigma_{b,c} = \frac{E_c D_c \kappa}{2} \tag{5.5}$$

The curvature is constant across the cross-section. Therefore, the CSF is defined as:

$$CSF = \frac{\sigma_{b,c}}{\kappa} = \frac{E_c D_c}{2} \tag{5.6}$$

The values for $D_c$ and the conductor's Young's modulus $E_c$ are provided by a cable manufacturer and are confidential.

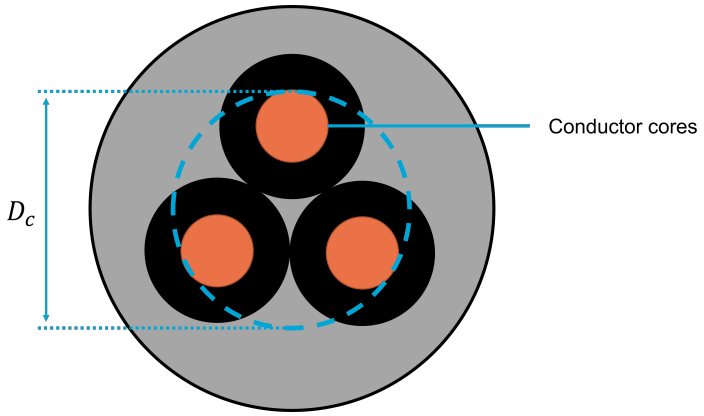


Figure 5.8: DPC conductors and conductor diameter

**Stress-Life Properties**

Review of previous studies on fatigue analysis of DPCs (see Section 3.3) shows that the fatigue properties of the copper conductor can either be expressed by a S-N curve, which considers only elastic deformation of the material, or a $\epsilon$-N curve, in which case plastic deformation is also included. To be able to make a decision on which method to use, it is necessary to make and estimation on whether there will be mostly high-cycle fatigue or low-cycle fatigue. Given that fatigue calculations are made for normal operational conditions and the design life time of DPCs can be as long as several decades, the occurrence of low-cycle fatigue is unlikely. Therefore, the S-N curve as proposed by Nasution et al. [65] (Figure 3.3a) is used for the fatigue calculations in this report.

**Fatigue Damage and Life**
The minimum calculated fatigue life can be expressed as the inverse of the calculated annual fatigue damage:

$$l_{ftg} = \frac{1}{D_{C,annual}} \tag{5.7}$$

However, recalling Equation 2.12, a safety factor for fatigue $DFF$ has to be taken into account. The maximum allowed annual fatigue damage on the DPC is therefore expressed as:

$$D_{ftg} = \frac{1}{l_{ftg} DFF} \tag{5.8}$$

Alternatively it is possible to define a design fatigue life as:

$$l_D = \frac{l_{ftg}}{DFF} = \frac{1}{D_{ftg} * DFF} \tag{5.9}$$

This design fatigue life must be larger than the minimum required fatigue life for reliable operation throughout the intended life-span of the cable.

**Limitations of the Fatigue Analysis**
The proposed analysis approach can have its limitation on the accuracy of the fatigue calculations. The main limitations are listed below:

- *Assumption of linear stress-strain behaviour*: The above equations for the fatigue behaviour of the conductor are only valid under the assumption of a linear stress-strain relationship. If the minimum yield strength of the copper were to be exceeded, plasticity occurs, in which case the used equation for stress $\sigma = \epsilon E$ no longer applies. In case of plasticity, Karlsen et al. [66] recommend the use of a $\epsilon$-N curve (Figure 3.3b). This allows for the inclusion of nonlinear deformation of the cable where small increase in stress causes a much larger strain than in the elastic domain, as shown in the stress-strain graph in Figure 5.9.
- *Global analysis*: The homogeneity of the cable cross-section does not allow the modelling of the individual cable components. Therefore, the influence of physical effects such as friction and relative motion of the components on the fatigue behaviour of the copper can not be calculated. Additionally, the simplified equations for the fatigue stresses, do not consider that the three conductors are helical components, which are wound under a certain pitch length. Therefore, the outermost strand of the conductor does not always align with the plane in which the cable bends, which means it is closer to the center line and the stresses are lower.

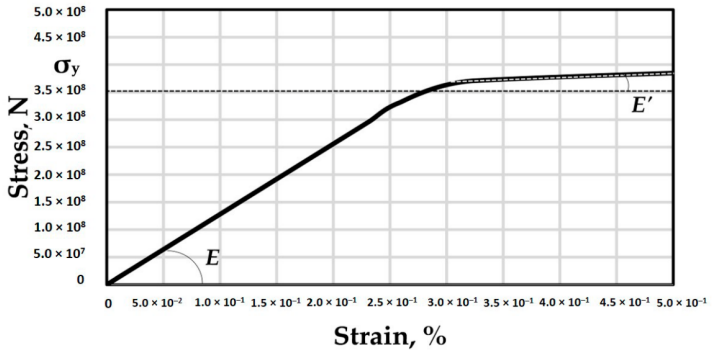


Figure 5.9: Example of nonlinear stress-strain curve [65]

## 5.2. Model Verifications

This section verifies the modelling decisions that were explained in the previous section and ensures that implementation in OrcaFlex is correct. Verification is done by comparing the theoretical loads on the cable to the results from an OrcaFlex test simulation.

### 5.2.1. Dry and Submerged Weight of the Cable

The objective of this test is to confirm that the OrcaFlex model correctly handles gravity and buoyancy forces on the DPC. At first, the cable is suspended in air between two points, as illustrated in Figure 5.10a. The reaction forces at the suspension points that result from gravity acting on the cable are calculated as:

$$F_r = \frac{1}{2}F_g = \frac{1}{2}w_{dry}Lg \tag{5.10}$$

When submerged in water, an upward buoyancy force opposing the gravitational force acts on the cable. This scenario is shown in Figure 5.10b. The resulting reaction forces are calculated as:

$$F_r = \frac{1}{2}(F_g - F_b) = \frac{1}{2}Lg(w_{dry} - \frac{\pi}{4}OD^2\rho_w) \tag{5.11}$$

Judging from the errors between theoretical and OrcaFlex results, which are shown in Table 5.6, gravity and buoyancy are estimated correctly by OrcaFlex. The percentile error is calculated as:

$$\text{Error} = \frac{|(\text{OrcaFlex value})*(\text{Theoretical value})|}{|(\text{Theoretical value})|}*100 \tag{5.12}$$

| Test | Error between theory and model |
|---|---|
| Dry weight reaction force | 7.05e-5% |
| Wet weight reaction force | 2.66e-8% |

Table 5.6: Dry and submerged cable weight verification results

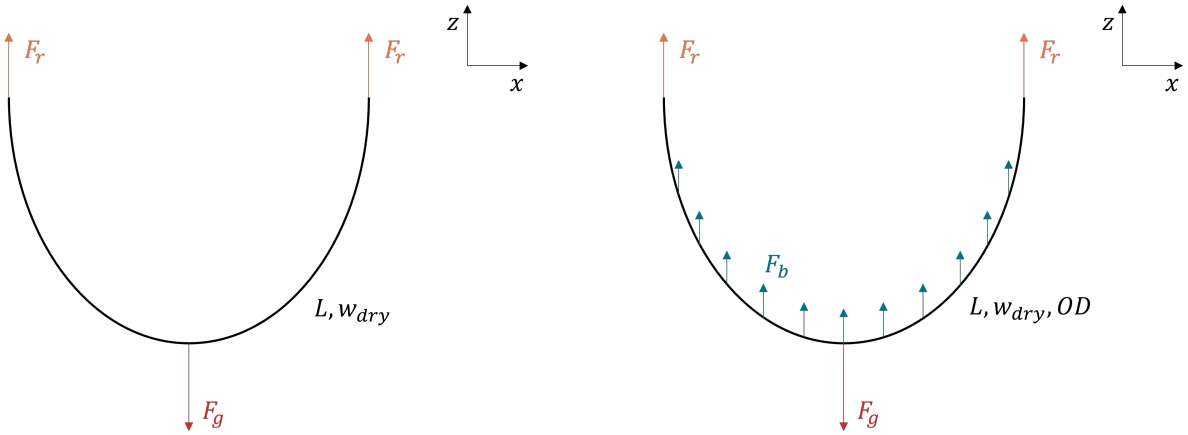


(a) Suspended in air

(b) Suspended in seawater

Figure 5.10: Forces on cable

### 5.2.2. Axial and Bending Stiffness of the Cable

The next test aims to verify that the axial stiffness of the cable is implemented correctly. Application of an axial force on the cable will result on an axial elongation of the cable, as is shown in Figure 5.11a. The relationship is as follows:

$$F_a = EA\frac{\delta L}{L} \tag{5.13}$$

The axial stress and strain on the cable are then calculated from Equations 3.1 and 3.2. The method for verification of the bending stiffness is similar. As shown in Figure 5.11b, a bending moment is applied to the cable. This results in a bending radius, from which the associated bending stress and strain can be calculated. Following up from Equations 3.3 and 3.4, the set of equations to calculate bending moment, stress and strain is:

$$M = \frac{EI}{R} \tag{5.14}$$

$$\sigma_b = \frac{M\frac{OD}{2}}{I} = \frac{32M}{\pi OD^3} \tag{5.15}$$

$$\varepsilon_b = \frac{OD}{2R} \tag{5.16}$$

From the results of the axial and bending stiffness tests (Table 5.7) it can be concluded that the axial and bending stiffness are correctly implemented in the OrcaFlex model. Therefore, the calculations of stresses and strains are correct too.

| Test | Error between theory and model |
|---|---|
| Axial force | 1.44e-4% |
| Axial stress | 1.44e-4% |
| Axial strain | 1.44e-4% |
| Bending moment | 5.37e-2% |
| Bending stress | 5.37e-2% |
| Bending strain | 5.37e-2% |

Table 5.7: Axial and bending stiffness verification results

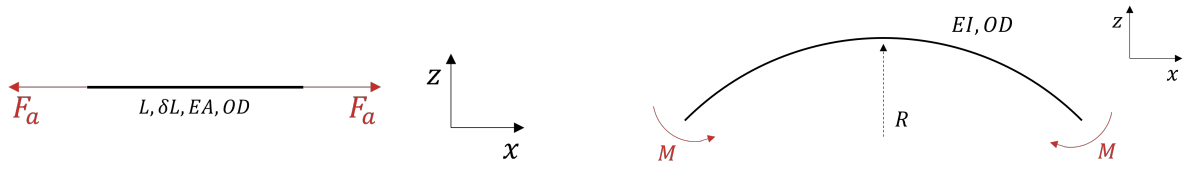


(a) Axial force on the cable

(b) Bending moment on the cable

Figure 5.11: Axial and bending stiffness verification scenarios

### 5.2.3. Buoyancy Module Forces

To check whether OrcaFlex accurately estimates the buoyancy force on the BM, first a massless module is modelled. The module is attached to a section of cable and, given that a buoyancy and gravitational force act on the cable section, the reaction force holding the system in position is expressed as:

$$F_r = F_{b,BM} + F_{b,Cbl} - F_{g,Cbl} = (V_{BM}\rho_w + \frac{\pi}{4}OD^2L\rho_w - w_{dry}L)g \tag{5.17}$$

In reality, the BMs do have a mass. To verify the gravity force on a BM in OrcaFlex, three BMs are attached to a cable section and the reaction force is calculated. The equation is as follows:

$$F_r = 3(F_{b,BM} - F_{g,BM}) + F_{b,Cbl} - F_{g,Cbl} \tag{5.18}$$

Both the BM tests are illustrated in Figure 5.12. The results in Table 5.8 show that the applied method for modelling individual BMs in OrcaFlex yields the correct results.

| Test | Error between theory and model |
|---|---|
| Buoyancy force | 1.83e-4% |
| Gravitational force | 2.22e-4% |

Table 5.8: BM forces verification results


(a) Buoyancy test (b) Gravity test

Figure 5.12: Buoyancy module verification scenarios

### 5.2.4. Fatigue Analysis

The fatigue analysis tool in OrcaFlex is verified by applying simple regular cyclic loading to the cable. This way, it is possible to calculate the estimated fatigue life analytically, according to S-N curves from reference literature, and compare them with the OrcaFlex results. Following assumptions and simplifications are made:

- Regular cyclic loading
- Linear stress-strain behaviour
- Homogeneous cross section
- Cross-sectional area of entire cable (outer diameter)

The case study presented here considers a cyclic loading amplitude that theoretically leads to a one-year fatigue life under pure axial loading. Axial cyclic loading is applied to a cable as shown in Figure 5.13. The number of load cycles in 1 year is calculated as the total number of seconds in one year over the duration of one stress cycle in seconds:

$$N_{year} = \frac{T_{year}}{T_{cycle}} \tag{5.19}$$

where $T_{year}$ = 31.536e6 s. According to Equation 3.6, the associated stress range is then:

$$\Delta\sigma = \sqrt[m]{\frac{A}{N_{year}}} \tag{5.20}$$

Herein $m$ = 6,238 and $A$ = 6.098e19 [65]. The motion applied to the OrcaFlex model to achieve a 1-year fatigue life is:

$$\delta L = \frac{\Delta\sigma L}{E} \tag{5.21}$$

Considering that the fatigue calculation is for the entire cross-section, the TSF can be expressed as:

$$TSF = \frac{1}{A} = \frac{4}{\pi OD^2} \tag{5.22}$$

The error between the theoretical fatigue life of 1 year and the OrcaFlex result is very small (Table 5.9). The deviations from the theoretical value can be attributed to an exposure time that is not exactly equal to one year and rounding errors. Therefore, the OrcaFlex fatigue analysis tool is perfectly adequate for the calculation of fatigue damage of a DPC.

| Test | Error between theory and model |
|---|---|
| Fatigue life | 2.10% |

Table 5.9: Fatigue analysis tool verification results

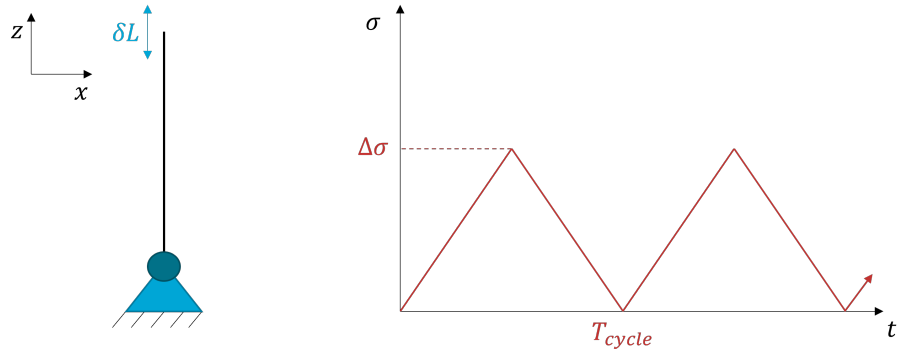


Figure 5.13: Fatigue analysis tool verification method

## 5.3. Convergence Study

The OrcaFlex simulations for the structural and fatigue analysis of the DPC configuration can be tuned by a number of simulation parameters. The value of these parameters can have influence on the performance of the simulations. Performance is measured by the following two indicators:

- *Accuracy of the results:* how close the simulation results are to ideal
- *Computational costs:* the time it takes for a simulation to run

It goes without saying that neither of these performance indicators can be satisfied perfectly and that a trade-off must be made. Therefore, this section presents a convergence study, in which the performance of the simulation model is tested for a number of different parameters. The objective of this study is to find the parameter values that will yield converging results, while keeping the computational costs acceptable.The following simulation parameters can be distinguished:

- The *time step* discretises the time space for time-domain simulations. Too small values can result in excessive computational costs, while too large values can cause numerical instability of the simulation.
- The *Cable Segment Length (CSL)* is responsible for the segment size of the lumped mass cable model. Large values result in fewer segments and therefore fewer calculations per time step are needed, however the results might become inaccurate.
- OrcaFlex has a build-up period feature, which is defined by the *build-up time* parameter. During the build-up period, the sea state is gradually increased. Therefore, longer build-up time values cause a smoother transition into the simulation period without peak stresses occurring due to an abrupt initialization of the sea state.
- The time-domain simulation period length is given by the *simulation time* parameter. This parameter needs to be chosen long enough to achieve a sufficiently developed sea state.

### 5.3.1. Setup

This section pictures the test scenario for the convergence study.

#### Model Parameters

The model parameters, as earlier described in Section 5.1, for the convergence study are listed in Table 5.10. Herein, the environmental conditions are adopted from Rentschler et al. [19], along with the global configuration parameters. The specifications of the auxiliary components are estimated from the work by Beerens [36].

| Parameter | Value | Unit |
|---|---|---|
| Environmental parameters | | |
| $D$ | 200 | m |
| $v_{wind}$ | 10 | $m\,s^{-1}$ |
| $d_{wind}$ | 0 | ° |
| $H_s$ | 5 | m |
| $T_p$ | 11.2 | s |
| $d_{wave}$ | 45 | ° |
| $U_0$ | 0 | $m\,s^{-1}$ |
| $d_{cur}$ | 0 | ° |
| Configuration parameters | | |
| $H$ | 180 | m |
| $L_1$ | 125 | m |
| $n_{BM}$ | 20 | - |
| $L$ | 500 | m |
| $x_{TP}$ | 360 | m |

Table 5.10: Model parameters for test scenario

**Simulation Parameters**

The simulation parameters in question are listed in Table 5.11, along with the values for which they are tested. The idea here is that only one variable is changed for each test, so that the influence of that variable on the performance of the simulation can be examined. The values for the fixed variables are chosen based on the convergence study results from the previously investigated value. For example, once an 'ideal' time step value has been chosen, this value is carried through to the next simulations. The base starting values for each simulation parameter are shown in Table 5.12.

| Parameter | Symbol | Test values | Unit |
|---|---|---|---|
| Time step | $t_{step}$ | [0.05, 0.10, 0.15, 0.20, 0.25] | s |
| Cable segment length | $CSL$ | [0.10, 0.25, 0.50, 1.0, 2.0, 3.0] | m |
| Build-up time | $t_{build}$ | [120, 240, 360, 480, 600] | s |
| Simulation time | $t_{sim}$ | [120, 300, 600, 1200, 2400, 3600, 4800, 6000] | s |

Table 5.11: Simulation parameter test values for convergence study

| Parameter | Base value | Unit |
|---|---|---|
| $t_{step}$ | 0.10 | s |
| $CSL$ | 1 | m |
| $t_{build}$ | 120 | s |
| $t_{sim}$ | 120 | s |

Table 5.12: Simulation parameter base values for convergence study

### 5.3.2. Results

The simulations that have been run for the convergence study produce several results that are relevant for the analysis of the simulation performance. They are listed below:

- Floating platform simulation time $t_{fpf}$: Duration of one floating platform model motion analysis simulation in seconds
- Cable simulation time $t_{cbl}$: Duration of one global DPC structural analysis simulation in seconds
- Fatigue simulation time $t_{ftg}$: Duration of one fatigue analysis simulation in seconds

The remainder of this section shows and discusses the results the convergence study for each simulation parameter.

### Time Step

The results for the time step convergence study are displayed in Figure 5.14. The time step size appears to have little to no influence on the fatigue results of the simulation, which is why the value $t_{step}$ = 0.2 s is chosen. A larger time step is not possible, because it leads to numerical instability in the floater simulations, which is why there are no results available for $t_{step}$ = 0.25 s. To further decrease the computational costs of the cable simulation time, the time step for the cable simulations could be enlarged as a multitude of the original time step. However, the effect of that measure on the accuracy of the results has not been investigated.

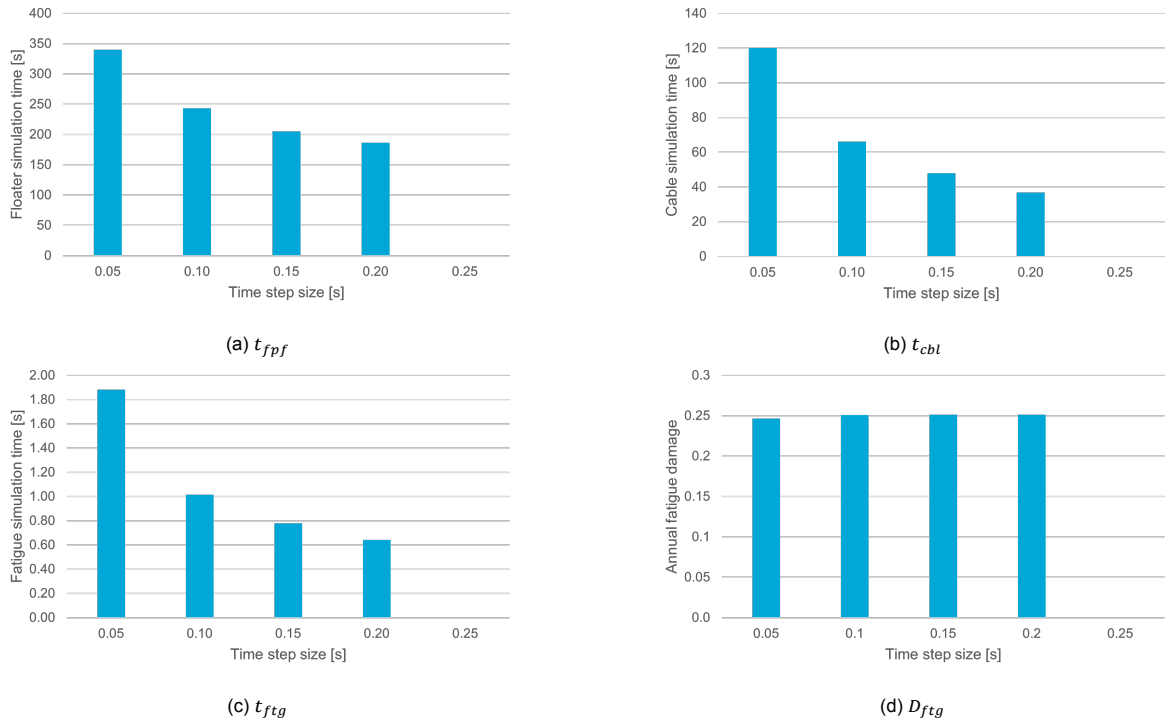


(a) $t_{fpf}$ (b) $t_{cbl}$

(c) $t_{ftg}$ (d) $D_{ftg}$

Figure 5.14: Results of time step convergence study

### Cable Segment Length

Figure 5.15 shows the outcome of the CSL convergence study. It shows that the CSL value does not have a significant influence on the accuracy of the results. The choice has been made to use $CSL$ = 2 m. A larger value could potentially cause inaccuracies if a simulation scenario with larger curvatures of the DPC were to occur. It also does not significantly improve computational efficiency. Be aware that the CSL value does not affect the floater simulation time, because the floating platform model does not include a power cable.

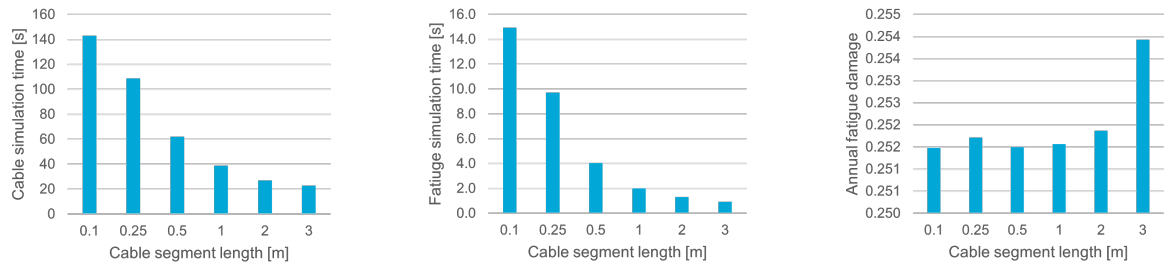


(a) $t_{cbl}$ (b) $t_{ftg}$ (c) $D_{ftg}$

Figure 5.15: Results of CSL convergence study

### Build-up time

The results in Figure 5.16 show that the annual fatigue damage converges to approximately $D_{ftg}$ = 0.18. The most computationally efficient build-up time value that yield accurate fatigue results is $t_{build}$ = 240 s. The build-up time length has no influence on the computational costs of the fatigue analysis, because the fatigue analysis does not include the build-up time and only calculates fatigue damage during the subsequent simulation time period. Short build-up times do have an impact on the fatigue damage, because a short build-up period can cause peak motions and loads during the early stages of the simulation.

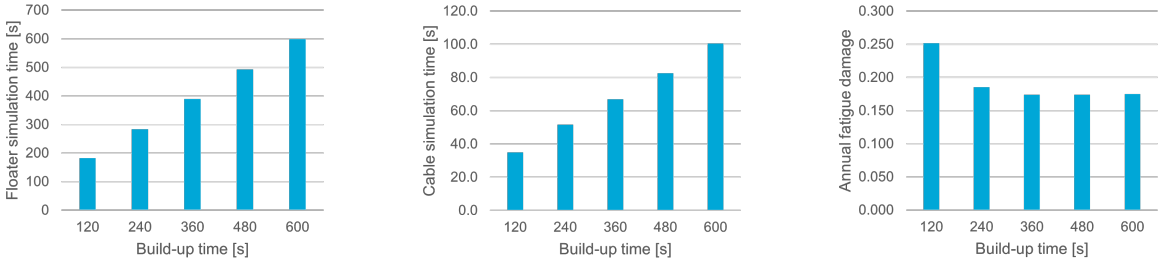


(a) $t_{fpf}$ (b) $t_{cbl}$ (c) $D_{ftg}$

Figure 5.16: Results of built-up time convergence study

### Simulation Time

The duration of the simulations needs to be long enough to capture enough different wave frequencies and amplitudes to create a good representation of long-term operation. Therefore, fairly long simulation times are required, which makes the simulations computationally expensive. The results of the simulation time convergence study (Figure 5.17) show that annual fatigue damage value stabilises after $t_{sim}$ = 2400 s. Total convergence with reasonable computational time cannot be reached, because of the highly irregular sea state.

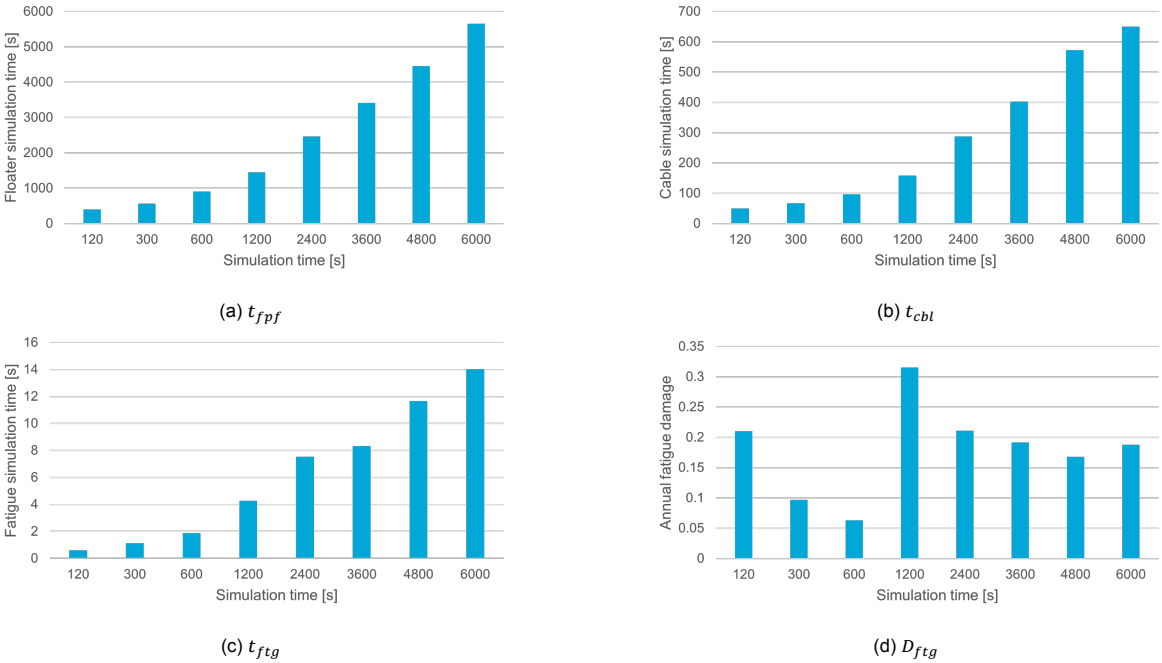


(a) $t_{fpf}$ (b) $t_{cbl}$

(c) $t_{ftg}$ (d) $D_{ftg}$

Figure 5.17: Results of simulation time convergence study

### Findings and Limitations

An overview of the best simulation parameter choices resulting from the convergence study is given in Table 5.13. It is important to note that while these parameter values work excellent for this specific

environmental scenario (see Table 5.10), they may not in other scenarios. For example, the following scenario changes can have influence on the desired simulation parameter values:

- An increase in wave length an wave height may require an extended time-domain simulation length to be able to capture enough physical effects and convergence of the fatigue damage results.
- A decrease in water depth can result in smaller bend radii on the cable. In order to be able to accurately model the curvature of the cable a smaller $CSL$ value may be required.

To get a better idea of the dependency of the simulation parameters on the environmental conditions, it would be beneficial to conduct a more elaborate convergence study. Several environmental load cases could be formulated, in which only one environmental parameter is changed to discover its influence on the simulation parameter values.

| Parameter | Selected value | Unit |
|---|---|---|
| $t_{step}$ | 0.2 | s |
| $CSL$ | 2 | m |
| $t_{build}$ | 240 | s |
| $t_{sim}$ | 2400 | s |

Table 5.13: Best simulation parameter selection

## 5.4. Parametric Sensitivity Study

A sensitivity study is conducted to assess the influence of the model parameters on the behavior of the DPC configuration. The purpose of this study is to identify the ranges within which each parameter delivers the best results and to make an assessment of which parameters are most suitable to use as decision variables for the optimization algorithm. Due to the limitations imposed by the scope of this research, the structural cable parameters (e.g. bending stiffness) will not be taken into consideration during this study. The assumption is made that these parameters are provided by a cable manufacturer and are not independent from each other. In similar fashion, the structural parameters for the auxiliary components are left unchanged too. The environmental parameters are not included in this study either, because in reality they cannot be influenced. This leaves the following parameters to be included in the parametric sensitivity study:

- Length of the first dynamic cable section $L_1$
- Length of the buoyant cable section $L_2$
- Length of the second dynamic cable section $L_3$
- Length of the static cable section $L_{ST}$
- Horizontal distance to the termination point $x_{TP}$
- Number of buoyancy modules $n_{BM}$
- Buoyancy module spacing $d_{BM}$

Herein, $L_1$ includes the length of the BS $L_{BS}$, which is fixed. $L_2$ defined by $n_{BM}$ and $d_{BM}$ as:

$$L_2 = (n_{BM} - 1)d_{BM} \tag{5.23}$$

Therefore, rather than investigating $L_2$, both $n_{BM}$ and $d_{BM}$ are considered as variables and are taken into consideration in this study.

Since $L_3$ and $L_{ST}$ are interdependent, for this sensitivity study the total length $L$ will be used as a variable in stead. This independent variable $L$ is then defined as:

$$L = L_1 + L_2 + L_3 + L_{ST} \tag{5.24}$$

By defining the cable length variables as above, in combination with parameter $x_{TP}$, a large number of different LWS configuration can be created. The remainder of this section presents the setup of the parametric sensitivity study and the results. The independent global model variables are shown in Figure 5.18.

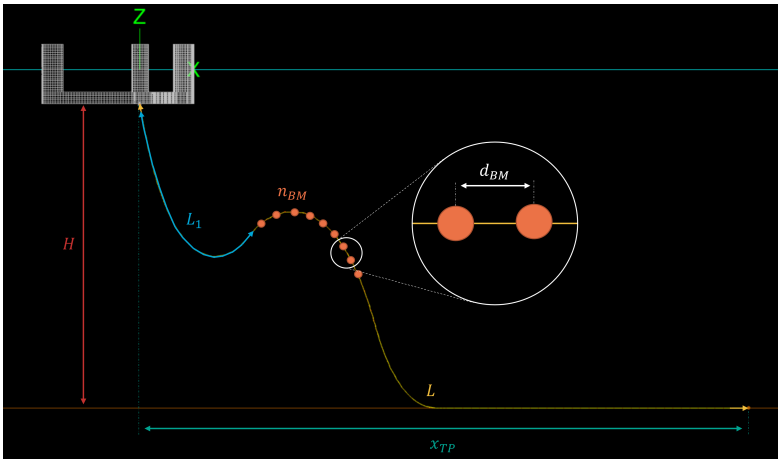


Figure 5.18: Independent global model parameters

### 5.4.1. Setup

The test scenario as described in Section 5.3.1 is used again for the parametric sensitivity study. An overview of the variable parameters is given in Table 5.14. The test values here are chosen based on intuition of the author and recommendations from previous research (e.g. [19]). Each parameter also has been assigned a base value, which remains constant during experiments in which the influence of another parameter is tested.

| Parameter | Test values | Base value | Unit |
|---|---|---|---|
| $L_1$ | [50, 75, 100, 125, 150, 175, 200, 225, 250] | 125 | m |
| $d_{BM}$ | [2, 4, 6, 8, 10] | 6 | m |
| $n_{BM}$ | [5, 10, 20, 30, 40] | 20 | - |
| $L$ | [405, 450, 495, 540, 585] | 504 | m |
| $x_{TP}$ | [270, 315, 360, 405, 450] | 360 | m |

Table 5.14: Parametric sensitivity study setup

### 5.4.2. Results

The performance of the configuration is rated by assessing the ultimate and fatigue loads. Even though the objective of this research is to minimise the fatigue damage in the DPC, the axial and bending loads on the cable must also stay within the operational limits that are specified by the cable manufacturer. Seeing as over tensioning of the DPC in the LWS configuration is highly unlikely, the following two simulation outcomes are of interest:

- Annual fatigue damage $D_{ftg}$
- Normalised curvature $C_N$

Now, the results of the sensitivity study for each variable are presented and discussed. The following results are shown in graphs and figures:

- *Bar graphs with maximum annual fatigue damage and maximum normalised curvature:* These results show the absolutes of both relevant simulation outputs at their respective most critical locations along the length of the cable.
- *Maximum annual fatigue and normalised curvature plots:* These figures show the magnitude of fatigue and maximum curvature that occurs at each point along the length of the cable. This serves to identify the critical locations and to see the influence of curvature on fatigue damage.

- *Figures from the OrcaFlex:* These figures support the explanations that are given about the structural response of the cable (e.g. what causes high fatigue damage for a certain configuration).

**Length of the First Dynamic Cable Section**

The outcome of the parametric sensitivity study for $L_1$ is shown in Figure 5.19. It appears that as the value for $L_1$ becomes larger, $D_{ftg}$ increases while $C_N$ decreases. Hence, a trade-off must be made. This effect can be explained when looking at the shape of two configurations in Figure 5.21. Shape (A) has a small $L_1$, which causes larger curvatures in the sag bend and the hog bend of the cable. For an even smaller $L_1$ this effect even causes over bending to the point where excessive fatigue damage occurs at the hog bend and the near the HOP (see Figure 5.20). Configuration (B) shows much less curvature overall, however the fatigue damage at the HOP is increased due to the longer length of free-hanging cable, which means the buoyancy modules can not dampen the motions near the HOP as effectively. Considering that fatigue resistance is the predominant performance indicator in this research, the best performing configurations for this particular environmental scenario are expected to have $L_1$ values ranging from 75 m to 125 m.

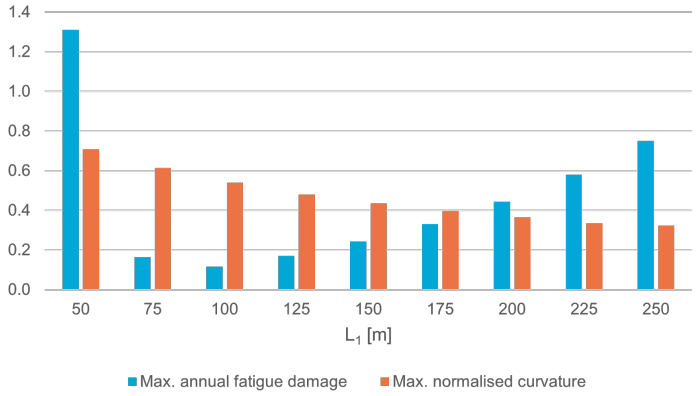


Figure 5.19: $L_1$ sensitivity study results


(a) $D_{ftg}$ (b) $C_N$

Figure 5.20: Annual fatigue damage and normalized curvature along length of the cable for different $L_1$ values

(a) $L_1$ = 75 m (b) $L_1$ = 200 m

Figure 5.21: Configurations for $L_1$ = 75m and $L_1$ = 200m

### Buoyancy Module Spacing

When evaluating the results of the $d_{BM}$ sensitivity study in Figure 5.22, it becomes evident that a $d_{BM}$ value between 4 m and 8 m gives the best performance. Figure 5.23 shows the maximum annual fatigue damage and maximum normalised curvature along the entire cable length for the different $d_{BM}$ values. Here can be seen that the buoyant cable section is exceptionally susceptible to fatigue damage for large values of $d_{BM}$. This is caused by curvature fluctuations between the BMs. The cable's bending stiffness is not great enough to span the large distance between the BMs, causing sagging and cyclic motions. This phenomenon is captured in Figure 5.24a. DPCs with very short BM spacing suffer from high curvature and fatigue at the hog bend, due to a high concentration of buoyancy force pulling the cable upwards and causing a sharp bend, as shown in Figure 5.24b.

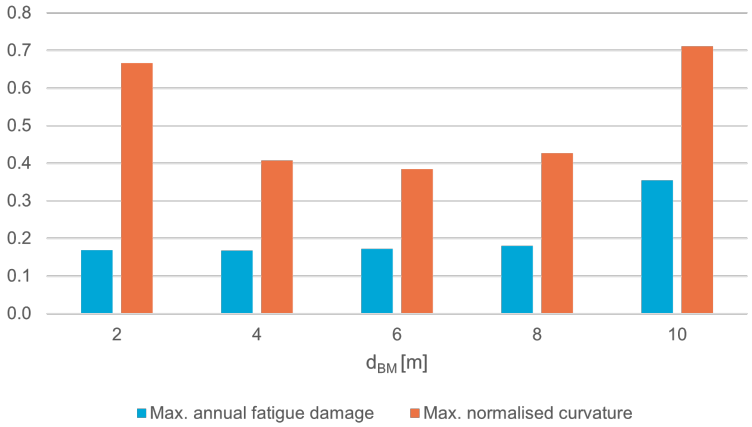


Figure 5.22: $d_{BM}$ sensitivity study results

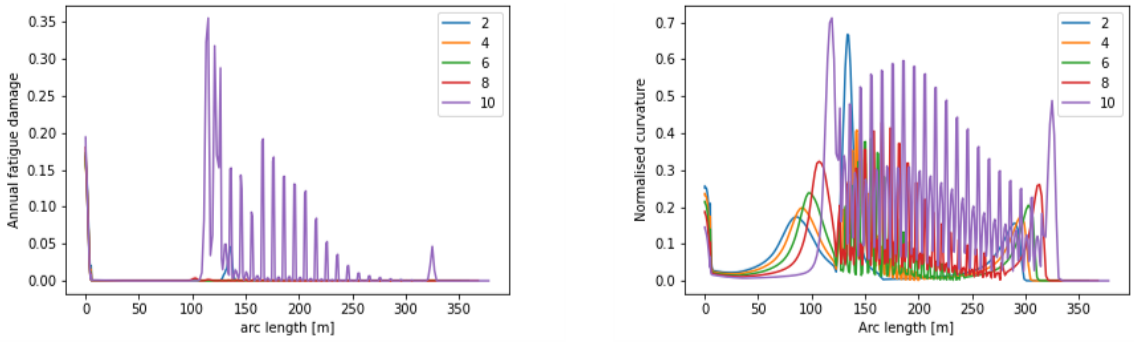


(a) $D_{ftg}$ (b) $C_N$

Figure 5.23: Annual fatigue damage and normalized curvature along length of the cable for different $d_{BM}$ values

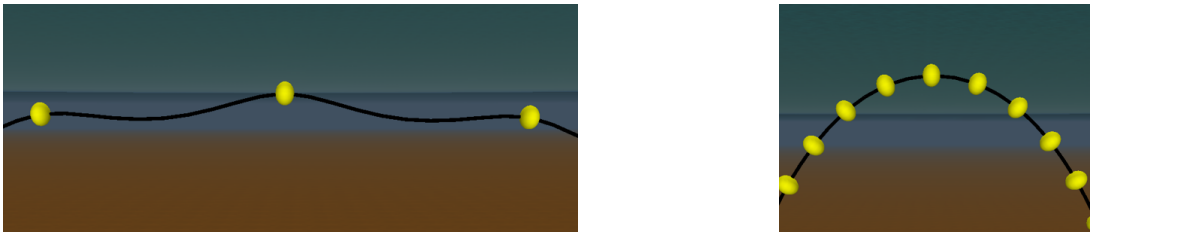

(a) Sagging of the DPC between the BMs (b) Large curvature at hog bend due to concentration of BMs

Figure 5.24: Shape of the buoyant cable section for small and large $d_{BM}$ values

### Number of Buoyancy Modules

Similarly to the parameter $d_{BM}$, $n_{BM}$ influences the length of the buoyancy section. The results of the parametric sensitivity study for $n_{BM}$ reveal that the configurations with 20 and 30 BMs outperform the variant with 10 BMs. For an even lower number of BMs major fatigue damage issues start to arise, which according to Figure 5.26a occur near the TDP. The explanation for this poor performance is found in Figure 5.27a. It shows that the amount of buoyant force generated by only 5 BMs is not strong enough to create an effective LWS. The water depth is far too great for a catenary-like configuration and therefore excessive stresses occur near the TDP, as well as increased fatigue damage at the HOP. For configurations with more than 40 BM other problems arise, namely that too much buoyancy force is generated and the cable rises to the surface. This situation is shown in Figure 5.27b. Surfacing of the cable causes errors in the OrcaFlex simulations, which is why no results are available for $n_{BM}$ = 40.

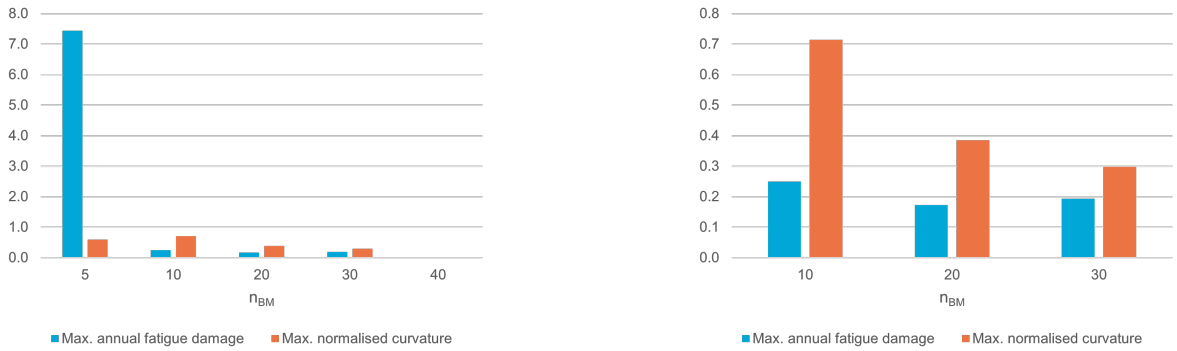


(a) All test values

(b) Zoomed in on feasible results

Figure 5.25: $n_{BM}$ sensitivity study results

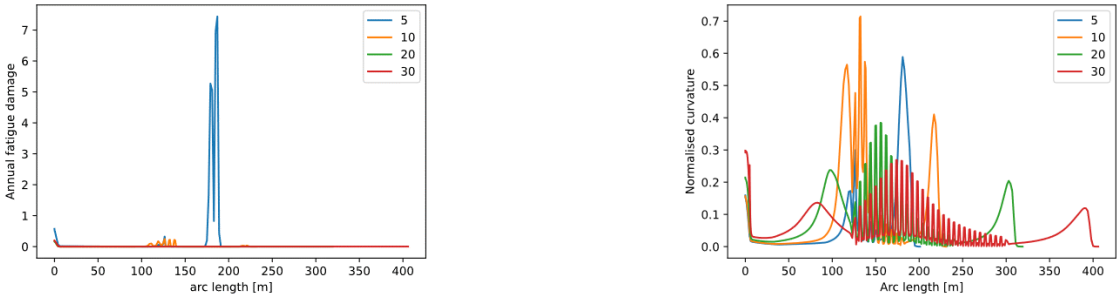


(a) $D_{ftg}$

(b) $C_N$

Figure 5.26: Annual fatigue damage and normalized curvature along length of the cable for different $d_{BM}$ values

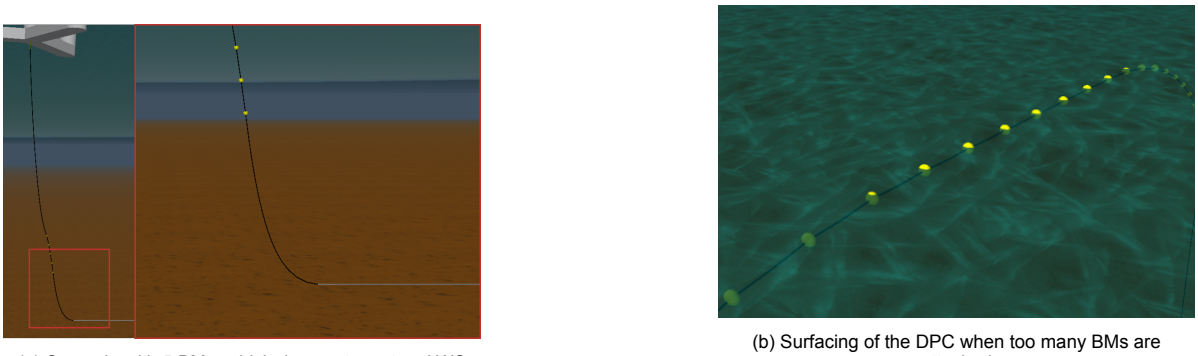

(a) Scenario with 5 BMs, which does not create a LWS

(b) Surfacing of the DPC when too many BMs are attached

Figure 5.27: Result of attaching too few or too many BMs to the cable

### Total Length

The maximum annual fatigue damage and maximum normalised curvature results from the parametric sensitivity study for the total cable length are shown in Figure 5.28. It is clear that short cable lengths perform poorly with regards to fatigue resistance. Figure 5.29a displays a giant peak in fatigue damage near the HOP. This happens because the cable length is too short when compared to the horizontal distance to the cable termination point. The cable is stretched out between its HOP and TDP, which causes large stresses and therefore fatigue at the HOP. This shape is shown in Figure 5.30a. For longer cable lengths, the fatigue damage results are much better, but the curvature increases at the sag bend, hog bend and TDP (see Figure 5.29b. At some point, the opposite happens to the short $L$ scenario, namely that the cable essentially becomes too long. Figure 5.30b reveals that a large part of the cable rests on the seabed while the remaining part experiences large curvatures. The most ideal total cable length values for this particular environmental scenario appear to be 495 m and 540 m.

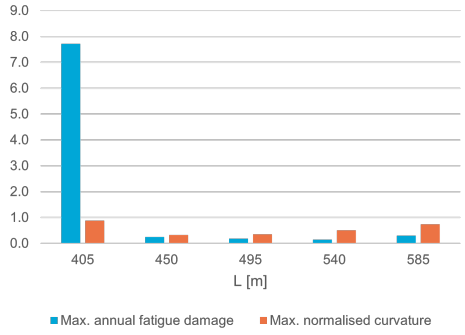


(a) All test values

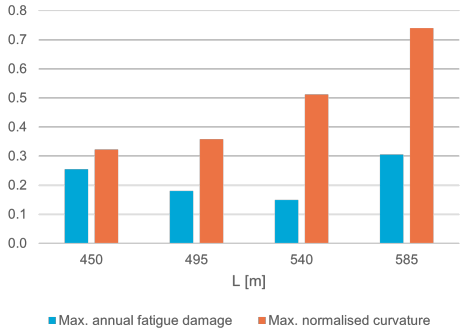


(b) Zoomed in on feasible results

Figure 5.28: $L$ sensitivity study results

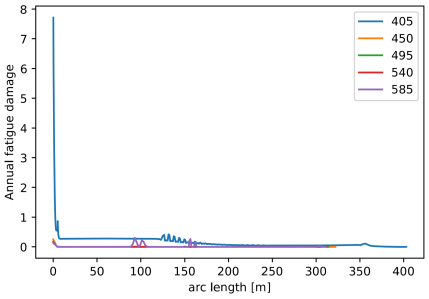


(a) $D_{ftg}$

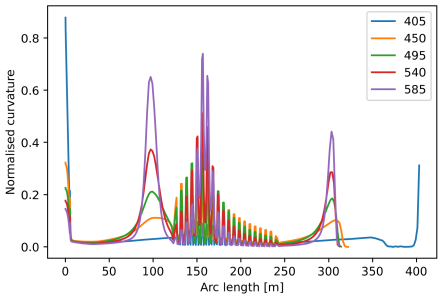


(b) $C_N$

Figure 5.29: Annual fatigue damage and normalized curvature along length of the cable for different $L$ values

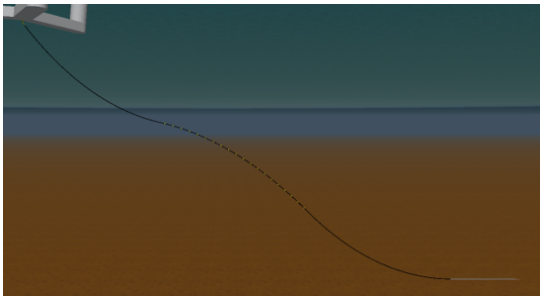

(a) $L$ = 405 m

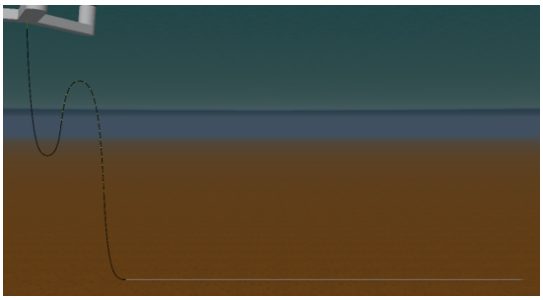

(b) $L$ = 585 m

Figure 5.30: Configurations for $L$ = 405 m and $L$ = 585 m

### Horizontal Distance to the Termination Point

To an extent, the $x_{TP}$ sensitivity study produces results that are similar to those from the $L$ sensitivity study. From Figure 5.31 the conclusion can be drawn that the performance of the configuration suffers for very large values of $x_{TP}$ and that the results improve for smaller values up until the point that the relative total cable length becomes too great and curvature peaks become excessive at the sag bend, hog bend and TDP of the cable. Figures 5.32 and 5.33 show the performance along the length of the cable and the most extreme configurations respectively. When comparing the results of the $L$ and $x_{TP}$ studies, the suspicion arises that good performance of the configuration relies on careful choice of the ratio between $L$ and $x_{TP}$.

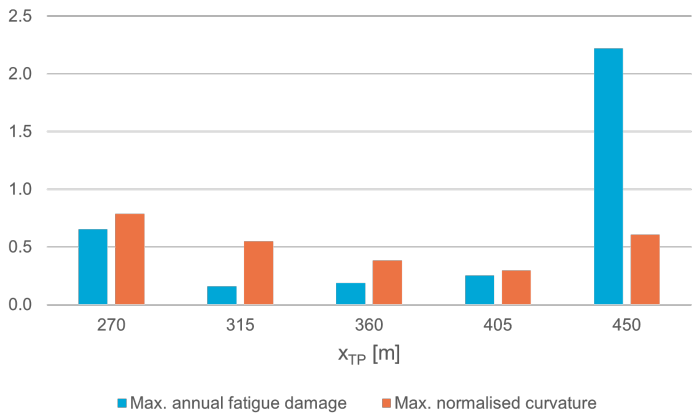


Figure 5.31: $x_{TP}$ sensitivity study results

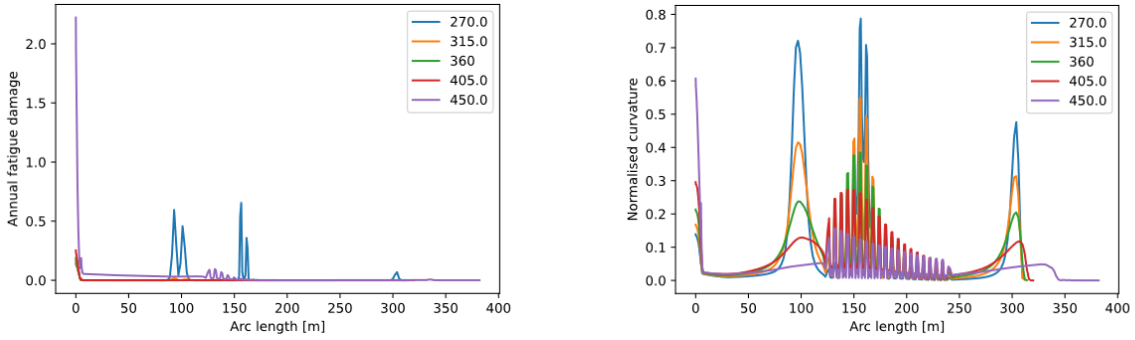


(a) $D_{ftg}$ (b) $C_N$

Figure 5.32: Annual fatigue damage and normalized curvature along length of the cable for different $x_{TP}$ values

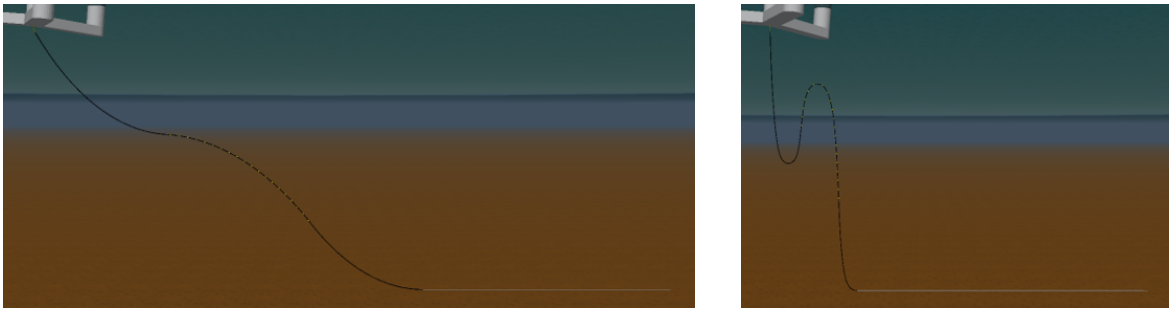

(a) $x_{TP}$ = 450 m (b) $x_{TP}$ = 275 m

Figure 5.33: Configurations for $x_{TP}$ = 275 m and $x_{TP}$ = 450 m

## 5.5. Conclusion

The global decoupled modelling of a DPC can be done with three individual parametric models. First, the motions of the floating platform system, consisting of a FOWT, semi-submersible platform and mooring lines, are calculated. Appropriate environmental conditions are used as input parameters for the floating platform model. The 6DoF motion time history output of the floater model is then used as an input for the global DPC model. The cable model requires accurate modelling of the DPC and the auxiliary components that are necessary to create a LWS configuration, by carefully selecting the parameters that define each component. Here, the DPC is represented as a lumped mass model, from which the motions and loads on the cable are calculated. After completing the structural analysis, fatigue analysis can be performed. The global load and motion time histories are converted into stresses on the copper conductor of the DPC using tension and curvature stress factors. The resulting stress cycles are counted with rainflow counting, after which the total accumulated fatigue damage is calculated as the sum of all individual damage contributions. In the case of high-cycle fatigue, a S-N curve is an appropriate tool to model the copper conductor's fatigue properties and to calculate the damage contribution of each stress amplitude.

In order to verify that the modelling decisions are correct, a number of verification tests can be conducted. This involves comparing analytically derived results of a test scenario to the numerical results from the equivalent OrcaFlex model. In each test case, the errors between the theoretical and OrcaFlex results were negligible, indicating correct implementation of the modelling aspects in OrcaFlex and correct interpretations of the loads that act on a DPC.

When performing numerical simulations, it is important to carefully choose the simulation parameters. Incorrect values can lead to numerical instability, inaccurate results or computational inefficiency. A convergence study can help to select appropriate parameter values. During this study, each parameter is tested for different values, while the other parameters remain fixed. The performance of the simulation is indicated as a combination of computational costs and accuracy of the results. The results are considered sufficiently accurate once they converge towards a steady value.

Before using the numerical DPC model in any kind optimization algorithm, the relevant decision variables must be identified. The performance of the DPC configuration for different model parameter values can be tested through a carefully formulated parametric sensitivity study. The purpose of this study is to assess the influence that the individual parameters have on the behaviour of the system and define ranges within which each parameter gives the best results. The findings can be used to make an educated decision on the choice of decision variables for the optimization and their upper and lower bounds. In the case of this research, the sensitivity study has also helped to eliminate potential decision variables and thus reduce the dimensionality and complexity of the problem.

Analysis of the sensitivity study results reveals that for this particular DPC model, it is possible to reduce the dimensionality of the problem without suffering noteworthy limitations. Varying the spacing of the BMs has little to no influence on the fatigue behaviour, so this variable can be fixed. Additionally, there is an interdependence between the total cable length and the horizontal distance to the termination point, so one can be expressed in terms of the other. This results in a total number of three decision variables.

# 6

# Optimization Algorithm

This chapter explains the development of a parametric optimization model for the optimization of the DPC configuration. As mentioned earlier in Section 4 of this report, the analysis of complex DPC systems involves blackbox simulation models, which is why a BBO method must be used for the optimization. The results of Section 5.3 reveal that the time-domain dynamic simulations are computationally expensive. It is therefore desirable to select an optimization method that requires a small number of function evaluations, in order to be able to obain results within reasonable time. On top of that, the research objective also specifies the development of a methodology that allows for the application of various environmental scenarios. The sub-question *"How can parametric optimization be performed on the DPC configuration?"* is answered by first describing the workings of the optimization algorithm and explaining the modelling decisions that were made. The selected modelling aspects are then verified to assure that they function correctly.

## 6.1. Description

The optimal DPC configuration is calculated using the simulation models as described in Section 5.1 in conjunction with a BBO method. Based on the research on available BBO methods that was presented in Section 4.1, the decision is made to use a model based optimization method. Model-based optimization or SMO tends to be more efficient than direct search and heuristic optimization, which is important when working with computationally expensive simulations. The basic structure of the SMO algorithm is as follows:

1. *Design of Experiment:* Create samples to obtain training data
2. *Surrogate modelling:* Fit an appropriate surrogate model to the training data
3. *Solving the optimization problem:* Select and evaluate candidate solutions until the optimum is reached

This optimization structure is integrated into the cable analysis models as shown in Figure 6.1. The remainder of this section first gives the mathematical formulation of the BBO problem. Thereafter, the three phases of the optimization algorithm as listed above are explained.

### 6.1.1. Mathematical Formulation

The general formulation of the BBO problem with $p$ constraints and $k$ decision variables is:

$$\begin{aligned} \min_{x} \quad & f(x) \\ \text{s.t.} \quad & c_i(x) \leq 0, \quad i = 1, ..., p \\ & x \in \mathbb{R}^k \end{aligned} \tag{6.1}$$

where vector $x$ represents the independent decision variables. The unknown objective function is represented by $f$, while $c$ denotes the constraints. The remainder of this section will explain how the objective, decision variables and constraints are defined.

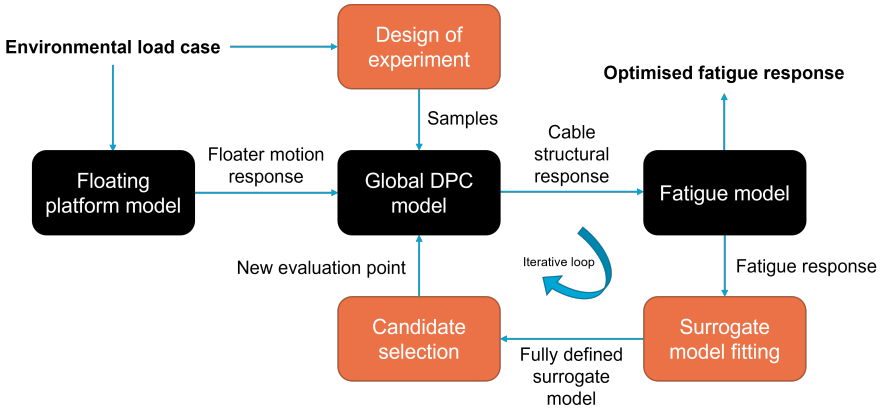


Figure 6.1: Optimization structure

**Objective Function**

Fatigue resistance is the most important design requirement of the DPC configuration is this research. When maximising, the performance indicator would be fatigue life of the DPC. However, this can be translated to a minimisation problem that seeks to minimize the inverse of fatigue life, namely the maximum annual fatigue damage. The objective function is then formulated as:

$$f(x) = D_{ftg} \tag{6.2}$$

**Decision Variables**

The decision variables are selected based on the parametric sensitivity study that was conducted in Section 5.4. This study investigated the influence that the global configuration parameters have on the dynamic and fatigue behaviour of the DPC. In order to filter out the irrelevant parameters and be able to more generally define the decision variables, the following modelling decisions are made:

- The BM spacing parameter $d_{BM}$ is fixed at $d_{BM} = 6$ m, which yielded the best overall performance. This parameter mainly seems to influence the dynamic behaviour locally within the buoyancy section, where large values cause accelerated fatigue due to curvature fluctuations between the BMs. Small values cause a concentration of buoyancy force at the hog bend, which leads to large curvatures in that area of the cable.
- The horizontal distance to the termination point $x_{TP}$ is fixed at $x_{TP} = 2H$. This value is chosen based on the results from Section 5.4 and supported by modelling decisions made in [19]. The decision to fix this variable simplifies the optimization problem, which is useful during the development phase of the model. A practical reasoning behind this might be that the location of the termination point is prescribed by the design of the FOWF (e.g. routing of the cables) rather than free to choose by the designers of the DPC configuration.
- The total cable length $L$ is chosen based on the horizontal distance to the cable's termination point $x_{TP}$ under the relationship $L = 1.5x_{TP}$. This relationship is established by calculating the length over horizontal distance ratio for the best performing value of $L$, yielding $L_{best}/x_{TP} = 540/360 = 1.5$. The inverse calculation for the best performing $x_{TP}$ value gives similar results, namely $L/x_{TP,best} = 504/315 = 1.6$. Note that, given the fixed value of $x_{TP}$, $L$ can also be expressed in terms of the HOP height as $L = 3H$.
- The other global configuration parameters, $L_1$ ans $n_{BM}$, are selected as independent decision variables for the optimization problem.

The above modelling decisions result in an optimization problem with a two-dimensional decision variable space. The mathematical formulation for the decision variables is:

$$x = \begin{bmatrix} x_1 \\ x_2 \end{bmatrix} = \begin{bmatrix} L_1 \\ n_{BM} \end{bmatrix} \tag{6.3}$$

**Constraints**
Several physical constraints are applied to the optimization model to assure that the DPC does not fail due to excessive loading or damage by its surroundings. The following constraints are defined:

1. The axial load on the DPC must remain below the Minimum Break Load (MBL) as specified by the cable manufacturer.
2. The bend radius on the DPC must remain above the Minimum Bend Radius (MBR) as specified by the cable manufacturer or the curvature on the DPC must remain below 1/MBR.
3. The DPC must not make contact with its surroundings (floater, water surface, sea bed) other than at the HOP and TDP. Therefore a minimum clearance between the sag bend and the seabed $d_{seabed}$ and the hog bend and the water surface $d_{surface}$ is defined.
4. Additionally, in order to prevent stress concentrations at the TP a minimum length of static cable section between the TDP and TP $d_{static}$ is required.

The mathematical formulation of the constraints is therefore:

$$c_1(x) \leq MBL \tag{6.4}$$

$$c_2(x) \leq \frac{1}{MBR} \tag{6.5}$$

$$-d_{surface} \leq g_{3,i}(x) \leq -D + d_{seabed} \quad \text{for} \quad i = 1, \ldots, N \tag{6.6}$$

$$c_4(x) \geq d_{static} \tag{6.7}$$

Where $c_1$ is the maximum axial load on the cable $T_{MAX}$, $c_2$ is the maximum curvature on the cable $\kappa_{MAX}$ and $c_{3,i}$ is the vertical location $z_i$ of each node $i$ that is part of either the sag or hog bend. $N$ stands for the total number of nodes on the sag and hog bends of the cables (these are most likely to make contact with the surroundings). The final constraint $c_4$ represents the length of the static cable section $L_{ST} = L - L_1 - L_2 - L_3$ (see Figure 5.3).

## 6.1.2. Design of Experiment

A well thought through DoE has good space-filling properties, no overlapping sample points and satisfies the constraints of the optimization problem. Given these requirements and based on the findings from Section 4.1.3, LHS seems like a suitable DoE method. An optimized LHS method in particular shows great promise for engineering design applications. That being said, true LHS can only be applied to box-constrained search spaces. It is possible to apply modified LHS to irregularly constrained spaces using the method developed by Petelet et al. [96]. However, when using this method the quality of the space-filling properties of the LHS design deteriorates [96], rendering this method inefficient and overly complex for the application to the problem at hand.

Due to the unknown nature of the dynamic cable model's behaviour, it is difficult to approximate the shape of the search space. A preliminary analysis of the search space is required to be able to define the boundaries of the search space and implement a suitable sampling method. This section describes how this analysis was carried out after which the sampling method is presented.

**Feasible Search Space Analysis**
The objective of the search space analysis is to identify the boundaries of a so-called 'feasible' search space. Samples that lie within the boundaries of the feasible search space will be feasible, meaning that they represent a configuration that does not break any of the constraints defined by Equations 6.4 through 6.7. Generation of infeasible samples is undesirable because of the following:

- The sample evaluations are computationally expensive. Generating infeasible samples, which cannot be effectively used for optimization purposes, is therefore a waste of time resources.
- Infeasible solutions do not yield a function value and therefore require special attention. A possibility is to assign them an artificial large function value, to prevent the optimizer from converging towards them, but this can cause a distorted perception of the model's response, especially towards the boundaries of the feasible search space.

To determine the boundaries of the feasible search space, a GS is performed on a two-dimensional box-constrained 'initial' search space. Due to the computational expense of time-domain dynamic simulations, only static analysis of each grid point is performed. This method can only guarantee satisfaction of the constraints partially, but reduces computational time significantly, therefore allowing to perform a GS with several hundreds of samples within minutes. The static solution does not provide an objective function values, but simply rejects samples that break any of the constraints. This GS is repeated for several water depths to be able to investigate the influence that the water depth has on the shape and size of the search space. The results for water depths $D$ = [100,150,200] m are shown in Figure 6.2.

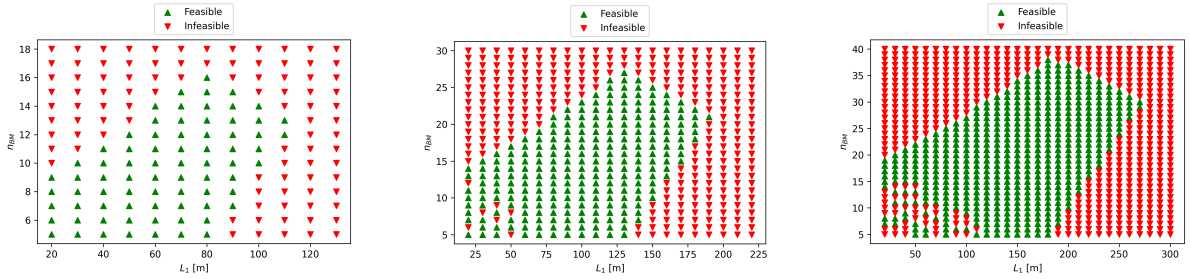


(a) $D = 100\ m$ (b) $D = 150\ m$ (c) $D = 200\ m$

Figure 6.2: Search space analysis results for different water depths.

The results from the static GS show that the feasible search space is certainly not box-constrained but rather a part of the initial search space constrained by linear boundaries. From these boundaries, inequality constraints for values of the decision variables can be formulated.

Analysis of the static GS results yields that the search space constraints can be defined as linear combinations of the water depth. The boundaries and vertices of the search space can be generalized as in Figure 6.3. The following constraints can be derived:

$$x_2 \geq A_2 + (x_1 - A_1)\frac{B_2 - A_2}{B_1 - A_1} \tag{6.8}$$

$$x_2 \leq C_2 + (x_1 - C_1)\frac{C_2 - B_2}{C_1 - B_1} \tag{6.9}$$

$$x_2 \leq D_2 + (x_1 - D_1)\frac{D_2 - C_2}{D_1 - C_1} \tag{6.10}$$

$$x_2 \geq D_2 + (x_1 - D_1)\frac{D_2 - A_2}{D_1 - A_1} \tag{6.11}$$

where $x$ is defined as in Equation 6.3 and the vertices are:

- $A = [D - 20, 5]$
- $B = [\frac{11}{7}D - \frac{320}{7}, \frac{6}{35}D - \frac{33}{7}]$
- $C = [D - 20, \frac{29}{140}D - \frac{39}{7}]$
- $D = [20, \frac{3}{35}D + \frac{8}{7}]$

Appendix C shows the derivation of the search space constraints.

With the above constraints, it is possible to quickly define the feasible search space for the optimization of a DPC for any reasonable water depth, without the need for a preliminary search space analysis. Note that these particular vertex values only hold for scenarios in which the the fixed parameters $d_{BM}$, $L$ and $x_{TP}$ have values as given in Section 6.1.1. If they are different, then the process of performing GS and static analysis for different water depths, based on which the vertex calculation can be performed, needs to be repeated.

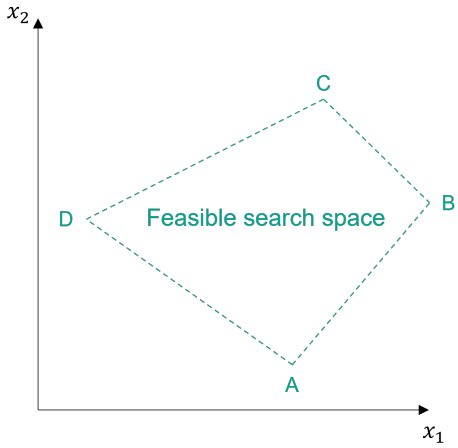


Figure 6.3: Generalized boundaries of the feasible search space

**Sampling**

Due to the particular shape of the feasible search space, LHS is not an ideal sampling method. Application of this DoE based on the findings of GS analysis would be possible but always compromised:

- In case of applying liberal box constraints (large search space that extends into infeasible territory), many infeasible solutions will be generated. In order to obtain enough feasible solutions, the number of samples needs to be increased significantly.

- In case of applying conservative box constraints (small search space that lies fully in the feasible region), the feasibility of the samples can be guaranteed. However, sections of the feasible search space are excluded from the sample space, therefore potentially missing out on the global optimum.

Regarding the apparent inability of LHS to meet the constraint-filling DoE requirement, a new method is developed for the generation of initial samples. This method is based upon defining search space constraints and performing random sampling with samples that must satisfy these constraints, i.e. all initial samples are feasible. The proposed DoE framework is as follows:

1. *Setup of the search space constraints:* This step can be executed by performing a GS of the initial box-constrained search space. However, if prior knowledge of the feasible search space's vertices is available, the constraints can be defined using Equations 6.8 through 6.11.

2. *Random sampling:* Random generation of samples within the feasible search space. While random sampling is not the most efficient sampling method, the assumption is made that it suffices for lower dimensionality problems.

3. *Test performance of DoE:* Since random sampling does not always fulfill the space-filling and non-collapsing requirements, the sampling is repeated until the initial samples are sufficiently well distributed and there are no duplicates. The distribution of samples is measured by setting a threshold to the minimum allowed euclidean distance between each sample, to prevent clustering. This approach also takes care of duplicates. The value for the threshold has to be chosen carefully. If it is too small the samples may be too clustered, while a too large threshold may be impossible to fulfill. A distance threshold based on the dimensions of the feasible search space and the number of samples is found to work sufficiently well across all water depths. It is formulated as:

$$\tau_d = \frac{3(B_1 - D_1)}{2(n-1)} \tag{6.12}$$

where $B_1$ and $D_1$ are the outer limits of the feasible search space in $x_1$ and $n$ is the number of initial samples.

### 6.1.3. Surrogate Modelling

SMO requires the selection of an appropriate interpolation method. RBF interpolation is the method of choice, due to its suitability for higher dimension nonlinear problems, good accuracy and robustness. This was previously explained in Section 4.1.3. This section describes the particularities that arise in the surrogate modelling phase of the proposed optimization method.

#### Surrogate Model Selection

The RBF model is fitted to the training data that was previously obtained in the DoE phase. In order get a good fit is is important to select the correct type of RBF, which are listed in Table 6.1. The RBFs are defined by the distance to the origin $r$ and a shape factor $\epsilon$. The choice of RBF type depends on the number of samples, the number of decision variables and on the shape of the (unknown) objective function. A good fit neither underfits nor overfits the training data. For simple models it is easy to tune the RBF settings an achieve an accurate RBF model without overfitting. However, for higher dimensionality models with many samples it can be more of a challenge. The RBF modelling is implemented in Python using the Interpolation package by SciPy [97].

Examples of surrogate models that are fitted to single-variable training data are shown in Figure 6.4. For a good fit, the solid blue line of the surrogate model needs to coincide as closely as possible with the dashed black line, which represents the real model. Note that the function of the real model is not known in the BBO problem, so a visual check is not possible when assessing the accuracy of the surrogate fit to the dynamic cable model.

| RBF type | General formulation |
|---|---|
| Gaussian | $e^{-(\epsilon r)^2}$ |
| Multiquadric | $\sqrt{1+(\epsilon r)^2}$ |
| Inverse multiquadric | $\frac{1}{\sqrt{1+(\epsilon r)^2}}$ |
| Linear | $r$ |
| Cubic | $r^3$ |
| Quintic | $r^5$ |
| Thin plate | $r^2 \ln r$ |

Table 6.1: RBF types and mathematical formulation

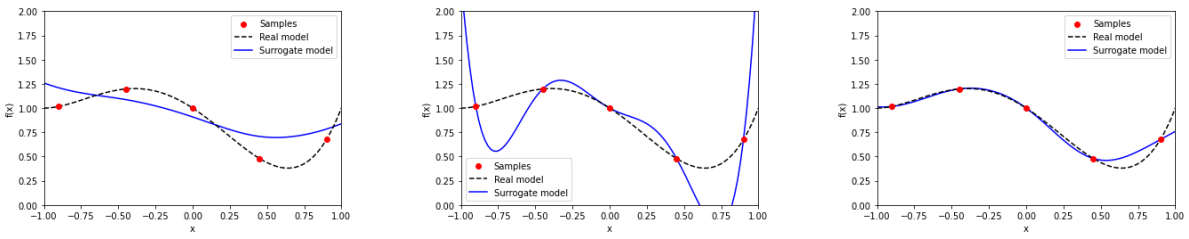


(a) Underfitted (b) Overfitted (c) Accurately fitted

Figure 6.4: Three surrogate model fits

#### Outlier handling

A problem that can occur when performing RBF interpolation is oscillations in the surrogate model. This effect is caused by large differences between function values [98]. The oscillations drastically reduce the accuracy of the surrogate fit and therefore make it difficult to find the true optimum of the function. A method to deal with high function values, from hereon referred to as 'outliers', is to modify their value to a value closer to that of the other data. This allows for a smoother surrogate fit, that is less susceptible to oscillations and false (local) optima. Similar to how outliers are treated in [99], a data point is a considered an outlier when its function value is larger than the median of all function values. Each outlier is then modified by assigning it this very same median value.

An example of how outliers are modified is shown in Figure 6.5. In this example, 10 arbitrary samples $(x, f(x))$ are generated. The median of this data happens to be 4.5, which is the function value that is assigned to the outliers.

The outlier handling step aims to improve the accuracy of the surrogate model near the global optimum of the optimization problem. Meanwhile, the overall accuracy is reduced, because 50% of the data (everything above the median) is modified to an artificial value. However, since the only real objective is to find the optimum, this is not considered a problem. Additionally, even though some high function values may be reduced to a much smaller value, the median value will still be considerably higher than the minimum. Therefore, poorly performing regions within the search space can still be clearly identified.

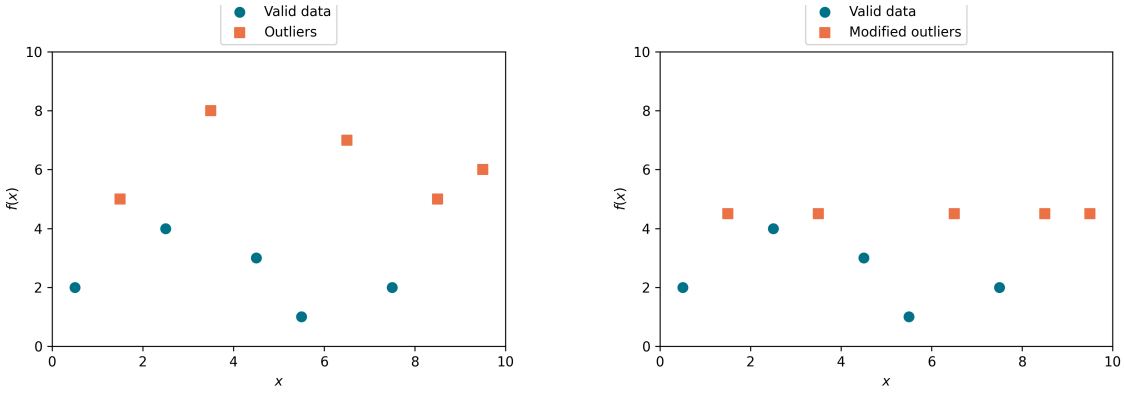


(a) Initial data

(b) Modified data

Figure 6.5: Outlier modification example

### 6.1.4. Optimization Problem Solving

After having fitted a surrogate model to the training data, the next step is to solve the optimization problem, i.e. find the optimal solution. Simply accepting the minimum value of the surrogate function as the optimal solution to the BBO problem is risky and does not guarantee a correct result. This is because the initial surrogate fit may not be accurate enough and the surrogate's optimum may therefore not be an accurate representation of the true optimum. It is therefore necessary to also investigate solutions that are not necessarily located at the surrogate's optimum, but which do give further insight on the shape of the real model. The following terms are defined:

- *Exploratory search*: Explore solutions that across the entire search space, far away from the existing data points. This procedure broadens the understanding of the real objective function and can possibly detect minima that were previously undetected due to inaccurate surrogate fitting.

- *Exploitative search*: Investigate solutions that are close to the surrogate optimum. If the surrogate fit is accurate, then it is likely that an optimal solution is found.

An effective search for the global optimum of the problem requires a dedicated searching algorithm. This algorithm iteratively selects candidate solutions and evaluates them until an optimum is found. For this task, an interpretation of the the Constrained Optimisation using Response Surfaces (CORS) algorithm [99] is used. This algorithm is suitable for the optimization of RBF surrogate models and can easily be integrated into the optimization framework as explained in the previous sections. CORS selects candidate points that are located at a minimum distance away from the previously evaluated points. The selected candidate is then evaluated and added to the training data. A new surrogate model is then fitted to the updated set of training data. This process is repeated for decreasing minimum distances at which the candidate points must be located, up until the whole search space is included in the search. Therefore, the algorithm starts by performing pure global search (exploratory search) and gradually moves towards pure local search (exploitative search). The iterative framework of CORS is shown in Figure 6.6.

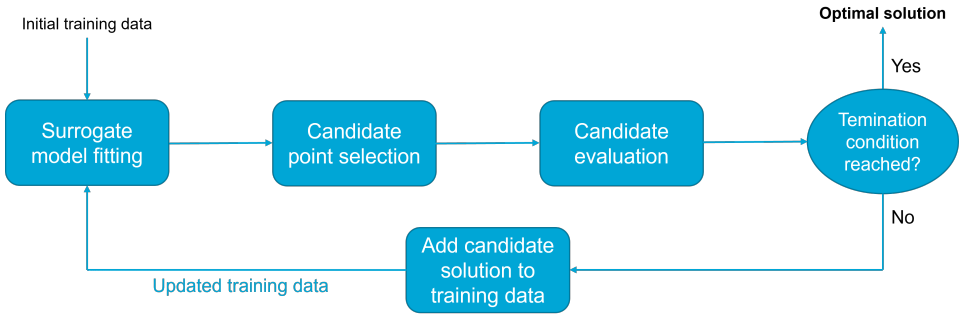


Figure 6.6: CORS framework

**Mathematical Formulation**

The iterative process of the CORS algorithm for an optimization problem with $n$ variables is formulated as follows:

1. *Surrogate fitting:* The surrogate model $\hat{f}_i$ is fitted to the set of training data $D_i = \{(x, f(x))$ for $x \in S_i\}$. Here $i$ is the current algorithm iteration, $S_i$ is the set of decision variable samples, and $f$ is the real model.

2. *Candidate selection:* The candidate selection step is the distinct feature of the CORS algorithm. The minimum distance between the existing data points and the candidate is governed by $\beta = \beta_1, ..., \beta_i$, where $0 \leq \beta_i \leq 1$. The new candidate point $x_{n+i}$ is then selected to be the point $x$ that solves the optimization problem:

$$\begin{aligned} \min \quad & \hat{f}_i(x) \\ \text{s.t.} \quad & ||x - x_j|| \geq \beta_i \Delta_i \quad \text{for} \quad j = 1, ..., n+i+1 \\ & x \in \mathcal{D} \end{aligned} \tag{6.13}$$

   where

$$\Delta_i = \max_{\tilde{x} \in \mathcal{D}} \min_{1 \leq j \leq n+i-1} ||\tilde{x} - x_j|| \tag{6.14}$$

   Herein $\mathcal{D}$ is the feasible decision variable space, as defined during the feasible search space analysis (Section 6.1.2).

3. *Candidate evaluation:* The next step is to evaluate the function $f$ for the new candidate $x_{n+i}$. After the simulation has finished, the values of $\hat{f}_i(x)$ and $f_i(x)$ are compared and an the relative error is calculated:

$$e_i = \frac{|\hat{f}_i(x) - f_i(x)|}{|f_i(x)|} \tag{6.15}$$

4. *Evaluate stopping criterion:* A stopping criterion is introduced to terminate the algorithm once a suspected optimum is reached. The algorithm terminates when the relative error between the surrogate and the real model [1] is smaller than a predefined error threshold:

$$e_i < \tau_e \tag{6.16}$$

   At this point, if the stopping criterion is reached, the algorithm is terminated and the final results can be reviewed. If this is not the case then candidate $x_{n+i}$ and its evaluated value $f_i(x)$ are added to the training data to form an updated training data set $D_{i+1}$. Subsequently, the algorithm returns to step 1 and a new iteration step is initialized.

[1] "Real model" refers to the blackbox DPC model, for which the algebraic form is unknown. However, for each candidate point the blackbox function is evaluated using a time-domain simulation in OrcaFlex. Therefore, the function values of the surrogate model and real model can be compared during each iteration of the algorithm.

## 6.2. Verification

This section verifies the modelling choices that were made to create the BBO method as described in Section 6.1. The following aspects are tested for performance and correct implementation:

- Definition of the feasible search space
- Outlier handling
- Optimization algorithm convergence

### 6.2.1. Feasible Search Space

From the feasible search space analysis in Section 6.1.2, a set of generalised constraints (Equations 6.8 through 6.11) was derived for the boundaries of the feasible search space. The performance of this approach is tested by taking a number of random samples around the boundaries of the feasible search space and evaluating how many of these samples actually yield a feasible solution. This procedure is conducted for different water depths, ranging from rather shallow to deep. A total of 40 samples is taken for depths $D$ = [60, 100, 140, 180, 200] m. The results of this verification step are presented in Table 6.2. The plotted results are shown in Appendix D.

Considering that all samples within the feasible search space are feasible, the overall performance of the feasible search space definition method is deemed satisfactory. While samples at the boundaries for shallow water depths have a higher probability of violating the constraints, the probability of this occurring is very small. If an infeasible sample were to arise, its influence on the performance of the algorithm could easily be minimized by assigning a dummy value and applying outlier modification, as explained in Section 6.1.3.

| $D$ | Pass | Fail | Succes rate |
|---|---|---|---|
| 60 m | 31 | 9 | 77.5% |
| 100 m | 35 | 5 | 87.5% |
| 140 m | 39 | 1 | 97.5% |
| 180 m | 37 | 3 | 92.5% |
| 220 m | 36 | 4 | 90.0% |

Table 6.2: Feasible search space verification results

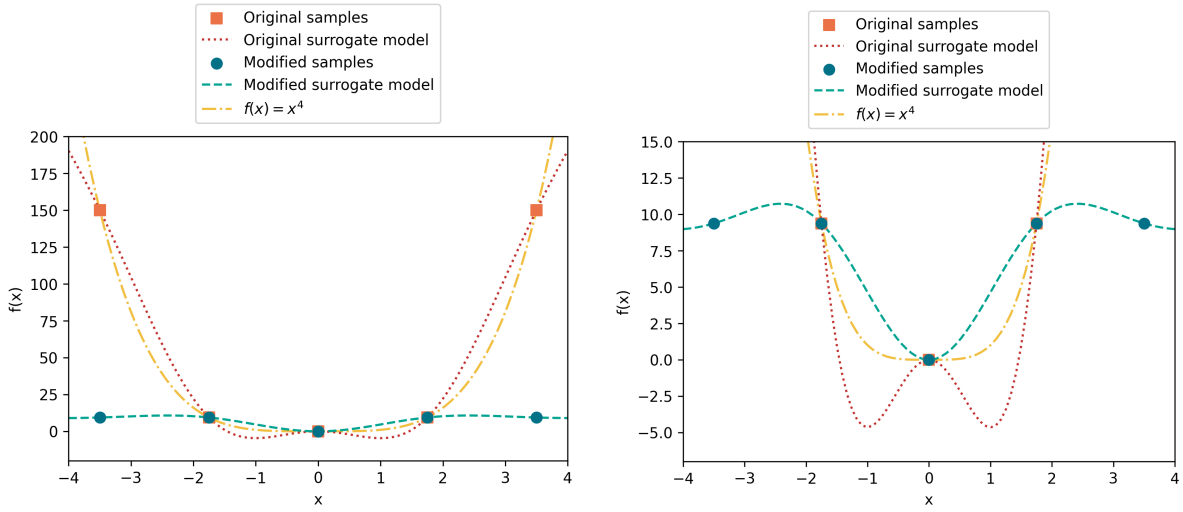


(a) Full overview

(b) Zoomed in on minimum

Figure 6.7: RBF model fit with and without modified outliers

### 6.2.2. Outlier Handling

The outlier handling step modifies the function value of samples that have a high function value or are infeasible. The objective here is to make it easier to fit an RBF model to the training data, and therefore be able to have a more accurate surrogate model. To test this feature, an attempt is made to fit a RBF model to a known function of the form $f(x) = x^4$, with and without modified outliers. This function has an optimum at $(x, f(x) = (0, 0)$, which given the simplicity of the function should be easy to locate with few samples.

The results in Figure 6.7 show that the accuracy of the surrogate model with modified outliers has indeed increased near the optimum. In fact, the non-modified example shows some of the earlier mentioned oscillations, causing two false minima to appear at $(x, f(x)) \approx (-1, -5), (1, -5)$. Therefore, without the outlier handling step, the optimum of the real function would be estimated incorrectly. Note that while after the application of outlier handling the fit of the surrogate model improves near the optimum, the accuracy vastly decreases in other regions of the search space. However, this is not a problem, because the algorithm's only objective is to find the optimum of the real function and not to produce an accurate representation of the entire search space.

### 6.2.3. Optimization Algorithm Convergence

The intricate optimization algorithm as presented in Section 6.1.4 is tested on a known function to be able to verify its performance. The performance is indicated by the convergence rate (i.e. the number of function evaluation required until an optimum is found) and the probability of convergence. This also provides the opportunity to test the problem with different values of the optimization parameters. Test cases are formulated with small and large numbers of initial samples, where $\beta$ dictates predominantly exploratory or exploitative search and with different RBF types. The following two $\beta$ sequences are used:

- $\beta_{exploitative}$ = [0.95, 0.75, 0.25, 0.05, 0.025, 0,...]
- $\beta_{exploratory}$ = [0.95, 0.9, 0.85, 0.75, 0.6, 0.4, 0.2, 0.1, 0.05, 0.025, 0,...]

The algorithm is terminated either if the error between surrogate and function evaluation reaches a value < 1% or if a maximum number of 15 iterations is reached.

A test function is formulated in the form $f(x) = (x_1^2 - 25)\cos x_1 + x_2^2$. This function is evaluated on the search domain $-2\pi \leq x_i \leq 2\pi$, on which it has a global minimum at $(x_1, x_2, f(x)) = (0.0, 0.0, -25)$ and a two local minima at $(x_1, x_2, f(x)) = (\pm 5.0, 0.0, 0.0)$. This function is non-convex, which means that the function contains various minima and maxima and contains local optima. This means that there is a risk that the optimizer converges to one of the local optima, rather than to the global optimum. The function also slopes steeply towards the edges of the search domain, which can cause extremely high function values, making the RBF interpolant susceptible to oscillations. A contour plot of the test function is shown in Figure 6.8.

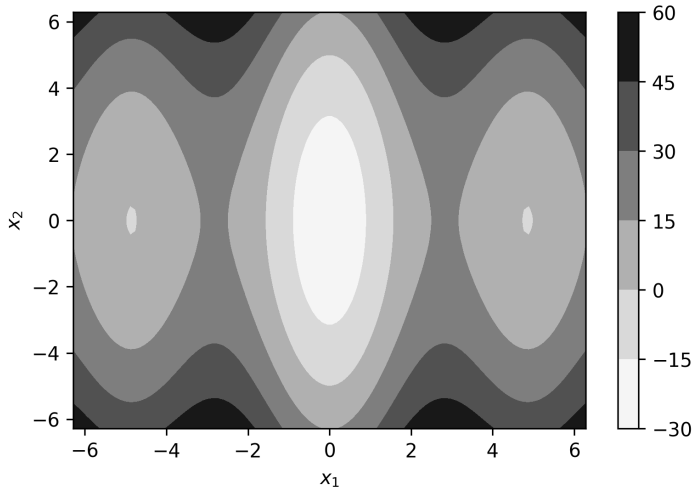


Figure 6.8: Contour plot of the test function

The proposed test function incorporates several local minima and areas with high function values. It therefore forms a suitable proving ground to test the ability of the algorithm to prevent convergence towards local optima and to handle outlier samples. The assumption is made that the actual blackbox function of the DPC model behaves similarly, in that there will be local minima and higher function values towards the boundaries of the search domain. However, to verify this, more knowledge about the response surface of the blackbox function is required. This can be obtained by performing a fine GS procedure across the entire feasible search space and fitting a surrogate model to the data. However, this step was left disregarded within this research due to time limitations.

**Results**

The algorithm was tested with 8 different settings for the optimization parameters. Each of the simulations was repeated 100 times. Table 6.3 shows the resulting performance of the algorithm. Two performance indicators are registered, namely the convergence rate (CR), which represents the average number of algorithm iterations that was performed until the stopping criterion was reached, and the convergence probability (CP), which shows in how many of the simulation runs the global optimum was found.

The results of this verification step show that it is crucial to select enough initial samples and use an appropriate parameter $\beta$ in order to achieve convergence towards the global optimum. With the correct settings, the proposed SMO algorithm shows good convergence properties, at least on this test function.

| # | $n$ | $\beta$ | RBF type | CR | CP |
|---|---|---|---|---|---|
| 1 | 10 | Exploitative | Multiquadric | 7.51 | 67% |
| 2 | 20 | Exploitative | Multiquadric | 5.49 | 83% |
| 3 | 10 | Exploratory | Multiquadric | 9.64 | 85% |
| 4 | 20 | Exploratory | Multiquadric | 8.10 | 91% |
| 5 | 10 | Exploitative | Gaussian | 7.59 | 74% |
| 6 | 20 | Exploitative | Gaussian | 5.46 | 80% |
| 7 | 10 | Exploratory | Gaussian | 9.45 | 89% |
| 8 | 20 | Exploratory | Gaussian | 8.18 | 96% |

Table 6.3: Algorithm performance on test function

**Further Remarks**

Selecting the optimization parameters based on the results from the experiments with a test function is somewhat risky. The propesed test function serves well to verify the outlier handling and iterative search strategy. Additionally, the results give insight into the influence of the optimization parameters on the performance of the algorithm and indicate that the algorithm works as intended. However, the blackbox objective function could look completely different, thus requiring different simulation parameters for maximum performance. The response surface may for instance be very flat, in which case the Gaussian RBF model, which emerges as a good interpolant for the test function, is unlikely to be efficient. A solution would be to formulate an arbitrary case study, perform a fine GS on it and fit a surrogate model to the data to achieve an algebraic approximation of the blackbox function. This can then be used as a test function to further fine tune the optimization parameters. However, this time-intensive procedure has not been conducted in this research.

## 6.3. Conclusion

Due to the computationally expensive simulations that are involved in the analysis of DPCs, it is important to use an optimization method that requires few function evaluations. Model-based optimization is a suitable method for the parametric optimization of the DPC configuration. The first step in formulating the optimization problem is defining the objective function, decision variables and constraints. When minimizing fatigue damage is the only objective, the constraints govern the ultimate loads on the cable. Additional distance constraints must be added to prevent that the DPC collides with its surroundings. In this research, the number of decision variable is limited to two, namely the length of the first dynamic section and the number of attached BMs. The goal of the optimizer is to find the values for these parameters for which the maximum annual fatigue damage on the DPC is minimized.

While applying LHS to generate initial samples is common practice, it is not an ideal solution for the optimization of the DPC configuration. The search space in which feasible samples can be generated is not box-shaped, which means that LHS would generate a large amount of infeasible samples. Therefore, there is need for a custom DoE method, which first performs a rudimentary analysis of the feasible search space and then defines the feasible search space boundaries as a function of the water depth. This makes the DoE method applicable to scenarios with different water depths. Finally, random sampling within the feasible search space is performed, until a sample set is achieved with a minimum euclidean distance requirement between each sample to prevent clustering.

A RBF surrogate modelling approach is used to construct surrogate models based on the sampled training data. Herein, it is important to select an appropriate RBF type, which neither underfits nor overfits the data and provides an accurate representation of the real model. The RBF is susceptible to oscillations if relatively high function values are part of the data set. To reduce the oscillations, an outlier handling step must be added, which modifies the value of the high function values and therefore limits their negative influence on the accuracy of the surrogate model. In this research, the outlier values are modified to the median value of the whole data set.

Even after elaborate sampling and surrogate modelling, the initial surrogate model is unlikely to be accurate enough to display the global minimum. An optimization solving strategy must be applied to find the true minimum of the blackbox function. The proposed method used an iterative approach to find the optimum to the optimization problem. During each iteration, a new candidate solution is selected and evaluated. The algorithm starts with exploratory search, only allowing new candidates to be selected far away from existing data points. With each next iteration, the minimum distance between the candidate and previous points is reduced until eventually the search is fully exploitative. The algorithm is terminated once the error between the surrogate model and the real function evaluation falls below a certain threshold. This optimization method prevents premature convergence towards a local optimum.

After defining the optimization problem and formulating the necessary operations to find the optimal solution, the proposed SMO method needs to be verified. Verification involves testing the individual modelling decisions that were made by subjecting them to artificial test problems. The feasible search space can be verified by taking random samples around the boundaries and determining is they yield valid function values. The outlier handling step can be subjected to a test function to test if it indeed prevents oscillations of the RBF interpolant and improves the fit around the optimum. Finally, the optimization strategy can be applied to a carefully selected test function to see if it finds the global and optimum and how many function evaluations are needed. This step can also serve to determine the values of the optimization parameters without needing to perform computationally expensive simulations.

# 7

# Model Validation

The proposed SMO method is validated by testing whether or not it meets its requirements. The following requirements are to be fulfilled:

- *Convergence:* The optimization algorithm must converge towards an optimum solution.
- *Robustness:* The optimization algorithm must perform well for a wide range of scenarios.
- *Efficiency:* An optimal solution must be found within acceptable time.

Additionally, the outcomes of the fatigue analysis are evaluated. From there, conclusions can be drawn about the properties of the fatigue optimized configurations and the quality of the fatigue calculations.

This section attempts to validate the proposed model by performing a number of experiments, gathering results and discussing the findings.

## 7.1. Experimentation

In order to test the performance of the optimization algorithm, two semi-fictional environmental case studies are formulated, which represent operation of a FOWT under varying conditions. The ability of the algorithm to solve optimization problems with vastly different input parameters proves its flexibility and robustness. The following experiments are carried out:

- *Tests of the SMO method:* Attempt to find the optimal solution for both case studies using the proposed RBF model-based optimization method.
- *GS:* Conduct a GS for both case studies to find a global optimum. The resulting optimum serves as a target optimum for comparison with the SMO results.
- *Analyse a reference configuration:* Calculate the fatigue performance of a reference DPC configuration and compare to the optimized configuration.

### 7.1.1. Environmental Conditions

Case study 1 represents a location with moderate sea state and water depth. This scenario is modelled after the location of the Hywind FOWF, which is located off Scotland's east coast. The Hywind FOWF is a 30 MW pilot project with 5 FOWTs, which are interconnected by a number of inter-array DPCs. The metocean data for the sea state is provided by a report by Statoil [100] (see Appendix E). Case study 2 places the FOWT system at a location with a larger water depth and harsher environmental conditions. The wave height, wave period and wind velocities are higher than in scenario 1, which causes higher loads and stresses on the DPC.

The environmental parameters for both case studies are presented in Table 7.1. The wave conditions are represented by a single JONSWAP wave spectrum (Equation 2.18), rather than a number of different load cases. This approach is taken to reduce the number of simulations that need to be performed. It is important that the correct spectral parameter values are chosen to get an accurate

JONSWAP representation of the wave data hindcast. Several studies ([101], [102]) have compared the JONSWAP spectrum to real-life measurements of wave data. Generally, the most accurate fit of the JONSWAP estimation compared to the observed spectrum was found for $\gamma \approx 1$, which corresponds with a Bretschneider spectrum. A peak enhancement factor value $\gamma = 1$ is therefore used to shape the wave spectra for the experiments. This value indicates operation under fetch-limited conditions [48]. This applies to the Hywind FOWF, which is located only about 5 km away from the coast.

For case study 1, $H_s$ and $T_p$ are selected as the mean of all sea states with an occurrence probability larger than 1% from the wave scatter table (Figure E.4). This covers 87% of all occurrences and excludes cases with low probability of occurrence, which are not expected to contribute to fatigue damage. The significant wave height resulting from this calculation corresponds with the data from Figure E.1. The surface current velocity $U_0$ and corresponding direction is taken from Figure E.3 and the current profile is calculated using Equation 2.21. Herein, current is considered to be generated by tidal movement only, which explains the offset between wind and current directions. Finally, the wind parameters are adopted from Figure E.2. The environmental conditions for case study 2 are defined by scaling up the wave and wind parameters from case study 1 to represent a rougher sea state, as defined in [103]. The tidal current remains the same.

| Parameter | Case study 1 | Case study 2 |
|---|---|---|
| $D$ | 120 m | 200 m |
| $H_s$ | 2 m | 4 m |
| $T_p$ | 8 s | 11 s |
| $U_0$ | 0.15 m/s | 0.15 m/s |
| $d_{cur}$ | 30° | 30° |
| $v_{wind}$ | 10 m/s | 14 m/s |
| $d_{wind}$ | 0° | 0° |

Table 7.1: Environmental parameters for both case studies

### 7.1.2. Optimization Model Settings

The parameter values for the numerical cable model and optimization algorithm are determined based on the knowledge gathered from the previously conducted studies and experiments in Sections 5 and 6.

**Simulation Parameters**

The optimal settings for the time-domain simulations were previously determined from the convergence study (Section 5.3). Consequently, the simulation settings for the experiments in Table 7.2 are based on the findings from the convergence study. The only change lies in the simulation time step $t_{step}$. The value had to be lowered due to numerical instability occurring during the floating platform simulations. The computational expense of the function evaluations is therefore higher than previously estimated.

Note that the simulation parameter values are constant across both environmental scenarios, as a result from the previously performed studies. While this approach is considered to be sufficiently well founded for this research, advances in accuracy of the fatigue calculations and computational efficiency can be achieved by selecting the parameter values based on the environmental conditions and global configuration parameters. An example could be to increase the $CSL$ for deeper water scenarios with longer cables.

| Parameter | Value |
|---|---|
| $t_{step}$ | 0.1 s |
| $CSL$ | 2 m |
| $t_{build}$ | 240 s |
| $t_{sim}$ | 2400 s |

Table 7.2: Simulation parameters for experimentation

**Global Model Parameters**

While $L_1$ and $n_{BM}$ were appointed as decision variables (see Section 6.1.1), the other global configuration parameters remain constant. Their values are based on the findings from the parametric study

in Section 5.4 and are presented in Table 7.3. Recall from Section 6.1.1 that the total cable length and the horizontal distance to the TP are dependent on the height of the HOP as $L = 3H$ and $x_{TP} = 2H$ respectively. The HOP height is taken as $H = D - 20$.

| Parameter | Case study 1 | Case study 2 |
|---|---|---|
| $H$ | 100 m | 180 m |
| $d_{BM}$ | 6 m | 6 m |
| $L$ | 300 m | 540 m |
| $x_{TP}$ | 200 m | 360 m |

Table 7.3: Global configuration parameters for both case studies

**Optimization Parameters**

The DPC configuration is optimized with the proposed method for DPC optimization, using the optimization parameter settings in Table 7.4. These settings are selected based on a refinement of the findings from Section 6.2.3. The number of initial samples is somewhat higher for case study 2, because the feasible search space for that scenario is significantly larger. A new $\beta$ is defined as $\beta = [0.95, 0.85, 0.75, 0.5, 0.3, 0.2, 0.1, 0, ...]$, which is a trade-off between the previously presented exploitative and exploratory variants of the parameter (see Section 6.2.3).

| Parameter | Case study 1 | Case study 2 |
|---|---|---|
| $n$ | 15 | 25 |
| RBF type | Gaussian | Gaussian |

Table 7.4: Optimization parameters for both case studies

## 7.1.3. Grid Search

A simple GS algorithm is applied to both case studies too. The GS algorithm requires a large number of function evaluations and is computationally expensive, which is why the mesh size of the grid is chosen relatively coarse. The settings for the GS are presented in Table 7.5. Herein, parameters $d_1$ and $d_2$ are the spacing between each sample point in $x_1$ and $x_2$ direction. The spacing is larger for case study 2, because of the larger feasible search space. The resulting sample spaces are shown in Figure 7.1.

| Parameter | Case study 1 | Case study 2 |
|---|---|---|
| $d_1$ | 10 m | 20 m |
| $d_2$ | 2 | 3 |

Table 7.5: GS parameters for both case studies

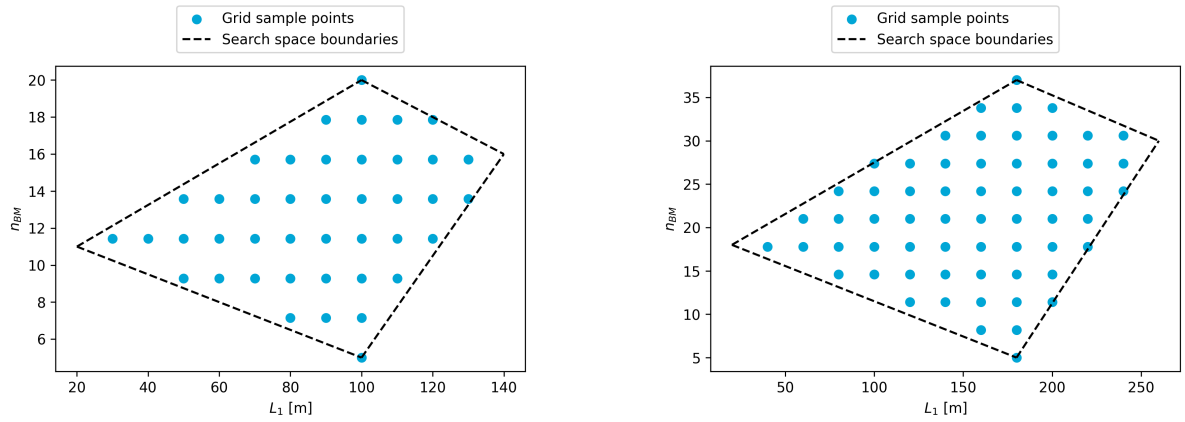


(a) Test case 1

(b) Test case 2

Figure 7.1: GS sample points

### 7.1.4. Reference DPC Configuration

For additional comparison, simulations of a reference DPC configuration are performed. The design of this configuration is according to a 1:1:2 ratio for the parameters $L_1$, $L_2$ and $L_3$ (including static section). Rentschler et al. [54] discovered this to be the best performing design across all water depths, in a static scenario. The conditions $x_{TP} = 2H$ and $L = 3H$ happen to apply to these scenarios too. The exact global configuration parameters for both test cases are listed in Table 7.6.

| Parameter | Case study 1 | Case study 2 |
|---|---|---|
| $H$ | 100 m | 180 m |
| $L_1$ | 75 m | 135 m |
| $n_{BM}$ | 14 | 24 |
| $d_{BM}$ | 6 m | 6 m |
| $L$ | 300 m | 540 m |
| $x_{TP}$ | 200 m | 360 m |

Table 7.6: Global configuration parameters of reference DPC configurations

## 7.2. Results

A total of 6 experiments was carried out to test the performance of the algorithm. Two of these were GS runs, one for each environmental case study. These experiments are denoted as ”GS-1” and ”GS-2”. Furthermore, four executions of the optimization algorithm were performed, two for each case study, which are referred to as ”SMO-1.1”, ”SMO-1.2”, ”SMO-2.1” and ”SMO-2.2”. This section gives an overview of the results from the GS and SMO computer experiments. The results are presented in graphs and tables and give a quantitative description of the performance of the optimization model. Some qualitative descriptions of the ongoing phenomena are given for additional support of the numerical results.

### 7.2.1. Optimization Algorithm Performance

The final results from the six experiments are shown in Table 7.7. This table presents the optimized annual fatigue damage $D_{ftg,opt}$ and life $l_{ftg,opt}$ [1]. Since the outcome of the GS is considered as a reference point for the global optimum, the error [2] between the best solution of each SMO experiment and the corresponding GS was calculated. This error is regarded as an indicator for convergence towards the global optimum. If it is very small or even negative (meaning that a better results was found than through the use of GS), then convergence was successful. The number of required function evaluations $n_f$ was also recorded for each experiment. This number serves as an indicator for efficiency. The percentile efficiency improvements are presented. Finally, the values of the decision variables that correspond to the optimal DPC configuration design are shown. Additionally, Figure 7.2 shows the location of these optimal solutions within the decision variable space.

| Experiment | $L_{1,opt}$ | $n_{BM,opt}$ | $D_{ftg,opt}$ | $l_{ftg,opt}$ | Error | $n_f$ | Time reduction |
|---|---|---|---|---|---|---|---|
| GS-1 | 110 m | 16 | 1.22e-5 | 8.23e5 years | - | 42 | - |
| SMO-1.1 | 108 m | 15 | 1.14e-5 | 8.76e5 years | -6.03e0% | 32 | 23.8% |
| SMO-1.2 | 115 m | 15 | 1.22e-5 | 8.17e5 years | 6.61e-1% | 30 | 28.6% |
| GS-2 | 100 m | 21 | 1.29e-2 | 7.74e1 years | - | 61 | - |
| SMO-2.1 | 99 m | 22 | 1.33e-2 | 7.52e1 years | 3.03e0% | 42 | 31.1% |
| SMO-2.2 | 114 m | 22 | 1.44e-2 | 6.95e1 years | 1.14e1% | 36 | 41.0% |

Table 7.7: Results of GS and SMO experiments

[1] Note that these are calculated fatigue damages/lives and NOT the design fatigue damages/lives. The latter requires the application of a safety factor.

[2] The error is calculated as $\text{Error} = \frac{\text{(SMO result)*(GS result)}}{\text{(GS result)}} * 100$

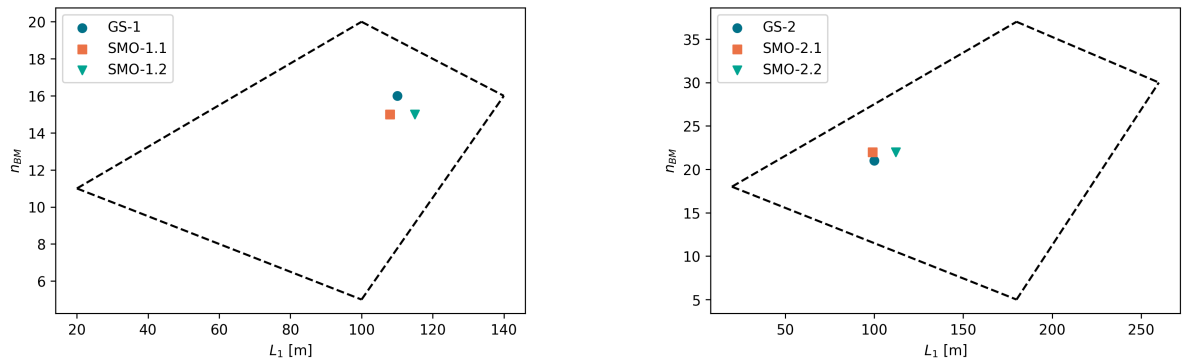


(a) Case study 1

(b) Case study 2

Figure 7.2: Optimal solutions for both case studies that were found through experimentation

### Convergence Properties

Table 7.8 shows the number of iterations that each optimization underwent until the stopping criterion was reached. The optimizer attempts to improve the best solution with each iteration, but does not always succeed. This is why the number of improvements over the course of the algorithm execution is registered as well. The iteration in which the best performing candidate solution was found is also of importance. In some instances, a good performing solution is found early on an no further improvements are discovered after that. The convergence behaviour of each SMO run is plotted in Figure 7.3. Here iteration 0 stands for the initial sampling step. The initial best solution is therefore the best performing sample from the initial sample set. Figure 7.4 shows the development of the best performing DPC shape for each experiment.

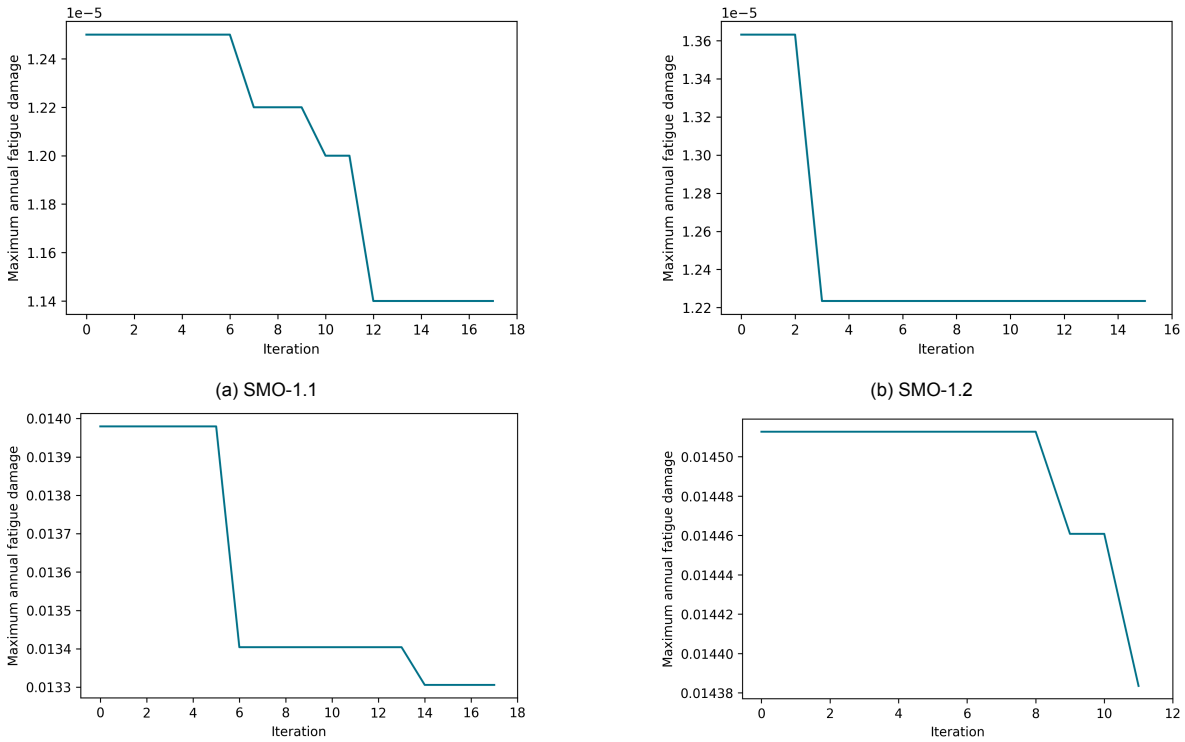


(a) SMO-1.1

(b) SMO-1.2

(c) SMO-2.1

(d) SMO-2.2

Figure 7.3: Best fatigue damage solution development for each SMO run

| Experiment | Iterations | Improvements | Best iteration |
|---|---|---|---|
| SMO 1.1 | 17 | 3 | 12 |
| SMO 1.2 | 15 | 1 | 3 |
| SMO 2.1 | 17 | 2 | 14 |
| SMO 2.2 | 11 | 2 | 11 |

Table 7.8: Convergence rate of the experiments

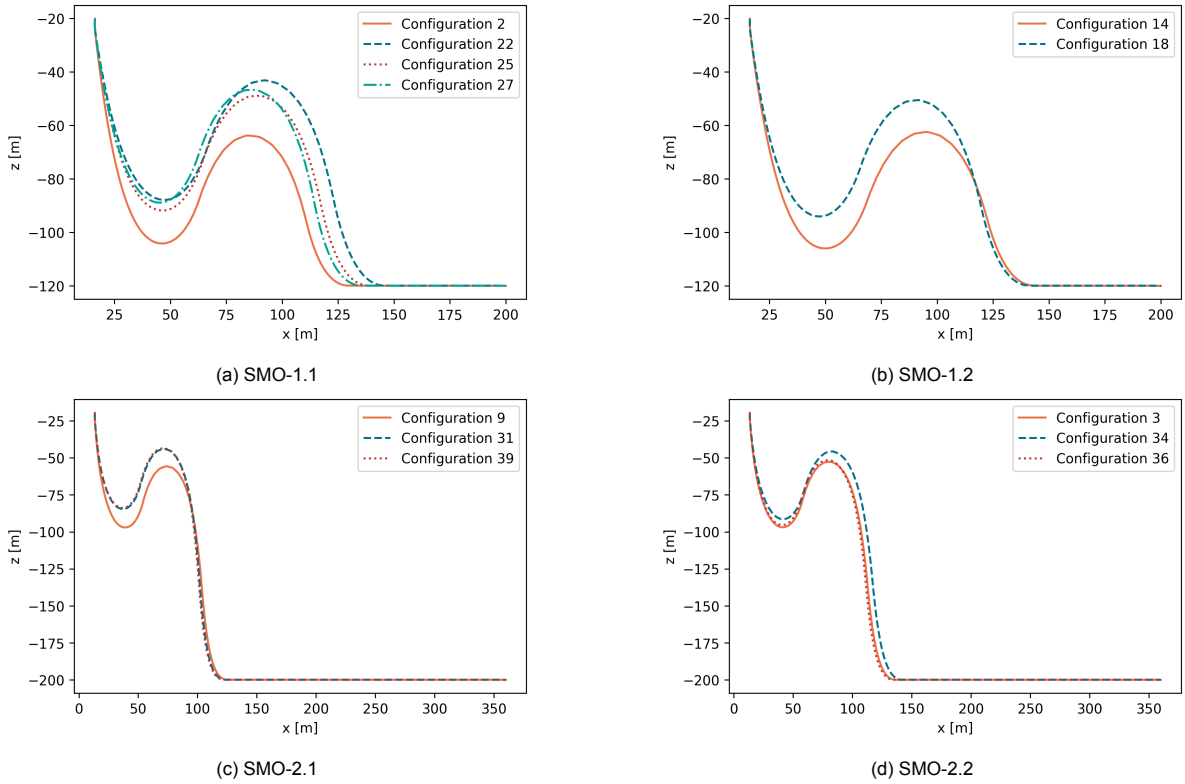


(a) SMO-1.1

(b) SMO-1.2

(c) SMO-2.1

(d) SMO-2.2

Figure 7.4: Best performing configurations for each SMO run

**Development of Surrogate and Function Evaluations**

Figure 7.5 displays how the evaluations of the surrogate model and real model develop over the course of the optimization algorithm runs. Plots of the error between surrogate and real function evaluation are added, along with the error threshold which acts as the stopping criterion for the optimizer. Naturally, the error is large during the early stages of the iterative process, when the surrogate fit is still poor due to lack of valuable training data. Eventually, as the surrogate fit improves, the error always reaches the threshold value of 1%. Note that in two instances, the scale of the axis displaying the evaluated function value is logarithmic, whilst on the others it is linear. This is because the logarithmic scale cannot display negative function values, which do occur for the surrogate evaluations of experiments SMO-1.1 and SMO-1.2.

**Surrogate Modelling and Candidate Selection**

Fragments the optimization sequence for optimization run SMO-1.1 are visualized in Figure 7.6. After initial sample selection, the iterative SMO process is started. During the first iterations, the candidate search space (indicated on the plots in green) is still very limited, as can be seen in the candidate selection step of iteration 2. The candidate here is selected nowhere near the current minimum of the surrogate model. This corresponds to exploratory search, as dictated by Equations 6.13 and 6.14. At iteration 4, the search space is already much less restricted, indicating a shift towards exploitative search. Looking at the contour plot at iteration 4, the new candidate is selected close to the optimum of the current surrogate model. During the final iteration of the algorithm, the candidate selection space

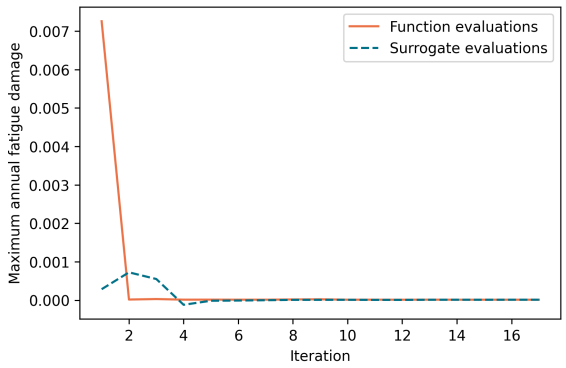


(a) Surrogate and function evaluations for SMO-1.1

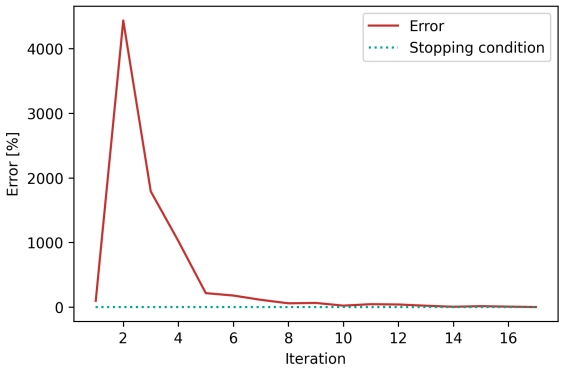


(b) Errors for SMO-1.1

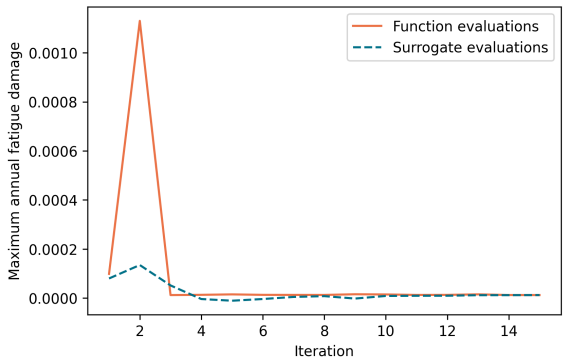


(c) Surrogate and function evaluations for SMO-1.2

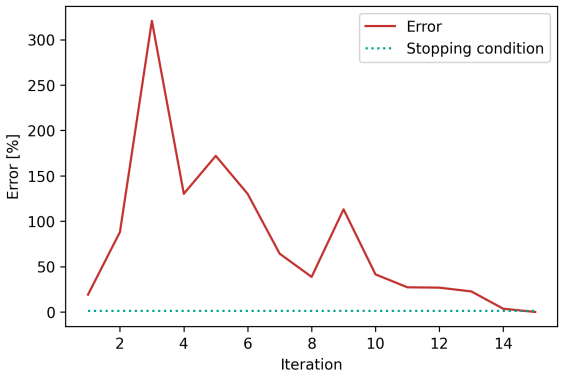


(d) Errors for SMO-1.2

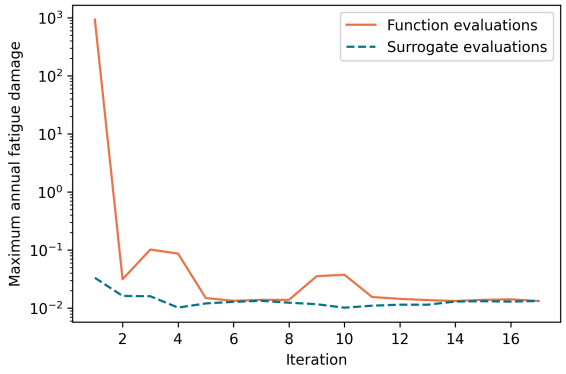


(e) Surrogate and function evaluations for SMO-2.1

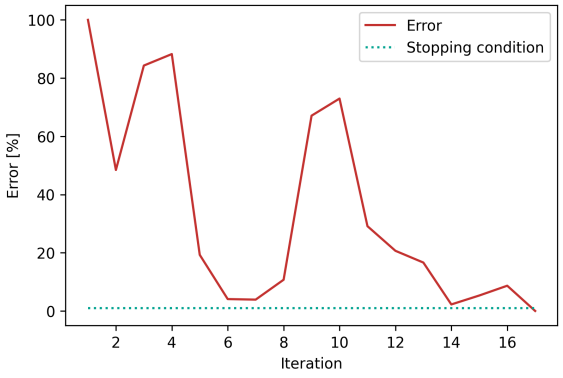


(f) Errors for SMO-2.1

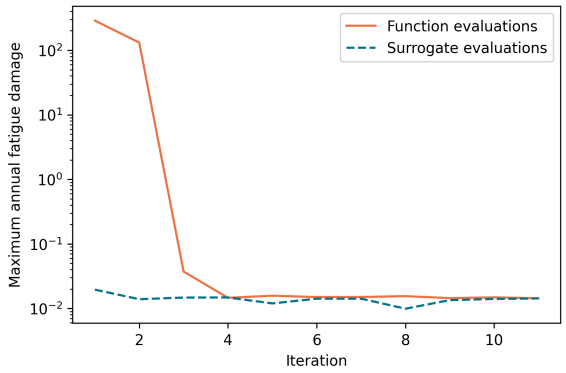


(g) Surrogate and function evaluations for SMO-2.2

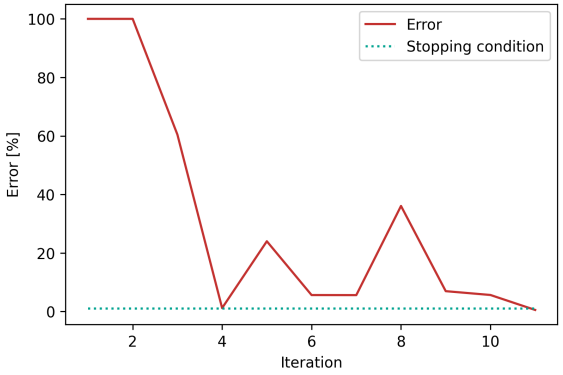


(h) Errors for SMO-2.2

Figure 7.5: Surrogate evaluations, function evaluations and associated errors for each SMO experiment

is completely unrestricted and many new data points have appeared in the vicinity of the suspected global optimum. At this point the search is fully exploitative. Note how the shape of the surrogate model has completely transformed from its earliest form and now shows a clear global optimum.

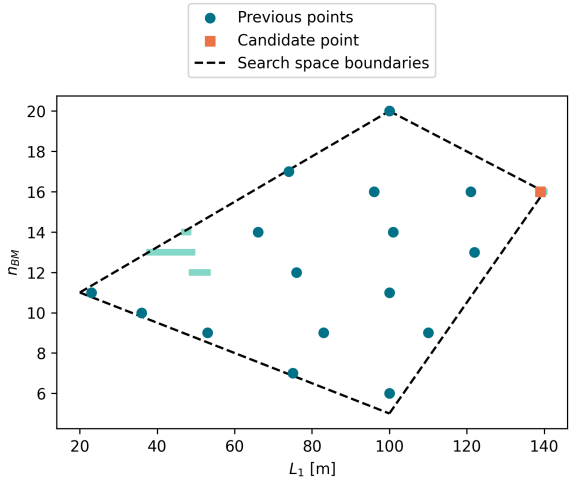


(a) Candidate selection space, iteration 2

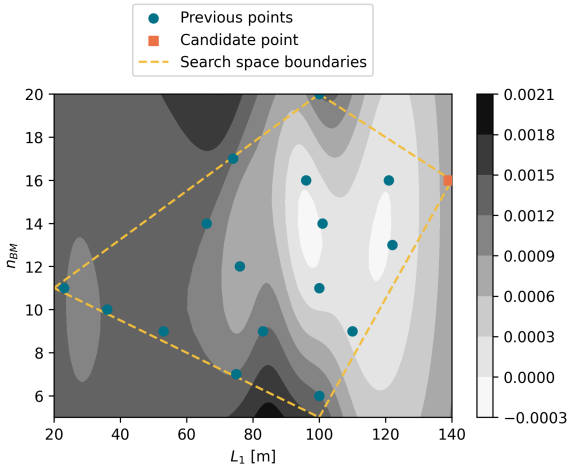


(b) Surrogate model fit, iteration 2

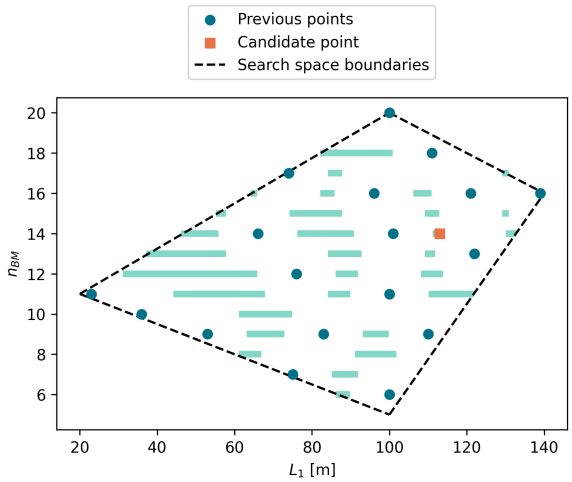


(c) Candidate selection space, iteration 4

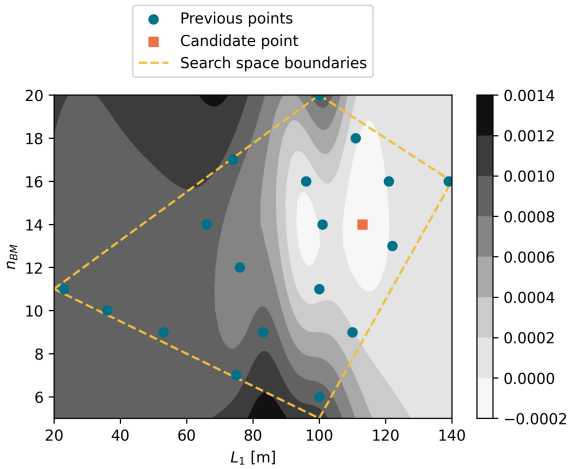


(d) Surrogate model fit, iteration 4

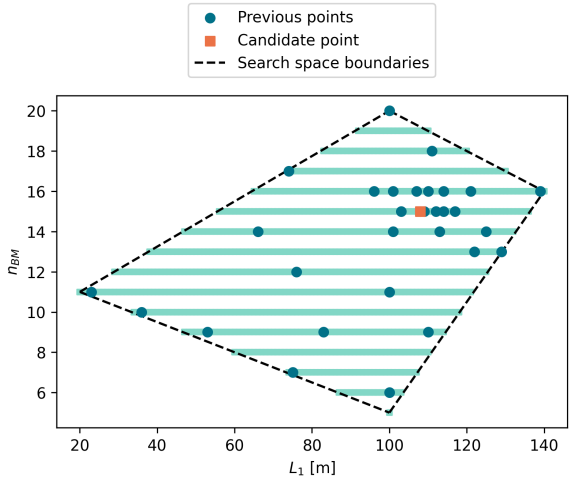


(e) Candidate selection space, iteration 17

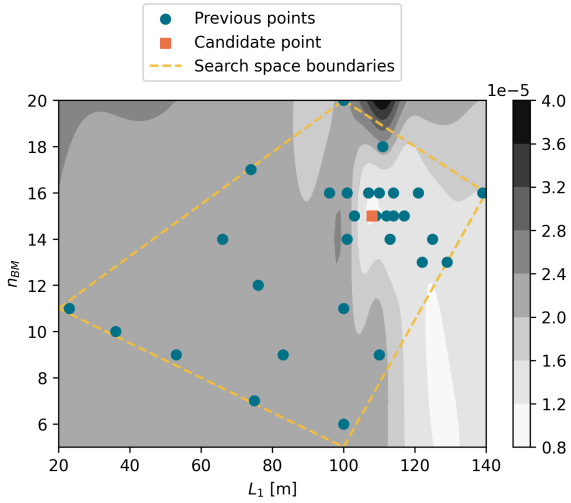


(f) Surrogate model fit, iteration 17

Figure 7.6: Surrogate model fit and candidate selection for each iteration of SMO run 2.1

### 7.2.2. Fatigue Behaviour

To gain insight into the fatigue behaviour of the 6 optized DPC configurations that were previously obtained through experimentation, Figure 7.7 presents the calculated fatigue damage between the HOP and TDP of each configuration. These plots identify the critical fatigue locations along the length of the cable:

*A*. HOP

*B*. Transition from BS to regular dynamic cable

*C*. Sag bend

*D*. Hog bend/buoyant cable section

*E*. TDP

Recall from Equations 5.7 through 5.9 that a safety factor $DFF$ has to be applied the calculated fatigue damage, resulting in a design fatigue damage. Considering a minimum life expectancy of the DPC of 20 years, this results in a maximum allowable calculated fatigue damage of 5.0e-3. If this value is exceeded, then the cable can not operate reliably over its whole life span.

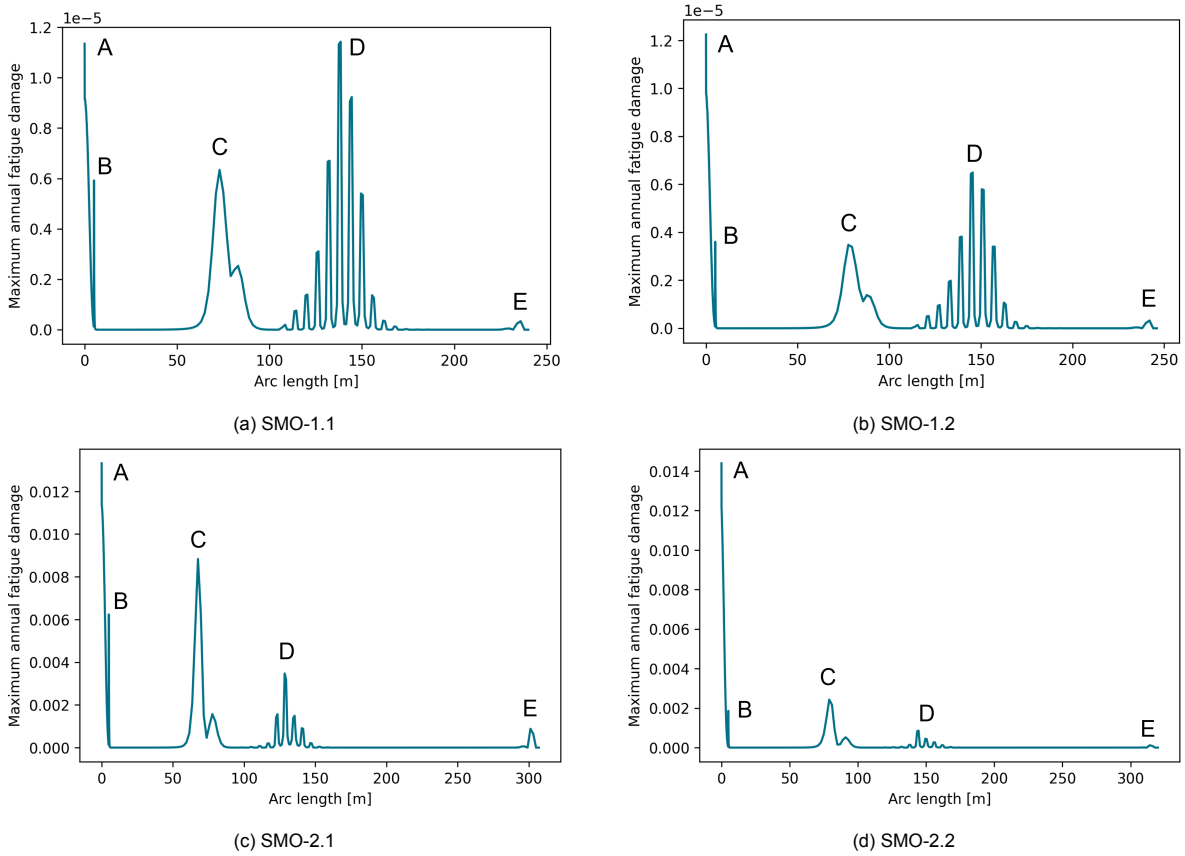


(a) SMO-1.1

(b) SMO-1.2

(c) SMO-2.1

(d) SMO-2.2

Figure 7.7: Fatigue damage along cable length of each best solution found with SMO method

#### Influence of the Decision Variables

To be able to analyse the influence that the two decision variables have on the fatigue response of the DPC, the performance of several different configuration shapes is compared. Herein, the optimized configuration is compared to intermediate solutions with either a large or small value of one of the variables, while the other variable remains approximately constant. Figures 7.8 and 7.9 show two cases of this comparison, for varying water depth scenarios. The plots show the different shapes that result from the decision variable values, as well as the resulting fatigue damage. Additionally, the location of the critical point is highlighted. The variable values are given in the legend of each plot.

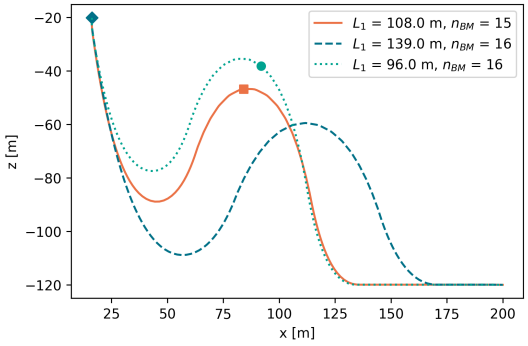


(a) Shapes for variable $L_1$

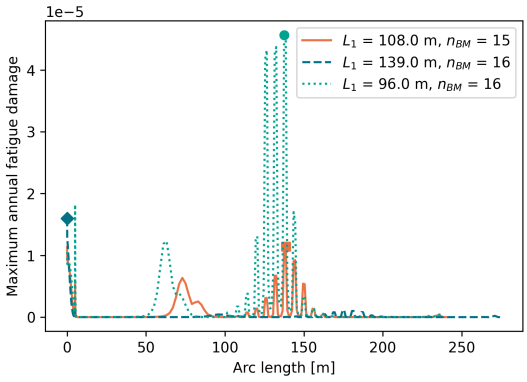


(b) Fatigue damages for variable $L_1$

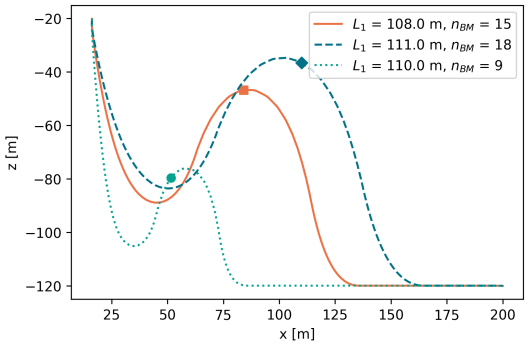


(c) Shapes for variable $n_{BM}$

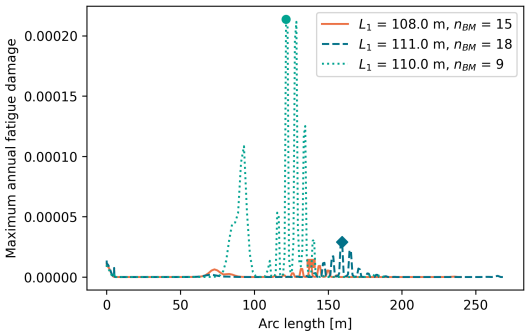


(d) Fatigue damages for variable $n_{BM}$

Figure 7.8: Influence of the decision variables on the fatigue behaviour for SMO-1.1

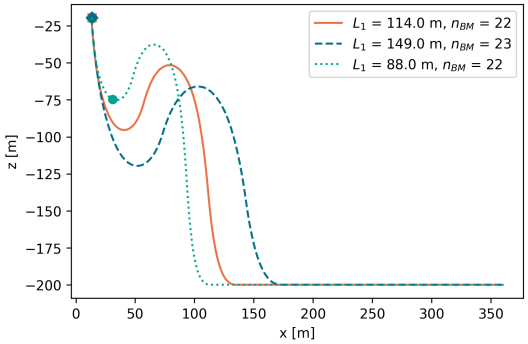


(a) Shapes for variable $L_1$

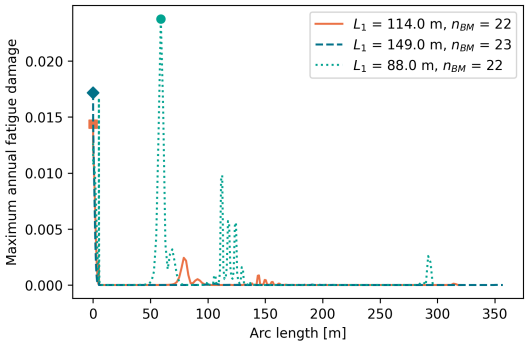


(b) Fatigue damages for variable $L_1$

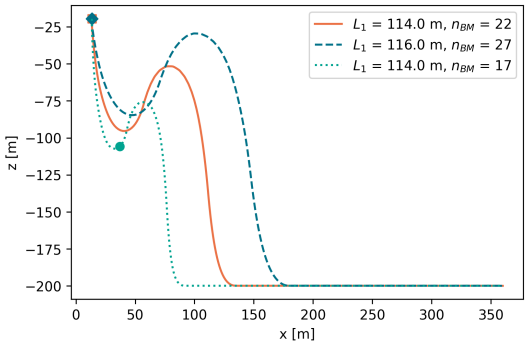


(c) Shapes for variable $n_{BM}$

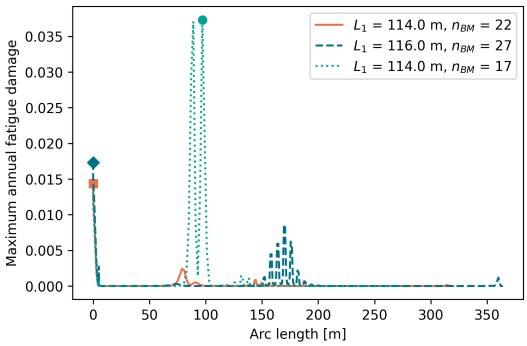


(d) Fatigue damages for variable $n_{BM}$

Figure 7.9: Influence of the decision variables on the fatigue behaviour for SMO-2.2

**Reference and Optimized Fatigue Performance**
The reference configurations as previously given by Table 7.6 were analysed and the fatigue performance is compared to the optimized configurations that were found using the SMO algorithm. Table 7.9 gives the maximum annual fatigue damage results and the calculated fatigue life improvement that an optimized configuration offers over the reference case. Figure 7.10 shows both the shapes of the initial reference configuration and the optimized DPC, for both test cases, while Figure 7.11 shows the calculated fatigue damage along the length of the cable. The critical fatigue locations of have shifted significantly due to the change in configuration shape. The most notable improvement occurs for case study 1, where the optimized configuration has a much longer section length $L_1$, creating a deeper hanging sag bend. This reduces curvature at the HOP and within the sag bend, leading to reduced fatigue stresses on these areas.

| Case study | $D_{ftg,ref}$ | $l_{ftg,ref}$ | $D_{ftg,opt}$ | $l_{ftg,opt}$ | Ftg. life improvement |
|---|---|---|---|---|---|
| 1 | 4.62e-3 | 21.6 years | 1.14e-5 | 8.77e4 years | 8.75e4 years |
| 2 | 1.66e-2 | 6.02 years | 1.29e-2 | 7.75 years | 1.73 years |

Table 7.9: Fatigue life performance of reference and optimized configurations

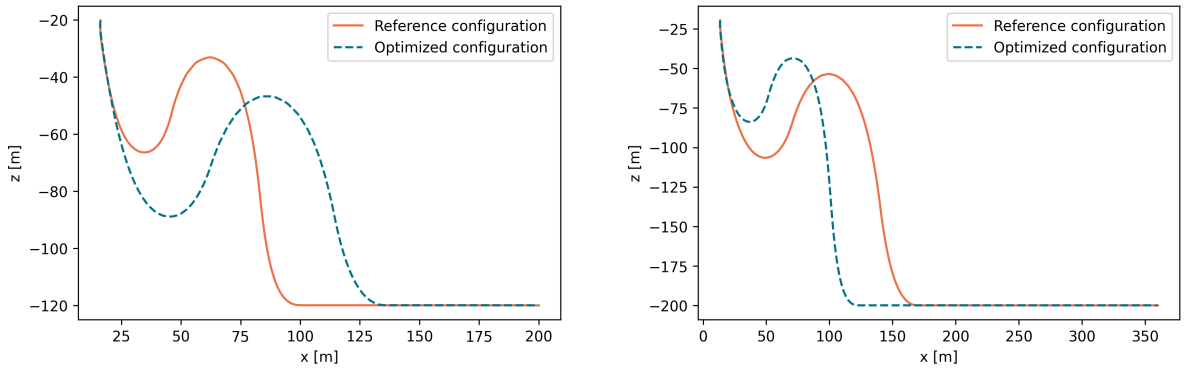


(a) Case study 1 (b) Case study 2

Figure 7.10: Comparison of reference and optimized cable configuration shapes

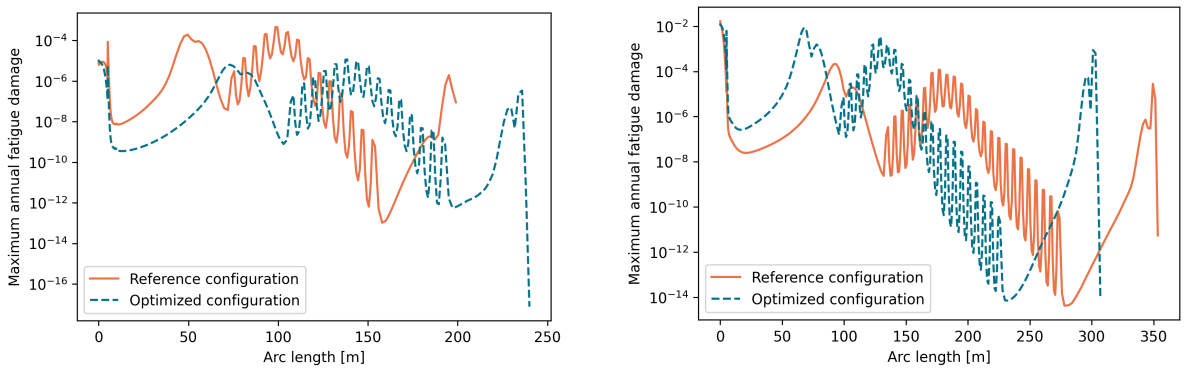


(a) Case study 1 (b) Case study 2

Figure 7.11: Comparison of calculated fatigue damage for reference and optimized configurations

## 7.3. Discussion

This section discusses the results with regards to the three requirements for a well-performing optimization method. Additionally, comments are included on the calculated fatigue performance of the optimized DPC configuration. Finally, the limitation of the optimization model are highlighted, along with the impact of these limitations on the results.

### 7.3.1. Optimization Algorithm

A discussion of the results and findings related to the performance of the proposed SMO method.

**Convergence**

Even after numerous experiments, the exact locations of the global optima for both case studies remain unknown. The GS gives a good indication of the approximate location of the optimum, but for a more definitive answer a finer GS is required. However, it is reasonable to assume that if the solution of the RBF optimization method is very close to the GS optimum or potentially even better than it, convergence to the optimum has been achieved.

Table 7.7 shows that the results from the SMO experiments correspond closely with the optimal solutions found by the GS method. One exception is the solution of experiment SMO-2.2, which deviates from the GS optimum by about 11%. This is an example of where the final solution has converged towards a local optimum. The reason for this mishap is caused by poorly distributed sampling and insufficient exploration of the search space, of which the latter is supported by the fast convergence of the error between surrogate and real model (Figure 7.5h).

All together, the performance of the optimization algorithm in terms of convergence can be considered good but not flawless. Not every execution of the optimization algorithm finds the exact same solution, given the exact same input variables to the optimization problem. This deficit is caused by inaccuracies of the RBF model fit. The surrogate model continues to have minima in the wrong locations, which can possibly lead the optimizer away from the true global optimum. This prevents exploration of new candidates near the current best solution, which is where an improved solution is likely to be. Increasing the number of initial samples and allowing for more algorithm iterations would surely improve the convergence properties, but this may well lead to unacceptably high computational costs. A more efficient solution could be to invert the inequality constraint from Equation 6.13 and gradually increase the value of the parameter $\beta$ towards the end of the iterative process. This forces candidate selection closer to the existing samples, thus closer to the current best solution. The risk of this method is convergence towards a local optimum if a solution close to the global optimum has not been found yet. However, this is unlikely if enough exploration of the search space has been conducted.

Figure 7.2 displays the location of the GS and optimized solutions within the search space. This plot shows that the solutions are located closely together within the same area of the search space, which is a good sign for consistency of the algorithm's convergence properties. Even though, as previously mentioned, the algorithm does not always find the exact same solution, it gets close each time. This solution can then be used as a starting point for a localized search strategy.

Note that finding an optimum using GS can be hit-or-miss. When applying a coarse GS algorithm, the global optimum might well be located relatively far from one of the grid samples, in which case the GS optimum is not very close to the true optimum of the blackbox function. In the case of experiments GS-1 and GS-2, very good solutions were found, which is can be considered pure luck. With this in mind, the ability to locate the optimum of the SMO algorithm is potentially much better than portrayed by the results in Table 7.7.

**Robustness**

The optimization method appears to perform well for varying input scenarios. The formulated case studies represent varying environmental conditions and water depths. For each case, the optimizer succeeds in finding a solution that is close to the estimated optimum (obtained through GS experiments), in more than one instance. Throughout the optimization process no particular irregularities, such as excessive generation of infeasible samples or convergence towards a particularly bad solution, occur for any of the test scenarios. This success can be attributed to the preliminary analysis and definition of the feasible search space boundaries and the successive sampling method.

Some remarks on robustness can certainly be made. Most notable is the need for careful selection of the optimization parameters. It was already mentioned that the larger feasible search space for the deep water scenario makes optimization more difficult. Therefore, more initial samples are needed to sufficiently cover the search space. The selection of this parameter was a trial and error process, something that should definitely be analysed more carefully and improved to achieve compliance to any arbitrary environmental scenario.

**Efficiency**
The indicator for efficiency is the total number of function evaluations needed for the algorithm to find the global optimum of the optimization problem. With the current simulations parameter settings, a single time-domain structural response and fatigue simulation of the numerical DPC model can take over 10 minutes to complete. This also depends on the water depth and corresponding cable length, a longer cable with more FEM elements requiring significantly higher computational effort.

When compared to the GS method, the proposed optimization method performs well with regards to efficiency. The required number of function evaluations can be reduced by up to 40%, which is valuable computational time. Keeping in mind that the current model only operates with two variables, but is expandable to higher dimensions, the computational savings may increase even more. The number of function evaluations needed in a GS for $p$ grid points per variable in $k$ dimensions is $p^k$. This exponential growth makes GS extremely inefficient for higher dimensionality problems [71].

Detailed information about the efficiency of similar optimization studies is sparsely available. The methods are insufficiently well described by the authors to be able to draw conclusions or the set of objective, decision variables and constraints is too different to make a fair quantitative comparison. Therefore, the author has decided that no comparative results would be presented amongst the other results. However, some coarse estimations can be made on the efficiency of some reference studies and how they compare to the work in this report:

- A GA has previously been used to optimize the DPC configuration [19]. This method used a population size of 20, which means that for each iteration of the algorithm 20 function evaluations are needed. A total of 25 iterations was performed, resulting in a total of 500 function evaluations. While this method is capable of locating BMs anywhere along the length of the cable and therefore allows for very intricate LWS configurations, one must ask if the computational effort to achieve this is feasible.

- Another model-based DPC optimization method has previously been developed, which makes use of a kriging surrogate model [18]. With 600 initial samples and over 100 iterations, the method appears to be computationally expensive, when compared to the proposed RBF based approach. That being said, 6 decision variables are included, which makes for a very comprehensive optimization problem.

The optimization method proposed in this method requires only 30-40 function evaluations, depending on the environmental scenario. However, the optimization problem incorporates only two decision variables. Once the dimensionality is increased, the performance can be re-evaluated for a more decisive comparison with other methods.

After inspecting the results of the conducted experiments, some adjustments come to mind that could potentially increase the efficiency of the optimization method. Raising the error threshold for the stopping criterion is an obvious way to reduce the number of iterations that are initiated before termination. Setting the threshold too high would surely have a negative effect on convergence towards the optimum, but even a small relaxation could benefit the efficiency. This can be seen when inspecting the error development for experiment SMO-2.1 (Figure 7.5h). At iteration 6 and 7 the error drops to less than 5%, after which it rises again because the surrogate model develops some oscillations which attract the new candidate. At this point, the best solution was already close to the final optimum (see Figure 7.3c). If the algorithm would have terminated at iteration 7, then this final best solution would have never been discovered. However, total computational costs would be reduced by over 25%. Considering these assumptions, raising the error threshold can be especially useful if the dimensionality of the problem is increased, or if the user is simply interested in a quick 'ballpark optimal' configuration design.

## 7.3.2. Fatigue Performance

A discussion of the results and findings related to the calculated fatigue damage.

**Critical Points and Distribution of the Fatigue Damage**
Fatigue damage is generally only an issue at certain points along the DPC's length. At these critical locations, the calculated fatigue damage peaks, which indicates that mechanical fatigue failure is a distinct possibility. Figure 7.7 shows the calculated fatigue damage along the length of the best performing

DPC configuration from each SMO experiment. Critical fatigue locations can clearly be identified at following locations:

- *HOP:* Even though a BS is modelled, the fatigue damage still tends to peak at the HOP.
- *After the BS:* The cable experiences a peak in curvature in the transitional section between BS. In the experimental cases the peaks are not affecting the total fatigue performance of the cable, but when the BS is poorly designed, the fatigue damage at this location can become critical.
- *Sag bend:* Curvature in the sag bend can cause significant fatigue damages. They tend to be more critical for the deep water configurations of case study 2, where the sag bend curvature is slightly higher, due to the shorter length of the first dynamic cable section.
- *Hog bend:* The calculated fatigue damage oscillates here, due to curvature fluctuations between the BMs. The relative effects are more severe for shallower water configurations, because there are less BMs to dampen the motions.

The best performing DPC configurations appear to be shaped in such a way that the fatigue damage is distributed along the cable as evenly as possible. This is clearly visible in the fatigue damage plot for SMO-1.1 (Figure 7.7a). Here, the magnitude of the calculated fatigue damage is almost identical at the two most critical locations (HOP and hog bend), while the fatigue analysis for the lesser performing solution of SMO-1.2 (Figure 7.7b) reveals that the damage at the HOP is dominant. Similar effects can be observed for the final configurations from case study 2 experiments, but to a lesser degree. After all, it has been proven that they are not exact global optimum solutions. However, a reduction in fatigue damage at the HOP at the cost of higher fatigue damages at other critical points can clearly be observed for the solution of experiment SMO-2.1. These findings may well be a good indicator for a fatigue optimized solution for the DPC configuration, but more investigation is required to validate this assumption.

**Calculated Fatigue Life**
When examining the quantitative fatigue damage results it becomes clear that the relevance of fatigue resistant design of the DPC is highly dependent on the environmental loading. The maximum calculated annual fatigue damage for the best solution of case study is 1 is 1.14e-5 (Table 7.7). Even after applying a $DFF$ of 10, as prescribed by the design requirement in Equation 2.12, this still results in a design fatigue life of approximately 8772 years (Equation 5.9). Assuming that the fatigue calculations were performed correctly, this indicates that failure of the conductor due to mechanical fatigue within the life span of the DPC is highly unlikely. In contrast, the fatigue results for the experiments of case study 2 show the opposite. The minimum design fatigue life of the conductor here is only about 7 years (Equation 5.9), which is not enough for reliable operation. This means that for deep water scenarios with rough sea conditions, a DPC with different structural properties is needed to limit the fatigue stresses on the conductor. Do note that the global fatigue analysis that was used in this research has its limitations, and that a more intricate fatigue calculation method could produce different results.

**Shape of the DPC Configuration**
The configuration shapes that arise as optimal or best solutions from the experiments are shown in Figure 7.4. Interesting to see is that the configuration shapes for the different water depths are not scaled with the water depth, but have vastly different proportions. The shallow water configurations perform well with a relatively long first cable section in relation to the total cable length, while the optimized configurations in deeper water have much smaller relative first section lengths. This can be explained by the critical fatigue stresses at the HOP. To reduce the cyclic loading at the HOP, the BMs need to be located relatively close in order to be able the dampen the motions of the cable. If they are located further away from the HOP, then the first cable section can behave almost like a simple catenary shape DPC, which is not suitable for a DPC application. This effect was previously already registered in Section 5.4.2, where an increasing value for parameter $L_1$ lead to an ever increasing maximum fatigue damage at the HOP (see Figures 5.19 and 5.20). The rough sea state of case study 2 potentially adds to this, causing even higher stresses at the HOP and therefore requiring additional damping of the cyclic motions. To determine the exact contributions that water depth and sea state have on the optimal configuration, more research with other environmental conditions is required.

The more extreme configuration comparisons from Figures 7.8 and 7.9 shed additional light on the previous findings. Figure 7.8b, shows that a shorter value for $L_1$ indeed dampens the motions at the HOP and shifts the critical fatigue damage to the hog bend. If $L_1$ is too large, excessive fatigue damage can occur at the HOP. Similar effects are registered for the deep water scenario (Figure 7.9b), but the fatigue peak occurs at the sag bend, rather than the hog bend. This can be explained by the close proximity of the sag bend to the HOP and the fact that the motions at the sag bend are not directly dampened by the presence BMs. The value of $n_{BM}$ appears to have a lesser influence of the location of the critical point than it has on the magnitude of the maximum fatigue damage. Figures 7.8c and 7.8d show critical points at the hog bend, but a clear increase in fatigue damage if not enough BMs are attached. The resulting curvatures in sag and hog bend are large, which most likely contributes to an increase of fatigue damage. Too many BMs is also undesirable, as it too leads to an increase of fatigue damage at the hog bend. Without further analysis, this effect can only be explained by closer proximity to the water surface, where influence of waves and currents is greater. The effect that the number of attached BMs has on the deeper water, rougher sea state scenario is somewhat different (Figures 7.9c and 7.9d). Again, an increase of fatigue damage can be observed if $n_{BM}$ is too large. Due to the more sever floater motions the critical points remains at the HOP. In case too few BMs are used, the peak stress occurs at the sag bend, which appears to be caused by a sharp curvature and a lack of damping.

Comparing the shapes of the reference and optimized configurations (Figure 7.10) further confirms the previous assumptions. For case study 1, where the environmental loading is moderate, a lower hanging sag bend is possible, which reduces the overall curvature and fatigue damage on the cable. As Figure 7.11 shows, the overall fatigue performance of the optimized configuration is superior at all critical points. The fatigue damage improvement over the reference case is much lower for case study 2 and the average fatigue damage across the whole arc length actually appears to be higher. However, the critical fatigue damage at the HOP is reduced through selection a particularly small value for $L_1$.

**Fatigue Damage Causes and Mitigation**

From the experimental results and the findings that were previously discussed, it is possible to identify the main contributions to fatigue damage of the DPC and measure that can be taken to limit the damage at the critical points:

- *Bending stresses at the HOP:* Across all simulated scenarios, but in particular for rougher sea states, the highest fatigue damage is calculated at the HOP. This is caused by the motions of the FOWT. The connection to the floating platform is rigid, which results in stress concentrations. The BS reduces the bending stresses at the HOP somewhat and partly relocates them to the cable section just after the BS. This is indicated by a second fatigue damage peak in the transitional section between BS and regular dynamic cable. A further measure to mitigate the bending stresses at the HOP is shortening the length of the first dynamic cable section, i.e. moving the buoyant cable section closer to the HOP. This increases the dampening effect that the BMs have on the first section of the cable and reduces the curvature at the HOP, both of which are beneficial to the fatigue life of the cable section close to the HOP.
- *Bending stresses at the sag/hog bend:* The sag and hog bend can be subject to fairly large curvatures resulting in high fatigue stresses. In fact, the fatigue damage at either can be higher than at the HOP, as is the case for reference configuration 1 (7.11a). In this example, the curvature at both bends is particularly high. The much improved solution found by using the optimization model (experiment SMO-1.1) prescribes a configuration shape with a much longer first dynamic cable section, which results in much softer sag and hog bends, thus reducing curvature. Additionally, when the sag and hog bend are located further away from the floating platform and in deeper water, the influences of platform motions, waves and currents (higher near the surface) are smaller. Of course, this mitigation measure contradicts the previous measure of limiting the bend stresses at the HOP. Depending on the severity of the waves, a trade-off must be made.
- *Bending stresses between the buoyancy modules:* The fatigue damage fluctuates heavily in the space between the BMs. While some stress concentration are to be expected, altering the distance between the BMs specific to the environmental scenario can help to lower the stress peaks.

The findings presented above can be valuable knowledge for future designs of the DPC configuration or, in an optimization context, determination of the decision variables and their bounds.

## 7.4. Conclusion

The optimization model is validated by testing the convergence, robustness and efficiency. Additionally, the fatigue performance of the optimized DPC configurations is evaluated by comparing them to some non-fatigue optimized reference configurations and making comments about the association between fatigue response and configuration properties.

Experimentation is carried out by formulation of two environmental case studies, representing a moderate sea state and water depth and a rougher sea state in deeper water. Herein the wave conditions are modelled by a single JONSWAP spectrum, defined by a significant wave height and peak wave period. The currents are considered to be generated by tidal movement and are the same for both case studies. The wind speeds are constant, independent of height, but somewhat higher for case study 2 to match the rougher sea state.

Experiments are conducted with the proposed SMO method and by applying a coarse GS algorithm, which serves as material for comparison. The settings of the simulation parameters, global model parameters and optimization parameters are chosen based on the preliminary analyses that were conducted in previous sections of the report, with slight alterations to match the test scenarios.

The results show that the optimization model performs well in terms of convergence. Even though the final solutions were never exactly the same, a near-optimal solution can consistently be found within a reasonable number of function evaluations. The method therefore offers a sound basis for a preliminary optimized DPC configuration design. Compared to the GS, there is a significant reduction in required function evaluations when using the SMO method. It is highly likely that this relative efficiency can further improve if the dimensionality of the problem is increased by introducing new decision variables. The optimization method performs satisfactory across both case studies, which indicates robustness and applicability to a wide variety of environmental scenarios. However, the experiments for the deeper water scenario require a greater number of initial samples to adequately fill the associated larger feasible search space.

The fatigue calculations show that the environmental conditions play a crucial role in fatigue life of the DPC. Where fatigue damage is insignificant in moderate conditions, rougher environmental conditions can lead to premature fatigue failure of the DPC in question. While this is to be expected to some degree, the difference in calculated fatigue life is extremely high. Tests with a local cable model or real-life experiments can help to better understand this behaviour. A more structurally robust DPC may be required for rough sea, deep water applications.

The most critical fatigue damage tends to occur at the HOP and at the hog bend. The stresses that contribute to fatigue at the HOP are caused by the motions of the floating platform. They can be mitigated by moving the buoyant cable section closer to the HOP, which increases the dampening effect of the BMs and reduces the curvature at the HOP. The drawback of this measure is that it causes increased fatigue stresses in the sag and hog bends due to the increased curvature and influence of waves and currents. Therefore, a good balance needs to be found. The best performing configurations tend to distribute the fatigue damage across the critical points as evenly as possible.

# 8

# Conclusions and Recommendations

This section presents conclusions about the conducted research and recommendations for future research. The conclusion section reflects back on the research objective and question and highlights the findings. Limitations to the current state of this research and possible improvements are covered by the recommendations section.

## 8.1. Conclusions

The objective of this research was to develop a parametric model of a DPC and apply an efficient and flexible optimization method to it in order to find the optimal preliminary DPC configuration. The research was driven by the main research question *"How can a parametric optimization model be developed to be used for the optimization of the dynamic power cable configuration?"*. The answer to this research question was investigated through a sequence of sections, all of which had their own research objective and question. The first part of the report gave an overview of the available knowledge about DPC design, analysis and optimization, after which the proposed method for parametric modelling and optimization of the configuration was presented.

The parametric modelling of the DPC involves the definition of three individual models in a commercial software package. The used floating platform model is a reference model, while the model for cable and fatigue calculation are fully parameterized custom models that were designed for the purpose of parametric optimization. The cable is represented as a FEM model that operates according to lumped mass theory. The fatigue model is set up to convert axial loads and curvatures into stresses on the conductor, according to analytically derived equations for axial and bending stresses. It is important to verify that the individual modelling aspects operate as intended. For this purpose, a series of tests in which simulated results are compared to analytically derived values needs to be conducted.

Once the workings of the model are verified, a convergence study is required to be able to select appropriate values for the simulation parameters. The goal is to gather accurate simulations results, without being unnecessarily computationally expensive. As irregular sea states are used, fairly long simulation time values are required until the fatigue results converge, which makes for computationally expensive time-domain structural response analyses of the floater and cable. A reasonably long build-up stage is required too, in order to reduce peak stresses during the early stages of the simulations. The computational time for one structural response analysis simulation is therefore several minutes. The fatigue analysis is much less computationally demanding and requires only seconds to complete.

The final step in analysing the parametric model is a parametric sensitivity study. Since the purpose of the model is to be used for optimization, it is important to gain insight into the influence that the physical model parameters have on the performance of the DPC configuration. Parameters that highly influence the fatigue response of the DPC can be used as decision variables, while others can be fixed to reduce the dimensionality of the optimization problem. A clear example of the latter case is the parameter that sets the distance between the BMs, which performs equally well for different values and can therefore be fixed at any of these values. Parameters can also display behaviour of interdependence, as do the parameters for total cable length and horizontal distance to the TP of the cable. In this case, one can be defined as a function of the other, reducing the amount of required

decision variables. Physical limitations, such as space limitations dictated by the layout of the wind farm, can also be a reason to leave out certain variables and reduce the model's complexity.

When constructing a SMO method for the optimization of the DPC configuration, the first step is to mathematically formulate the optimization problem. This involves the minimization of an objective, which is a function of a set of decision variables, subject to a set of inequality constraints. In the case of single-objective minimization of fatigue damage, the objective function value is directly proportional to the calculated maximum annual fatigue damage or the inverse of minimum fatigue life. The constraints govern the MBL and MBR limits of the cable, as well as the minimum distance to the seabed and the water surface, to prevent collisions with the surroundings. The number of decision variables can be limited to two, namely the length of the first dynamic cable section and the total number of BMs that are attached. This model setup is capable of producing a wide variety of solutions without creating an overly complex optimization problem.

The constraints impose an oddly shaped feasible region of the search space. This makes the application of LHS difficult, because it would produce too many infeasible samples. Generating infeasible samples is computationally inefficient and distracts from the feasible solutions. Therefore, a method for sampling within the feasible search space is required. This feasible search space can be found by carrying out static analysis on grid samples for different water depths, which is computationally feasible. Correlations between the water depth and the location of the search space boundary's vertices can be established, from which equations for the boundary lines can be formulated. These boundaries hold for all water depths within the scope of the research. Random sampling within the boundaries with a minimum distance requirement between each sample ensures a feasible sample set without clustering.

A RBF interpolant is used for the construction of the surrogate model. Along with selection of an appropriate RBF type, it is important to handle high function values within the data set with care. The oscillations in the surrogate model fit caused by these high function values can be reduced by assigning a lower value to the outliers. Choosing the median of the whole data set as this value proved to be an effective method of reducing oscillations and improving the surrogate model's accuracy.

Solving the optimization problem requires a dedicated algorithm. An iterative search strategy that starts with global "exploratory" search and gradually moves to local "exploitative" search prevents convergence to a local optimum. Preliminary testing of the optimization algorithm on a known test function serves to validate the method and identify the appropriate values for the optimization parameters. The optimization parameters consist of the number on initial samples, a parameter that governs the transition from exploratory to exploitative search and the RBF interpolant type with which to construct the surrogate model. The results indicate that both an increase of initial samples and exploitative search improve the probability of successful convergence, but at the cost of computational efficiency. Careful tuning of the parameters is required for good optimization results that don't require an excessive amount of function evaluations.

Experimental case studies were formulated to test the performance of the SMO algorithm at optimizing the blackbox DPC configuration model. Herein, performance was measured in terms of convergence ability, robustness and efficiency of the optimizer. The results were compared to results from a GS study. As expected, the proposed optimization model turns out to be much more efficient than the GS procedure. The convergence results of the SMO experiments were good, but not perfect because the optimizer did not always end up finding the exact same result. Deviations from the suspected optimal fatigue damage, which was discovered through GS, of up to 11% were registered. That being said, the best solutions of each experiment were located close together, which means that the optimization method is clearly capable of finding a near-optimal DPC configuration withing a short time frame.

No particular problems were discovered when applying the optimization method to problems with varying environmental conditions and water depths. However, a larger amount of initial samples was required for the optimization of scenarios with a deeper water depth. This is because the feasible search space grows as the water depth is increased and a greater amount of data points is required to sufficiently fill the search space.

There are some interesting findings about the fatigue behaviour of the DPC. Firstly, the best performing DPC configuration showed that the magnitude of the fatigue damage at the two most critical locations was equal. One could say that for this configuration, the fatigue stresses were most evenly spread out along the length of the cable. Secondly, while fatigue damage seems to be insignificant to the cable's reliability for shallower water conditions with moderate environmental loads, critical minimum fatigue life values were registered for deeper water configurations with higher sea states. The

calculated design life time was as low as 7 years, which means that that a more structurally robust DPC is required for operation under rough conditions. Mitigation of the fatigue stresses at the critical HOP can be achieved by shortening the first dynamic section of the cable, thus moving the BMs closer to the surface and the HOP. This does increase the fatigue stresses on the hog bend. Therefore, a good balance must be found.

Reflecting back on the main research question, it can be concluded that an appropriate method has been developed for the optimization of the DPC configuration. The report provides a complete overview of the approach for solving the global DPC optimization problem. The choices for modelling and analysis of the cable were motivated, keeping the research goal in mind, which involved creating an efficient and flexible optimization method. The proposed optimization method was formulated so that it can be expanded with additional decision variables and is applicable to any environmental scenario. Even though some understanding of the optimization algorithm is needed to select appropriate values for the optimization parameters, the other input parameters are easily implemented and can mostly be gathered from manufacturer specifications or reference studies. Using the proposed optimization method, it is therefore possible to make a global design of the DPC configuration, without the need of extensive preliminary knowledge about the behaviour of DPCs. Some further generalization of the DoE and optimization parameter selection can further improve this feature.

## 8.2. Limitations and Recommendations

This section sums up the limitations to the current optimization model and gives recommendations on future research to improve the model.

### 8.2.1. Limitations

Over the course of developing the parametric optimization model, certain assumptions and simplifications were introduced, which caused some limitations to the model. The following physical limitations to the cable model can be identified:

- A number of loads was not considered when conducting the hydrodynamic and structural analyses of the DPC. From the loads introduced in Section 2.2, both VIV and loads caused by marine growth were not included in the analysis. The influence of VIV could be significant on the fatigue of the DPC.
- Due to the decupled modelling approach, the coupling effects of interaction between floating platform and DPC are lost. While it was decided that these effects are not particularly significant for the LWS configuration, there may still be inaccuracies in the structural response of the DPC.
- The effect of torsion is not included in the fatigue calculations. Additional axial loads on the DPC can occur when the cable is under torsion, due to the helical winding of the armouring wires [104].
- The fatigue analysis was only conducted on a global level, without modelling the internal components of the cable. While some approximations were introduced of the effect of the global loads on the local loads on the conductor, expressed as TSF and CSF (Equations 5.4 and 5.6), these cannot be considered fully accurate. For more accurate fatigue calculations, the interaction between the internal components needs to be included by using a detailed local model.

The limitations to the optimization method are the following:

- In order to better understand the behaviour of the model and more easily enable development, the dimensionality of the optimization problems was limited. With only two decision variables, the flexibiliy of the model in discovering fatigue optimized solutions is somewhat compromised.
- The DoE method allows the generation of feasible samples, but is currently only applicable for scenarios with specific water depths and global configuration parameter settings. Additionally, its performance for higher dimensionality optimization problems is unknown.
- The optimization parameter values have been tuned using a test function that was not based on the response surface of a numerical cable model. Therefore, the quality of the settings can not be assured. The performance of the optimization algorithm can be improved when performing tests with a more appropriate test function.

### 8.2.2. Recommendations

*Increasing the dimensionality of the model* by adding decision variables is a logical next research step in expanding the optimization model. New decision variables can be explored, such as changing the orientation of the LWS or the parameters of the auxiliary components. Additional parametric studies are required if such changes were to be made to the model. The addition of a third decision variable in the form of total cable length is an addition that certainly has to be made to be able to create a wider range of DPC configurations. Adding decision variables does increase the complexity of the optimization problem. More initial samples will be required, which raises the computational costs. This effect can be limited by *formulating a more efficient DoE*. Additionally, careful analysis and selection of the optimization parameters is important to maintain good convergence and efficiency properties. Selection of an appropriate test function can aid with the development of the model and selecting the best performing optimization parameter values. A time-intensive but effective approach would be to perform a fine grid search of the search space for a reference environmental scenario and using the resulting response surface to test the optimization algorithm on.

A number of flaws within the optimization model have been discovered. The following aspects of the optimization method can be improved through future research:

- The *selection of the optimization parameters* can be improved. This can potentially increase the accuracy of the surrogate model and the overall efficiency of the algorithm. A trial-and-error process with the blackbox DPC model would be extremely tedious and inefficient. Formulating fitting test functions, based on the already accumulated knowledge about the response of the model, can enable more accurate and efficient testing of the optimization method than currently available.

- One of the problems with convergence of the model is that once a near-optimal solution is found, the optimizer often starts exploring unexplored regions of the search space that are far away from the current best solution. This lowers the efficiency significantly and can even prevent discovery of the true optimum. Research into an *alternative search strategy throughout the later algorithm iterations* is advised to prevent this behaviour. One possibility is to force greedy search in the vicinity of existing points.

- The *definition of the stopping criterion* can be revised in order to increase convergence probability or efficiency. Raising the error threshold can cause the algorithm to terminate sooner, but may interfere with convergence. It is advised that additional research about this matter is conducted, possibly including a complete redefinition of the stopping criterion. A possibility is to further investigate the earlier mentioned equal distribution of fatigue damage and use it as an indicator for optimality.

Further *investigation into the calculation of fatigue damage* is desirable. The excessive fatigue damages experienced during the experiments with case study 2 raise questions regarding the validity of the calculations. The environmental conditions may indeed be too rough for a cable of this specification, but there is also a possibility that the global fatigue model is not capable of accurately calculating the fatigue response under these conditions. Further research is required. Testing the fatigue damage more systematically under a wider range of environmental scenarios can help to discover the source of the excessive fatigue damages and verify the calculations. For validation of the results, experimental tests can be used. If those resources are not available, the utilization of a more detailed local fatigue model may help to better understand the fatigue behaviour of the DPC configuration.

# Bibliography


[1] M. Moser, *Future Population Growth - Our World in Data*, 2014. [Online]. Available: https://ourworldindata.org/future-population-growth (visited on 02/22/2022).

[2] U.S. Energy Information Administration, *International Energy Outlook 2021*, Washington, D.C., 2021. [Online]. Available: https://www.eia.gov/outlooks/ieo/.

[3] United Nations, *Paris agreement*, Paris, France, 2015.

[4] BP, *Statistical Review of World Energy 2020*, 2020. [Online]. Available: https://www.bp.com/en/global/corporate/energy-economics/statistical-review-of-world-energy.html.

[5] International Energy Agency, *Net Zero by 2050: A Roadmap for the Global Energy Sector*, Paris, France, 2021. [Online]. Available: https://www.iea.org/reports/net-zero-by-2050.

[6] I. Komusanac, G. Brindley, D. Fraile, and L. Ramirez, *Wind energy in Europe: 2020 Statistics and the outlook for 2021-2025*, Brussels, Belgium, 2021. [Online]. Available: https://windeurope.org/intelligence-platform/product/wind-energy-in-europe-2020-statistics-and-the-outlook-for-2021-2025/.

[7] R. Collombet, *Ocean Energy: Key trends and statistics 2020*, 2021. [Online]. Available: https://www.oceanenergy-europe.eu/files/ocean-energy-key-trends-and-statistics-2020/.

[8] Technology Collaboration Programme on Ocean Energy Systems, *Spotlight on Ocean Energy*, 2018. [Online]. Available: https://www.ocean-energy-systems.org/publications/oes-documents/market-policy-/document/spotlight-on-ocean-energy-2018-/.

[9] W. Musial, S. Butterfield, and B. Ram, "Energy From Offshore Wind," in *Proc. 2006 Offshore Technology Conf.*, Houston, Texas, USA: Offshore Technology Conference, 2006.

[10] J. Rhodri and M. Costa Ros, *Floating Offshore Wind: Market and Technology Review*, London, UK, 2015. DOI: 10.1016/j.jcp.2016.01.012.

[11] M. J. Dvorak, C. L. Archer, and M. Z. Jacobson, "California offshore wind energy potential," *Renewable Energy*, vol. 35, no. 6, pp. 1244–1254, 2010, ISSN: 0960-1481. DOI: 10.1016/j.renene.2009.11.022.

[12] L. Duckers, "Wave power," *Engineering Science and Education Journal*, vol. 9, no. 3, pp. 113–122, 2000. DOI: 10.1049/esej:20000303.

[13] P. R. Thies, L. Johanning, and G. H. Smith, "Assessing mechanical loading regimes and fatigue life of marine power cables in marine energy applications," in *Proc. of the Institution of Mechanical Engineers, Part O: Journal of Risk and Reliability*, vol. 226, 2012, pp. 18–32. DOI: 10.1177/1748006X11413533.

[14] M. Lerch, M. De-Prada-Gil, and C. Molins, "A metaheuristic optimization model for the inter-array layout planning of floating offshore wind farms," *International Journal of Electrical Power and Energy Systems*, vol. 131, 2021, ISSN: 01420615. DOI: 10.1016/j.ijepes.2021.107128.

[15] DNV GL, *Floating Wind: The Power To Commercialize*, Høvik, Norway, 2020. [Online]. Available: https://www.dnv.com/Publications/floating-wind-the-power-to-commercialize-192334.

[16] Ocean Energy Europe, *2030 Ocean Energy Vision: Industry analysis of future deployments, costs and supply chains*, Brussels, Belgium, 2020. [Online]. Available: https://www.etipocean.eu/knowledge_hub/2030-ocean-energy-vision/.

[17] GCube Insurance Services, *An insurance buyer's guide to subsea cabling incidents*. [Online]. Available: www.gcube-insurance.com.

[18] Y. Poirette, M. Guiton, G. Huwart, D. Sinoquet, and J.-M. Leroy, “An Optimization method for the Configuration of Inter Array Cables for Floating Offshore Wind Farm,” in *Proc. ASME 2017 36th Int. Conf. on Ocean, Offshore and Arctic Engineering*, Trondheim, Norway, 2017. DOI: 10.1115/OMAE2017-61655.

[19] M. U. T. Rentschler, F. Adam, and P. Chainho, “Design optimization of dynamic inter-array cable systems for floating offshore wind turbines,” *Renewable and Sustainable Energy Reviews*, vol. 111, pp. 622–635, 2019, ISSN: 1364-0321. DOI: 10.1016/j.rser.2019.05.024.

[20] A. Aninthaneni, “Optimization of offshore wind floater from dynamic cable and mooring perspective,” M.S. thesis, University of Liège, 2021. [Online]. Available: https://matheo.uliege.be/handle/2268.2/13300.

[21] DNV GL, *DNVGL-RP-0360: Subsea power cables in shallow water*, 2016. [Online]. Available: https://www.dnv.com/energy/standards-guidelines/dnv-rp-0360-subsea-power-cables-in-shallow-water.html.

[22] M. P. van der Tholen, *Failure Prediction of Submarine Power Cables*, Delft, The Netherlands, 2020.

[23] Y. Bai and Q. Bai, “Design of Deepwater Risers,” in *Submarine Pipelines and Risers*, 1st ed., Oxford, UK: Elsevier Ltd, 2005, ch. 22, pp. 401–412, ISBN: 978-0-08-044566-3. DOI: 10.1016/B978-0-08-044566-3.50024-5.

[24] S. Zhao and Y. Cheng, “A comparison of two dynamic power cable configurations for a floating offshore wind turbine in shallow water,” *AIP Advances*, vol. 11, no. 3, 2021. DOI: 10.1063/5.0039221.

[25] M. Ikhennicheu, M. Lynch, S. Doole, *et al.*, *D3.1: Review of the state of the art of dynamic cable system design*, 2020. [Online]. Available: https://corewind.eu/wp-content/uploads/files/publications/COREWIND-D3.1-Review-of-the-state-of-the-art-of-dynamic-cable-system-design.pdf.

[26] L. Shi, W. Yang, K. Chen, *et al.*, “Performance Evaluation of W Shape Dynamic Inter-Array Cable Configuration for Floating Offshore Wind Turbine,” in *Proc. Offshore Technology Conf. Asia*, Kuala Lumpur, Malaysia, 2022. DOI: 10.4043/31344-ms.

[27] K. Bakken, “Fatigue of dynamic power cables applied in offshore wind farms,” M.S. thesis, Norwegian University of Science and Technology, 2019.

[28] Balmoral, *Balmoral distributed buoyancy solutions*, 2021. [Online]. Available: https://www.balmoraloffshore.com/solutions/buoyancy/distributed-riser-buoyancy (visited on 04/19/2022).

[29] T. Kvarts and F. Lesur, *CIGRE TB 610 - Offshore generation cable connections*, 2015. [Online]. Available: https://e-cigre.org/publication/610-offshore-generation-cable-connections.

[30] N. Sødahl and T. Ottesen, “Bend Stiffener Design for Umbilicals,” in *Proc. ASME 30th International Conf. on Ocean, Offshore and Arctic Engineering*, Rotterdam, The Netherlands, 2011, pp. 449–460. DOI: 10.1115/OMAE2011-49461.

[31] Exsto, *Bend stiffeners*. [Online]. Available: https://www.exsto.com/en/solutions/solutions-subsea/surf/bend-stiffeners (visited on 04/11/2022).

[32] R. Weerheim, *Development of dynamic power cables for commercial floating wind farms*, Delft, The Netherlands, 2018. [Online]. Available: https://repository.tudelft.nl/islandora/object/uuid:487ba1e5-2764-4e96-808c-a9ee2772219d?collection=research.

[33] J. P. Grainger, A. M. Sykulski, P. Jonathan, and K. Ewans, “Estimating the parameters of ocean wave spectra,” *Ocean Engineering*, vol. 229, 2021, ISSN: 00298018. DOI: 10.1016/j.oceaneng.2021.108934. arXiv: 2008.10437.

[34] S. Rasool, K. M. Muttaqi, and D. Sutanto, “Modelling Ocean Waves and an Investigation of Ocean Wave Spectra for the Wave-to-Wire Model of Energy Harvesting,” in *Proc. 1st Int. Conf. on Energy, Power and Environment*, M. B. Niazi, Ed., Gujrat, Pakistan: MDPI, 2021. DOI: 10.3390/engproc2021012051.

[35] DNV GL AS, *DNVGL-ST-0437: Loads and site conditions for wind turbines*, 2016. [Online]. Available: https://www.dnv.com/energy/standards-guidelines/dnv-st-0437-loads-and-site-conditions-for-wind-turbines.html.

[36] M. A. Beerens, "Installation of a dynamic power cable for a floating offshore wind turbine: A comparative study," M.S. thesis, Delft University of Technology, 2016. [Online]. Available: https://repository.tudelft.nl/islandora/object/uuid%5C%3A281447cc-8e04-45eb-904f-f3f1ed95d7d6.

[37] B. M. Sumer and J. Fredsøe, "Forces on a cylinder in regular waves," in *Advanced Series on Ocean Engineering, Volume 12: Hydrodynamics around Cylindrical Structures*, World Scientific Publishing Co. Re. Ltd., 1997, pp. 123–168, ISBN: 978-1-61583-039-8.

[38] C. S. Mihelcic, "Hydrodynamic force coefficients of a vertical circular cylinder," M.S. thesis, Univeristy of British Columbia, 1989.

[39] Orcina, *K01 5MW spar FOWT*, 2021. [Online]. Available: www.orcina.com.

[40] Y. Yu, T. D. Pham, H. Shin, and K. Ha, "Study on the Motion Characteristics of 10 MW Superconducting Floating Offshore Wind Turbine Considering 2nd Order Wave Effect," *Enegies*, vol. 14, no. 19, 2021. DOI: 10.3390/en14196070.

[41] M. S. Triantafyllou, R. Bourguet, J. Dahl, and Y. Modarres-Sadeghi, "Vortex-Induced Vibrations," in *Springer Handbook of Ocean Engineering*, M. R. Dhanak and N. I. Xiros, Eds., Springer, 2016, pp. 819–849, ISBN: 9783319166490. DOI: 10.1007/978-3-319-16649-0.

[42] M. W. Broer, "Vortex induced vibrations on power cables of floating tidal energy converters," M.S. thesis, Delft University of Technology, 2014.

[43] J. Journée and W. Massie, *Offshore Hydromechanics*, 2001.

[44] European Committee for Standardization, *EN 1990:2002+A1*, 2005.

[45] DNVGL, *DNVGL-ST-0359: Subsea power cables for wind power plants*, 2016. [Online]. Available: https://www.dnv.com/energy/standards-guidelines/dnv-st-0359-subsea-power-cables-for-wind-power-plants.html.

[46] DNV, *DNV-OS-J103: Design of Floating Wind Turbine Structures*, 2013. [Online]. Available: https://dokumen.tips/documents/dnv-os-j103-design-of-floating-wind-turbine-structures.html?page=1.

[47] DNV, *DNV-OS-F201: Dynamic Risers*, 2010. [Online]. Available: https://www.dnv.com/oilgas/download/dnv-st-f201-riser-systems.html.

[48] L. H. Holthuijsen, *Waves in Oceanic and Coastal Waters*. Cambridge University Press, 2007, ISBN: 978-0-511-27021-5.

[49] W. D. Corson, D. T. Resio, R. M. Brooks, *et al.*, "Atlantic Coast Hindcast, Deepwater Significant Wave Information," Hydraulics Laboratory, U.S. Army Engineer Waterways Experiment Station, Vicksburg, Mississippi, USA, Tech. Rep., 1981. [Online]. Available: https://apps.dtic.mil/sti/citations/ADA095497.

[50] H. Chun and K. Ahn, "Wave Hindcasting on the Storm Waves at the Korean Straits of April , 2016," *Journal of Korean Society of Coastal and Ocean Engineers*, vol. 29, no. 1, pp. 36–45, 2017. DOI: 10.9765/KSCOE.2017.29.1.36.

[51] K. Ewans and J. Mcconochie, "Optimal Methods for Estimating the JONSWAP Spectrum Peak Enhancement Factor From Measured and Hindcast Wave Data," in *Proc. ASME 2019 38th Int. Conf. on Ocean, Offshore and Arctic Engineering*, Glasgow, Scotland: ASME, 2019. DOI: 10.1115/OMAE2019-95451.

[52] Y. Goda, *Random Seas and Design of Maritime Structures*, 2nd ed. Singapore: World Scientific Publishing Co. Pte. Ltd., 2000, ISBN: 981023256X.

[53] S.-h. Yang, "Parametric study of the dynamic motions and mechanical characteristics of power cables for wave energy converters," *Journal of Marine Science and Technology*, vol. 23, pp. 10–29, 2017, ISSN: 1437-8213. DOI: 10.1007/s00773-017-0451-0.

[54] M. U. T. Rentschler, F. Adam, P. Chainho, K. Krügel, and P. C. Vicente, “Parametric study of dynamic inter□array cable systems for floating offshore wind turbines,” *Marine Systems & Ocean Technology*, vol. 15, pp. 16–25, 2020, ISSN: 2199-4749. DOI: 10.1007/s40868-020-00071-7.

[55] C. H. Jo, D. Y. Kim, and Y. H. Rho, “A comparison of coupled and uncoupled dynamic analysis for the flexible riser in shallow water,” *Journal of the Korean Society of Marine Engineering*, vol. 38, no. 2, pp. 195–201, 2014. DOI: 10.1115/OMAE2013-11035.

[56] S. H. Yang, J. W. Ringsberg, E. Johnson, Z. Q. Hu, and J. Palm, “A comparison of coupled and de-coupled simulation procedures for the fatigue analysis of wave energy converter mooring lines,” *Ocean Engineering*, vol. 117, pp. 332–345, 2016, ISSN: 00298018. DOI: 10.1016/j.oceaneng.2016.03.018.

[57] L. Martinelli, A. Lamberti, P. Ruol, *et al.*, “Power Umbilical for Ocean Renewable Energy Systems-Feasibility and Dynamic Response Analysis,” in *Proc. 3rd Int.Conf. on Ocean Energy*, Bilbao, Spain, 2010. [Online]. Available: https://www.researchgate.net/publication/228814942_Power_Umbilical_for_Ocean_Renewable_Energy_Systems-Feasibility_and_Dynamic_Response_Analysis.

[58] K. S. Kim, H. S. Choi, and K. S. Kim, “Preliminary optimal configuration on free standing hybrid riser,” *International Journal of Naval Architecture and Ocean Engineering*, vol. 10, no. 3, pp. 250–258, 2018, ISSN: 20926790. DOI: 10.1016/j.ijnaoe.2017.10.012.

[59] D. G. Young, C. Ng, S. Oterkus, Q. Li, and L. Johanning, “Predicting failure of dynamic cables for floating offshore wind,” in *Proc. 3rd Int. Conf. on Renewable Energies Offshore*, 2019, pp. 821–828, ISBN: 9781138585355. [Online]. Available: https://www.researchgate.net/publication/328198603_Predicting_failure_of_dynamic_cables_for_floating_offshore_wind.

[60] DNV, *DNV-RP-C205: Environmental Conditions and Environmental Loads*, 2010. [Online]. Available: https://www.dnv.com/oilgas/download/dnv-rp-c205-environmental-conditions-and-environmental-loads.html.

[61] M. Sobhaniasl, F. Petrini, M. Karimirad, and F. Bontempi, “Fatigue life assessment for power cables in floating offshorewind turbines,” *Energies*, vol. 13, no. 12, 2020, ISSN: 19961073. DOI: 10.3390/en13123096.

[62] I. A. Assakkaf and B. M. Ayyub, “Reliability-Based Design for Fatigue of Marine Structures,” in *Proc. of Int. Workshop on Very Large Floating Structures*, vol. 1, 1999, pp. 388–397.

[63] M. Biot, L. Moro, and M. Urcia Larios, *State of the Art of Life Prediction Methods for Fatigue Design of Marine Structures*, 2009.

[64] J. Homan, *Description of a S-N Curve*, 2018. [Online]. Available: https://www.fatec-engineering.com/2018/02/20/description-of-a-s-n-curve/ (visited on 05/12/2022).

[65] F. P. Nasution, S. Sævik, and J. K. O. Gjosteen, “Fatigue Analysis of Copper Conductor for Offshore Wind Turbines by Experimental and FE Method,” *Energy Procedia*, vol. 24, pp. 271–280, 2012. DOI: 10.1016/j.egypro.2012.06.109.

[66] S. Karlsen, R. Slora, K. Heide, S. Lund, F. Eggertsen, and P. A. Osbor, “Dynamic Deep Water Power Cables,” in *Proc. 9th Int. Conf. and Exh. for Oil and Gas Resources Development of the Russian Arctic and CIS Continental Shelf*, 2009, pp. 194–203.

[67] J. Schijve, “Fatigue Properties,” in *Fatigue of Structures and Materials*, 2nd, Springer Dordrecht, 2008, pp. 141–169, ISBN: 978-1-4020-6808-9. DOI: 10.1007/978-1-4020-6808-9.

[68] Y.-l. Lee and T. Tjhung, “Rainflow Cycle Counting Techniques,” in *Metal Fatigue Analysis Handbook*, Elsevier Inc., 2012, pp. 89–114, ISBN: 978-0-12-385204-5. DOI: 10.1016/B978-0-12-385204-5.00003-3.

[69] D. G. Young, C. Ng, S. Oterkus, Q. Li, and L. Johanning, “Assessing the mechanical stresses of dynamic cables for floating offshore wind applications,” *Journal of Physics: Conference Series*, vol. 1102, 2018, ISSN: 17426596. DOI: 10.1088/1742-6596/1102/1/012016.

[70] I. Bajaj, A. Arora, and M. M. F. Hasan, “Black-Box Optimization: Methods and Applications,” in *Black Box Optimization, Machine Learning, and No-Free Lunch Theorems*, P. M. Pardalos, V. Rasskazova, and M. N. Vrahatis, Eds., 1st ed., Springer Cham, 2021, pp. 35–65. DOI: 10.1007/978-3-030-66515-9.

[71] C. Audet and W. Hare, *Derivative-Free and Blackbox Optimization*, 1st ed. Springer Cham, 2017, ISBN: 978-3-319-68913-5. DOI: 10.1007/978-3-319-68913-5.

[72] T. G. Kolda, R. M. Lewis, and V. Torczon, “Optimization by direct search: New perspectives on some classical and modern methods,” *SIAM Review*, vol. 45, no. 3, pp. 385–482, 2003, ISSN: 00361445. DOI: 10.1137/S003614450242889.

[73] S. Le Digabel, *Direct Search Methods*, 2020. [Online]. Available: https://www.gerad.ca/Sebastien.Le.Digabel/MTH8418/8_direct_search.pdf.

[74] M. Duinkerken and B. Atasoy, *Quantitative Methods for Logistics*, 2018.

[75] M. Gilli, *An Introduction to Optimization Heuristics*, 2004. [Online]. Available: http://www.unige.ch/ses/dsec/static/gilli/CyprusLecture2004.pdf.

[76] A. G. Gad, “Particle Swarm Optimization Algorithm and Its Applications: A Systematic Review,” *Archives of Computational Methods in Engineering*, vol. 29, no. 5, pp. 2531–2561, 2022, ISSN: 18861784. DOI: 10.1007/s11831-021-09694-4.

[77] J. A. Nelder and R. Mead, “A Simplex Method for Function Minimization,” *The Computer Journal*, vol. 7, no. 4, pp. 308–313, 1965, ISSN: 0010-4620. DOI: 10.1093/comjnl/7.4.308.

[78] B. Zhao, C. X. Guo, and Y. J. Cao, “A Multiagent-Based Particle Swarm Optimization Approach for Optimal Reactive Power Dispatch,” *IEEE Transactions on Power Systems*, vol. 20, no. 2, pp. 1070–1078, 2005. DOI: 10.1109/TPWRS.2005.846064.

[79] V. K. Ky, C. D’Ambrosio, Y. Hamadi, and L. Liberti, “Surrogate-based methods for black-box optimization,” *International Transactions in Operational Research*, vol. 24, no. 3, 2016, ISSN: 0890-9091. DOI: 10.1111/itor.12292.

[80] A. A. Giunta, S. F. Wojtkiewicz, and M. S. Eldred, “Overview of modern design of experiments methods for computational simulations,” in *Proc. 41st Aerospace Sciences Meeting and Exh.*, Reno, Nevada, USA, 2003, ISBN: 9781624100994. DOI: 10.2514/6.2003-649.

[81] F. A. Viana, “A Tutorial on Latin Hypercube Design of Experiments,” *Quality and Reliability Engineering International*, vol. 32, no. 5, pp. 1975–1985, 2016, ISSN: 10991638. DOI: 10.1002/qre.1924.

[82] B. G. M. Husslage, G. Rennen, E. R. van Dam, and D. den Hertog, “Space-filling Latin hypercube designs for computer experiments,” *Optimization Engineering*, vol. 12, pp. 611–630, 2011. DOI: 10.1007/s11081-010-9129-8.

[83] J. Cheng and M. J. Druzdzel, “Computational Investigation of Low-Discrepancy Sequences in Simulation Algorithms for Bayesian Networks,” in *Proc. 16th Conf. on Uncertainty in Artificial Intelligence*, 2000, pp. 72–81. DOI: 10.48550/arXiv.1301.3841.

[84] S. Kucherenko, D. Albrecht, and A. Saltelli, “Exploring multi-dimensional spaces: a Comparison of Latin Hypercube and Quasi Monte Carlo Sampling Techniques,” 2015. arXiv: 1505.02350.

[85] S. Bagheri, W. Konen, and T. Bäck, “Comparing Kriging and Radial Basis Function Surrogates,” in *Proc. 27th Workshop on Computational Intelligence*, Dortmund, Germany, 2017, pp. 243–259. [Online]. Available: https://www.researchgate.net/publication/328222483_Comparing_Kriging_and_Radial_Basis_Function_Surrogates.

[86] W. C. M. Van Beers and J. P. C. Kleijnen, “Kriging Interpolation in Simulation: A Survey,” in *Proc. 2004 Winter Simulation Conf.*, R. Ingalls, M. Rossetti, J. Smith, and B. Peters, Eds., Washington, DC, USA: IEEE, 2004, pp. 113–121. DOI: 10.1109/WSC.2004.1371308.

[87] J. Chen, J. Yan, Q. Yue, and M. Tang, “Flexible riser configuration design for extremely shallow water with surrogate-model- based optimization,” *Journal of Offshore Mechanics and Arctic Engineering*, vol. 138, no. 4, pp. 1–7, 2016, ISSN: 1528896X. DOI: 10.1115/1.4033491.

[88] I. Fylling and P. A. Berthelsen, “WINDOPT - An optimization tool for floating support structures for deep water wind turbines,” in *Proc. ASME 2011 30th Int. Conf. on Offshore Mechanics and Arctic Engineering*, Rotterdam, The Netherlands: ASME, 2011, pp. 767–776, ISBN: 9780791844373. DOI: 10.1115/OMAE2011-49985.

[89] S. Bhowmik, G. Noiray, and H. Naik, “Riser Design Automation with Machine Learning,” in *Abu Dhabi Int. Petroleum Exh. & Conf.*, Abu Dhabi, UAE: Society of Petroleum Engineers, 2019, pp. 1–12, ISBN: 9781613996720. DOI: 10.2118/197219-ms.

[90] A. C. Pillai, P. R. Thies, and L. Johanning, “Development of a Multi-Objective Genetic Algorithm for the Design of Offshore Renewable Energy Systems,” in *Proc. 12th World Congr. on Structural and Multidisciplinary Optimization*, Braunschweig, Germany, 2017. DOI: 10.1007/978-3-319-67988-4_149.

[91] Orcina, *Lines*. [Online]. Available: https://www.orcina.com/ (visited on 11/17/2022).

[92] C. Allen, A. Viselli, H. Dagher, *et al.*, “Definition of the UMaine VolturnUS-S Reference Platform Developed for the IEA Wind 15-Megawatt Offshore Reference Wind Turbine,” Tech. Rep., 2020. DOI: 10.2172/1660012.

[93] Orcina, *K03 15MW semi-sub FOWT*. [Online]. Available: www.orcina.comrenewables:K0315MWsemi-subFOWT.

[94] Orcina, *Lines*. [Online]. Available: https://www.orcina.com/ (visited on 11/17/2022).

[95] G. Giannini, P. Rosa-Santos, V. Ramos, and F. Taveira-Pinto, “On the development of an offshore version of the CECO wave energy converter,” *Energies*, vol. 13, no. 5, pp. 1–25, 2020, ISSN: 19961073. DOI: 10.3390/en13051036.

[96] M. Petelet, B. Iooss, O. Asserin, and A. Loredo, “Latin hypercube sampling with inequality constraints,” *Advances in Statistical Analysis*, vol. 94, no. 4, pp. 325–339, 2010, ISSN: 18638171. DOI: 10.1007/s10182-010-0144-z. arXiv: 0909.0329.

[97] SciPy, *Interpolation (scipy.interpolate)*. [Online]. Available: https://docs.scipy.org/doc/scipy/reference/interpolate.html.

[98] H. Gutmann, “A Radial Basis Function Method for Global Optimization,” *Journal of Global Optimization*, vol. 19, pp. 201–227, 2001. DOI: https://doi.org/10.1023/A:1011255519438.

[99] R. G. Regis and C. A. Shoemaker, “Constrained global optimization of expensive black box functions using radial basis functions,” *Journal of Global Optimization*, vol. 31, no. 1, pp. 153–171, 2005, ISSN: 09255001. DOI: 10.1007/s10898-004-0570-0.

[100] M. Mathiesen, A. K. Meyer, and B. Kvingendal, *RE2014-002: Hywind Buchan Deep Metocean Design Basis*, 2014. [Online]. Available: https://marine.gov.scot/sites/default/files/metocean_design_basis_hywind_buchan_deep_mdb_rev2_0.pdf.

[101] J. Prendergast, M. Li, and W. Sheng, “A Study on the Effects of Wave Spectra on Wave Energy Conversions,” *IEEE Journal of Ocean Engineering*, vol. 45, no. 1, 2018. DOI: 10.1109/JOE.2018.2869636.

[102] U.-J. Lee, W.-M. Jeong, and H.-Y. Cho, “Estimation and Analysis of JONSWAP Spectrum Parameter Using Observed Data around Korean Coast,” *Journal of Marine Science and Engineering*, vol. 10, no. 5, 2022. DOI: 10.3390/jmse10050578.

[103] Japan Oceanographic Data Center, *Weather information code table*, 1997. [Online]. Available: https://www.jodc.go.jp/data_format/weather-code.html.

[104] P. Fang, X. Jiang, H. Hopman, and Y. Bai, “Mechanical responses of submarine power cables subject to axisymmetric loadings,” *Ocean Engineering*, vol. 239, 2021, ISSN: 0029-8018. DOI: 10.1016/j.oceaneng.2021.109847.

# A

# Paper: A Radial Basis Function Method for the Parametric Optimization of Dynamic Power Cable Configurations

Paper begins on the next page.

# A Radial Basis Function Method for the Parametric Optimization of Dynamic Power Cable Configurations

M.P. van der Tholen, X. Jiang, S. Schreier
Department of Maritime and Transport Engineering
Delft University of Technology, Netherlands

***Abstract*— Floating offshore wind turbines offer opportunities to harvest wind energy at deep-water locations, where the construction of fixed-base turbines is infeasible. The dynamic power cables, which interconnect turbines and transport the generated electricity, are under large dynamic stresses due to the environmental loads and the motion of the floating platform. Limited knowledge about the structural behaviour of these cables is available, which is why there is need for new analysis and design methods. This paper presents a method for the preliminary design optimization of the dynamic power cable configuration. A parametric model of a dynamic power cable is built in the commercial software package OrcaFlex, from which motions, loads and fatigue on the cable can be calculated. Following that, a radial basis function surrogate model based optimization algorithm is applied to find the optimal cable configuration for an arbitrary environmental scenario. The key performance indicator here is fatigue damage, which is expected to be critical due to the cyclic loading on the cable. Experiments are carried out to test the optimization model's validity in terms of convergence, robustness and efficiency. The final method is capable of consistently finding a near-optimal dynamic power cable configuration design within reasonable time.**

## I. Introduction

The worldwide demand for energy is ever growing. Between 2020 and 2050, the demand for energy is expected to grow by 50% [1]. At the same time, the emission of greenhouse gases must be reduced drastically in order to reach the climate goals. To be a able to achieve 'net zero' greenhouse gas emissions in 2050, two thirds of total energy supply must come from renewable sources such as wind, solar, bio, geothermal and hydro energy [2].

Offshore wind energy plays an important role in the energy transition. Most current offshore wind technology makes use of turbines with bottom-fixed foundations. These turbines are only suitable for installation in waters up to 60 m [3], which limits their deployment to shallow coastal areas. The deeper water areas however offer much greater wind potential. In Europe alone, a potential of 4000 GW of wind energy is found in areas with depths between 50 m and 220 m [4]. For this reason the development of Floating Offshore Wind Turbines (FOWT) has taken a leap in recent years. These floating turbines can be placed in much deeper waters, offering an opportunity to harvest wind energy in deeper waters.

A crucial component of a FOWT system is the inter-array power cable, often referred to as Dynamic Power Cable (DPC). This cable segment is under cyclic dynamic loading from the environment which makes it susceptible to mechanical failures, potentially much more so than a fixed static submarine cable. Therefore, DPCs must be designed differently than static cables, namely as flexible umbilicals that must be strong enough to withstand the dynamic loads exerted on them. The configuration of a DPC can be changed and designed to mitigate the effects of the dynamic loads and therefore limit the risk of damage occurring to the cable during operation. Research has shown that a change in configuration or 'shape' in which the cable is suspended can lead to significant reductions of internal stresses and fatigue damage [5].

Due to the immaturity of FOWT technology, knowledge about design of an appropriate DPC is still limited. In order to accelerate the preliminary design of DPC configurations, dedicated methods for numerical analysis and design are required. This paper presents a method for the optimization of the DPC configuration, making use of a global parametric cable model and a dedicated optimization algorithm. The objective for the optimization is to minimize the fatigue damage on the conductors of the cable. The conductors are made out of electrolytic tough pitch copper, which has good electrical properties, but poor mechanical properties, making it susceptible to fatigue damage [6]. The goal of this research is to develop an optimization method that is both computationally efficient and can be applied to a flexible range of environmental scenarios.

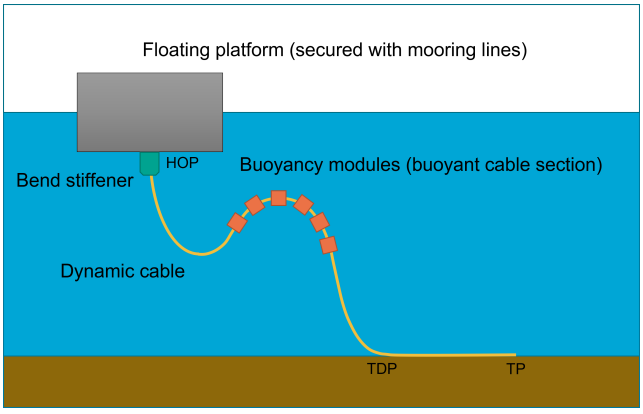


Fig. 1: LWS cable configuration

The basic DPC configuration shape that is used in this research is the Lazy Wave Shape (LWS). This configuration is suspended down the water column in an S-shape, which

is created by the addition of a buoyant cable section. This buoyant section is formed by a number of Buoyancy Modules (BM), which are clamped around the cable. For additional bend protection at the critical Hang-off Point (HOP) of the cable, a polymeric sleeve is attached around the cable, referred to as the Bend Stiffener (BS). An overview of the LWS and its components is shown in Figure 1. Notice how a sag bend and a hog bend are created due to the placement of the BMs. Additional points of interest are the Touchdown Point (TDP) and Termination Point (TP).

## II. Previous Work

A number of previous studies have been conducted on the global optimization of DPCs and flexible risers. Each of those studies begins by defining a numerical model of the floater and umbilical system using a software package, after which a tailored optimization method is applied. The main differences lie in the formulation of the optimization problem and the type of optimization method.

Work on the optimization of the DPC configuration has previously been done by Poirette et al. [7]. Their goal was to optimize the overall costs of the cable by varying the length of the different cable sections, total cable length, cable diameter and auxiliary component specifications. Constraints assured that none of the mechanical ultimate limits of the cable were exceeded. A model-based optimization method was applied, in which initial samples were taken through Latin Hypercube Sampling (LHS), after which a surrogate model was fitted to the training data. The final solution was obtained through an optimization method based on sequential quadratic programming.

Another relevant study was presented by Rentschler et al. [8]. After building a parameterized cable model, a multi-objective optimization problem was formulated in which the objective function was defined as a combination of ultimate loads, fatigue damage and total cable length, all of which needed to be minimized. Starting from an initial cable configuration that was found through static analysis of the system, the only decision variables for the optimization were the location of each BM on the cable. A Genetic Algorithm (GA) was used to find an improved DPC configuration.

Chen et al. [9] presented a design optimization method for flexible risers in shallow waters. To limit the required number of computationally expensive time-domain simulations, a model-based optimization approach was used. The performance of kriging and Radial Basis Function (RBF) surrogate models was compared, from which the RBF model proved to be more accurate and easier to construct. Subsequently, a GA was applied to further improve the solution. The objective was to minimize the curvature at the hog bend of the riser.

The common denominator between the above reference studies, is the usage of numerical simulation models. This calls for the need of a Blackbox Optimization (BBO) method. When working with simulation models, the analytical forms of the underlying algebraic equations is unknown, which makes it impossible to apply classical gradient-based optimization methods [10]. BBO methods are purely data driven and can therefore be applied if the structure of the objective function is unknown.

## III. Problem Description

The goal of this research is to create an efficient optimization method for the optimization of the DPC configuration. To achieve this, a model-based BBO method is formulated to optimize the fatigue behaviour of the numerical cable model. The time-domain simulations of the DPC are computationally expensive, which is why the optimizer must be able to find an optimum using as few function evaluation as possible.

### A. Parametric DPC Model

A parametric simulation model of the cable was created using the commercial software package OrcaFlex. Since decoupled analysis of the FOWT is considered adequate for the analysis of a LWS configuration, three individual models for the floating platform, DPC and fatigue calculations were formulated. The interaction between these models is illustrated in Figure 2. The global DPC model is defined by the global configuration parameters:

- $H$: HOP height above the seabed
- $L_1$: Length of the first dynamic section
- $n_{BM}$: Number of BMs
- $d_{BM}$: Distance between each BM
- $L$: Total cable length
- $x_{TP}$: Horizontal distance to the Termination Point (TP)

The role of the above parameters in the LWS configuration is illustrated in Figure 3.

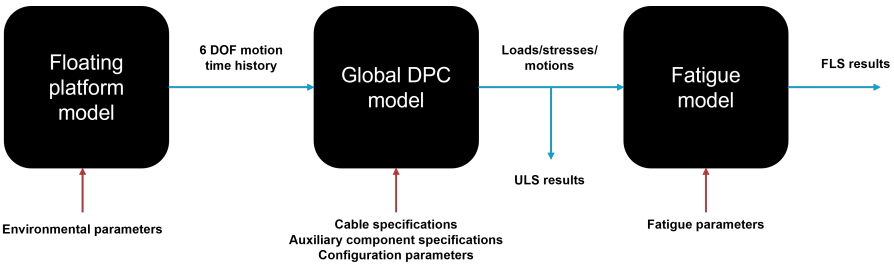


Fig. 2: Interaction between simulation models

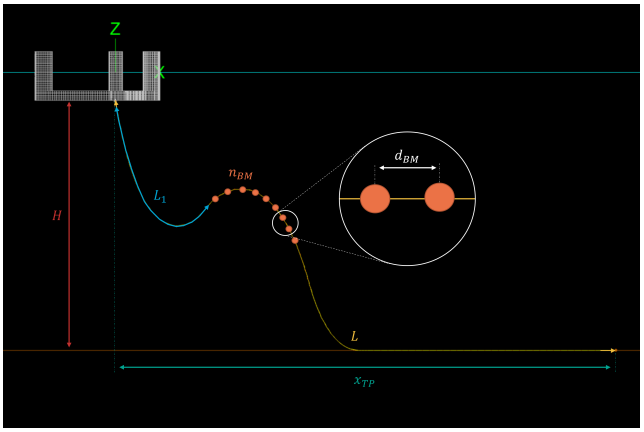


Fig. 3: LWS cable configuration and parameters

The simulation output of this model gives the stress and motion time histories on each node of the cable. Since the most fatigue critical component of the cable is the copper conductor, the motions and loads on the cable are translated into axial and bending stresses on the conductor, via the following equations:

$$\sigma_{a,c} = \frac{E_c F_a}{EA} \tag{1}$$

$$\sigma_{b,c} = \frac{E_c D_c \kappa}{2} \tag{2}$$

where $F_a$ is the axial load on the cable, $\kappa$ is the curvature of the cable, $EA$ is the axial stiffness of the cable and $E_c$ is the Young's modulus of the copper material within the conductor. $D_c$ is the diameter between the outer strains of the conductor, as shown in Figure 4.

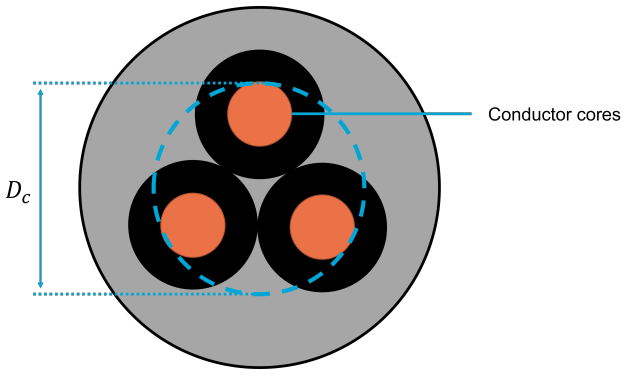


Fig. 4: Simplified DPC cross-section and conductor diameter

The load cycles that contribute to fatigue damage are counted using the rainflow counting method. This method was first introduced by Matsuichi and Endo [11] and is still widely applied for fatigue damage calculations in engineering applications. The accumulated fatigue damage is then calculated using the Miner-Palmgren rule [12]:

$$D_{ftg} = \sum_{i=1}^{k} \frac{n_i}{N_i} \tag{3}$$

where $k$ is the number of different stress levels from the rainflow analysis, $N_i$ is the average number of cycles to failure at stress level $S_i$ and $n_i$ is the number of stress cycles at stress level $S_i$.

### B. Optimization Problem Formulation

The general formulation of the optimization problem with $p$ constraints and $k$ decision variables is:

$$\begin{aligned} \min_{x} \quad & f(x) \\ \text{s.t.} \quad & g_i(x) \leq 0, \quad i = 1, ..., p \\ & x \in \mathbb{R}^k \end{aligned} \tag{4}$$

where vector $x$ represents the independent decision variables. The unknown objective function is represented by $f$, while $g$ denotes the constraints. As minimizing the maximum annual fatigue damage $D_{ftg}$ is the sole objective of the optimization problem, the objective function can simply be formulated as:

$$f(x) = D_{ftg} \tag{5}$$

Two decision variables are selected for solving the optimization problem, based on a parametric sensitivity study that is outside the scope of this paper. These are $L_1$ and $n_{BM}$. Both these parameters proved to have a significant influence on the fatigue behaviour of the DPC and are independent of other variables. Therefore, the mathematical formulation of the decision variables is:

$$x = \begin{bmatrix} x_1 \\ x_2 \end{bmatrix} = \begin{bmatrix} L_1 \\ n_{BM} \end{bmatrix} \tag{6}$$

The other configuration parameters that were previously introduced are fixed to limit the dimensionality of the optimization problem for research purposes. A number of constraints is introduced, which assure that none of the ultimate stress limits of the cable are exceeded and to prevent collisions with the surroundings. The constraints are formulated as:

$$g_1(x) \leq MBL \tag{7}$$

$$g_2(x) \leq \frac{1}{MBR} \tag{8}$$

$$-d_{surface} \leq g_3(x) \leq -D + d_{seabed} \tag{9}$$

$$g_4(x) \geq d_{static} \tag{10}$$

where $MBL$ is the minimum break load, $MBR$ is the minimum bend radius, $D$ is the water depth, $d_{surface}$ and $d_{seabed}$ are the minimum required distances between hog bend and water surface and sag bend and seabed respectively and $d_{static}$ is a minimum required length of stationary cable section before the TP.

### C. Optimization Algorithm

To solve this BBO problem, a Surrogate Model Optimization (SMO) method is used. The basic structure of the SMO algorithm is as follows:

1) *Design of experiment:* Perform sampling to obtain training data

2) *Surrogate modelling:* Fit a surrogate model to the training data
3) *Optimization problem solving:* Select and evaluate candidate solutions until the optimum is found.

This optimization structure is integrated into the cable analysis models as shown in Figure 5.

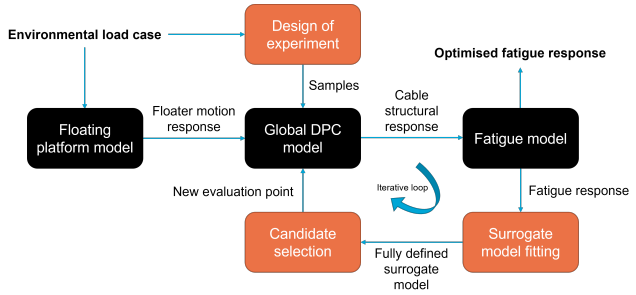


Fig. 5: Optimization structure

*1) Design of Experiment:* A conventional Design of Experiment (DoE) with LHS is not suitable for this optimization problem, because the feasible region of the search space is irregularly shaped. Therefore, an analysis of the feasible search space was performed, which yielded a generalization of the search space boundaries based on the water depth $D$. The general shape of the feasible search space is shown in Figure 6. The vertices can all be expressed as linear combinations of $D$. The resulting non-box-shaped boundaries make it difficult to apply efficient LHS.

Initial sampling is performed by randomly selecting samples within the boundaries of the feasible search space. Since some degree of space-filling (uniform distribution of the samples) is desirable to create a good initial sample set [13], a minimum Euclidean distance threshold is required between each sample and sampling is repeated until the sample distribution meets this condition.

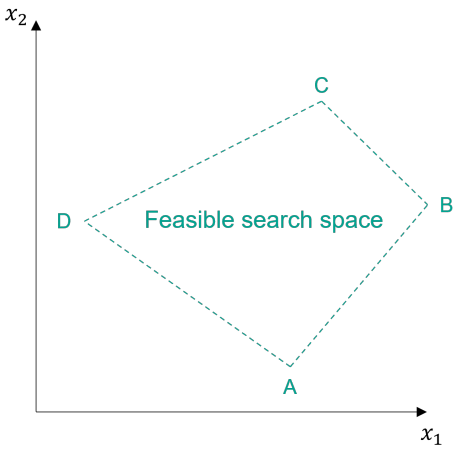


Fig. 6: Generalised feasible search space

*2) Surrogate Modelling:* A surrogate model, which represents an approximation of the real model function, is fit to the data set from the initial sampling. The RBF surrogate modelling method is used for this purpose. A radial function is a function whose value only depends on the Euclidean distance between the point at which it is evaluated and the origin and therefore has the form $\phi(x) = \varphi(|x|)$, where $\varphi$ is a real function [13]. The output of the system as estimated by the RBF surrogate model is then formulated as follows [14]:

$$\hat{f}(x) = \sum_{i-1}^{n} \theta_i \phi(||x - x_i||) \tag{11}$$

where the weights $\theta_i$ are determined by solving:

$$\theta = \Phi^{-1} f \tag{12}$$

Herein $n$ is the number of samples, $\Phi \in \mathbb{R}^{nxn} : \Phi_{i,j} = \varphi(||x - x_i||), i, j = 1, ..., n$ represents the RBFs and $f = f_1, ..., f_n$ is the vector of sampled function evaluations.

*3) Optimization Problem Solving:* Simply assuming that the minimum of the initial surrogate model is the optimum is risky. The surrogate model fit is most likely to be inaccurate, due to shortage of initial training data. Therefore, an iterative search strategy is required. This research makes use on an interpretation of the Constrained Optimization using Response Surfaces (CORS) algorithm by Regis and Shoemaker [15]. CORS selects candidate points that are located at a minimum distance away from the previously evaluated points. The selected candidate is then evaluated and added to the training data. A new surrogate model is then fitted to the updated set of training data. This process is repeated for decreasing minimum distances at which the candidate points must be located, up until the whole search space is included in the search. Therefore, the algorithm starts by performing pure global search (exploratory search) and gradually moves towards pure local search (exploitative search). The purpose of this approach is to find the global optimum and prevent premature convergence to a local optimum.

The iterative process described above is formulated as follows:

1) *Surrogate fitting:* The surrogate model $\hat{f}_i$ is fitted to the set of training data $D_i = \{(x, f(x)) \text{ for } x \in S_i\}$. Here $i$ is the current algorithm iteration, $S_i$ is the set of decision variable samples, and $f$ is the real model.
2) *Candidate selection:* The candidate selection step is the distinct feature of the CORS algorithm. The minimum distance between the existing data points and the candidate is governed by $\beta = \beta_1, ..., \beta_i$, where $0 \leq \beta_i \leq 1$. The new candidate point $x_{n+i}$ is then selected to be the point $x$ that solves the optimization problem:

$$\begin{aligned} \min \quad & \hat{f}_i(x) \\ \text{s.t.} \quad & ||x - x_j|| \geq \beta_i \Delta_i \\ & j = 1, ..., n + i + 1 \\ & x \in \mathcal{D} \end{aligned} \tag{13}$$

where

$$\Delta_i = \max_{\tilde{x} \in \mathcal{D}} \min_{1 \leq j \leq n+i-1} ||\tilde{x} - x_j|| \tag{14}$$

Herein $\mathcal{D}$ is the feasible decision variable space, as defined during the feasible search space analysis.

3) *Candidate evaluation:* The next step is to evaluate the function $f$ for the new candidate $x_{n+i}$. After the simulation has finished, the values of $\hat{f}_i(x)$ and $f_i(x)$ are compared and an the relative error is calculated:

$$e_i = \frac{||\hat{f}_i(x) - f_i(x)||}{||f_i(x)||} \tag{15}$$

4) *Evaluate stopping criterion:* A stopping criterion is introduced to terminate the algorithm once a suspected optimum is reached. The algorithm terminates when the relative error between the surrogate and the real model is smaller than a predefined error threshold:

$$e_i < \tau_e \tag{16}$$

At this point, if the stopping criterion is reached, the algorithm is terminated and the final results can be reviewed. If this is not the case then candidate $x_{n+i}$ and its evaluation $f_i(x)$ are added to the training data to form an updated training data set $D_{i+1}$. Subsequently, the algorithm returns to step 1 and a new iteration step is initialized.

## IV. Experimentation

The validity of the proposed optimization method is tested through a number of experiments. The following requirements are to be fulfilled:

- *Convergence:* The optimization algorithm must converge towards an optimum solution.
- *Robustness:* The optimization algorithm must perform well for a wide range of scenarios.
- *Efficiency:* An optimum solution must be found within acceptable time.

### A. Case Studies

Two case studies are formulated which represent different environmental operating conditions for the FOWT and its DPC. Case study 1 places the FOWT in moderately deep water and under a moderate sea state. The water depth and metocean conditions are based on the location of the HYWIND floating wind farm in Scotland, which are documented in a report by Statoil [16]. Case study 2 represents rougher environmental conditions and a larger water depth. The environmental conditions for both case studies are listed in Table I.

| Parameter | Symbol | Case study 1 | Case study 2 |
|---|---|---|---|
| Water depth | $D$ | 120 m | 200 m |
| Significant wave height | $H_s$ | 2 m | 4 m |
| Peak wave period | $T_p$ | 8 s | 11 s |
| Surface current velocity | $U_0$ | 0.15 m/s | 0.15 m/s |
| Current direction | $d_{cur}$ | 30° | 30° |
| Wind velocity | $v_{wind}$ | 10 m/s | 14 m/s |
| Wind direction | $d_{wind}$ | 0° | 0° |

TABLE I: Environmental parameter settings

The optimization parameters settings are shown in Table II. The values $\beta_i$ are defined as $\beta = [0.95, 0.85, 0.75, 0.5, 0.3, 0.2, 0.1, 0, ...]$. The parameter choices are based on previous experiments with a known test function. The number of initial samples has been adjusted for the case study 2 experiments to accommodate for the larger feasible search space.

| Parameter | Case study 1 | Case study 2 |
|---|---|---|
| $n$ | 15 | 25 |
| RBF type | Gaussian | Gaussian |

TABLE II: Optimization parameter settings

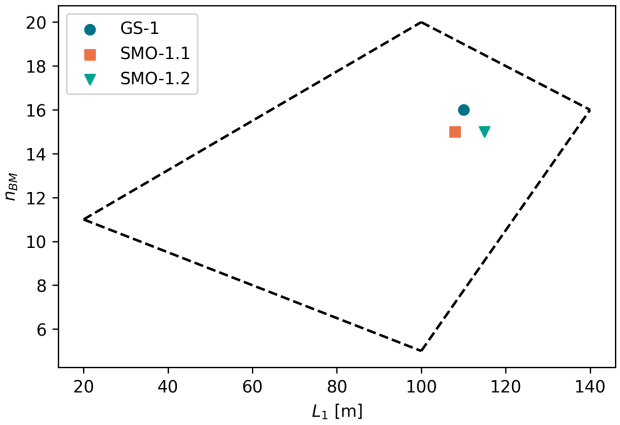


(a) Case study 1

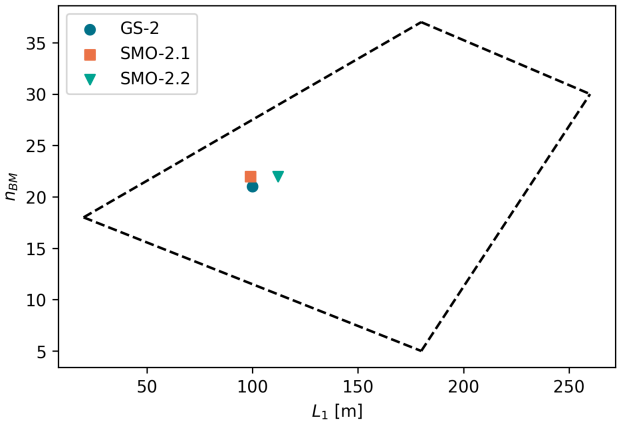


(b) Case study 2

Fig. 7: Optimal solutions

### B. Results

Several experiments are carried out using both the SMO method and a Grid Search (GS) algorithm with a relatively coarse grid mesh. The GS serves as material for comparison and to find the global optimal solution to the optimization problem. The four experiments using the SMO algorithm are named “SMO-1.1”, “SMO-1.2”, “SMO-2.1” and “SMO-2.2”, while the GS procedures for both case studies are referred to as “GS-1” and “GS-2”.

| Experiment | $L_{1,opt}$ | $n_{BM,opt}$ | $D_{ftg,opt}$ | $l_{ftg,opt}$ | Error | $n_f$ | Improvement |
|---|---|---|---|---|---|---|---|
| GS-1 | 110 m | 16 | 1.22e-5 | 8.23e4 years | - | 42 | - |
| SMO-1.1 | 108 m | 15 | 1.14e-5 | 8.76e4 years | -6.03e0% | 32 | 23.8% |
| SMO-1.2 | 115 m | 15 | 1.22e-5 | 8.17e4 years | 6.61e-1% | 30 | 28.6% |
| GS-2 | 100 m | 21 | 1.29e-2 | 7.74e1 years | - | 61 | - |
| SMO-2.1 | 99 m | 22 | 1.33e-2 | 7.52e1 years | 3.03e0% | 42 | 31.1% |
| SMO-2.2 | 114 m | 22 | 1.44e-2 | 6.95e1 years | 1.14e1% | 36 | 41.0% |

TABLE III: Results of GS and SMO experiments

The results showing the final solutions from each experiment are shown in Table III. Along with the variables that create the best performing final configuration, results for the efficiency are presented. Efficiency is measured as the total number of function evaluations that were performed until the algorithm terminated. The location of the final solutions of each experiment within the search space are plotted in Figure 7.

The GS algorithm runs identify two 'suspected' global optima. The results show that the final outcome of the SMO experiments is often very close to this optimal fatigue damage or in the case of SMO-1.1 even somewhat better. Figure 7 confirms that the solutions are indeed located closely within the same area of the search space, which indicates that the optimization algorithm indeed converges towards the global optimal solution. The worst performing experiment is SMO-2.2, which appears to have converged to a local optimum that is located very closely to the global optimum, showcasing the intricacy of the cable model's fatigue response. An improved accuracy of the surrogate model is required to improve this convergence behaviour.

In terms of efficiency, the proposed SMO method clearly outperforms the GS method. Improvements of up to 30% were achieved for successful runs, which is valuable time given that the function evaluations are computationally expensive. On top of that, the computational costs of the GS increase exponentially when the problem is expanded with additional decision variables, which is not the case for the SMO method [17].

## V. Conclusions and Recommendations

This section gives conclusions about the findings from the proposed SMO method and gives recommendations for future research on the matter.

### A. Conclusions

The goal of this research was to develop a method for the global optimization of the DPC configurations that is both computationally efficient and can be applied to a flexible range of environmental scenarios. This involved the formulation of a parametric cable model for the analysis of loads, motions and fatigue damage and the implementation of a surrogate model-based optimization method.

The proposed SMO method shows good performance in terms of its ability to converge to an optimal solution. The results are not perfect, but a near-optimal solution can be found reliably. This holds for different environmental scenarios, which indicates that the model is robust and applicable to a wide range of scenarios. This success can be attributed to the developed DoE method, which re-defines the search space boundaries for each different water depth. The efficiency of the optimization method is superior to that of a coarse GS algorithm. This property will most likely increase when more decision variables are added to the optimization problem.

### B. Recommendations

The first step in improving the optimization model can be to increase its design flexibility by adding new decision variables. A global configuration parameter, such as the total cable length, can easily be integrated into the model as a new variable. This allows for a wider variety of DPC configuration shapes. Naturally, this increases the complexity of the optimization problem, but the optimization method is theoretically capable of solving higher dimensionality optimization problems.

To improve the accuracy of the surrogate model, further analysis of the optimization parameters is required. This involves adjusting the number on initial samples, the parameter that governs the transition from exploratory to exploitative search and the RBF type. A strategic approach using a more appropriate test function is advised.

The option of an alternative search strategy towards the end of the optimization algorithm can be investigated. Currently the whole search space is eligible for candidate selection, which can make the optimizer drift away from the optimum if the surrogate model accuracy is poor in unexplored regions of the search space. A more greedy search near the current best solutions can help to prevent this.

## References


[1] U.S. Energy Information Administration, "International Energy Outlook 2021," 2021.

[2] International Energy Agency, "Net Zero by 2050: A Roadmap for the Global Energy Sector," 2021.

[3] W. Musial, S. Butterfield, and B. Ram, "Energy From Offshore Wind," in *Proc. 2006 Offshore Technology Conf.*, (Houston, Texas, USA), Offshore Technology Conference, 2006.

[4] J. Rhodri and M. Costa Ros, "Floating Offshore Wind: Market and Technology Review," 2015.

[5] P. R. Thies, L. Johanning, and G. H. Smith, "Assessing mechanical loading regimes and fatigue life of marine power cables in marine energy applications," in *Proc. of the Institution of Mechanical Engineers, Part O: Journal of Risk and Reliability*, vol. 226, pp. 18–32, 2012.

[6] S. Karlsen, R. Slora, K. Heide, S. Lund, F. Eggertsen, and P. A. Osbor, "Dynamic Deep Water Power Cables," in *Proc. 9th Int. Conf. and Exh. for Oil and Gas Resources Development of the Russian Arctic and CIS Continental Shelf*, pp. 194–203, 2009.

[7] Y. Poirette, M. Guiton, G. Huwart, D. Sinoquet, and J.-M. Leroy, "An Optimization method for the Configuration of Inter Array Cables for Floating Offshore Wind Farm," in *Proc. ASME 2017 36th Int. Conf. on Ocean, Offshore and Arctic Engineering*, (Trondheim, Norway), 2017.

[8] M. U. T. Rentschler, F. Adam, and P. Chainho, "Design optimization of dynamic inter-array cable systems for floating offshore wind turbines," *Renewable and Sustainable Energy Reviews*, vol. 111, pp. 622–635, 2019.

[9] J. Chen, J. Yan, Q. Yue, and M. Tang, "Flexible riser configuration design for extremely shallow water with surrogate-model- based optimization," *Journal of Offshore Mechanics and Arctic Engineering*, vol. 138, no. 4, pp. 1–7, 2016.

[10] I. Bajaj, A. Arora, and M. M. F. Hasan, "Black-Box Optimization: Methods and Applications," in *Black Box Optimization, Machine Learning, and No-Free Lunch Theorems* (P. M. Pardalos, V. Rasskazova, and M. N. Vrahatis, eds.), pp. 35–65, Springer Cham, 1 ed., 2021.

[11] M. Matsuichi and T. Endo, "Fatigue of metals subjected to varying stress," 1968.

[12] D. G. Young, C. Ng, S. Oterkus, Q. Li, and L. Johanning, "Predicting failure of dynamic cables for floating offshore wind," in *Proc. 3rd Int. Conf. on Renewable Energies Offshore*, pp. 821–828, 2019.

[13] V. K. Ky, C. D'Ambrosio, Y. Hamadi, and L. Liberti, "Surrogate-based methods for black-box optimization," *International Transactions in Operational Research*, vol. 24, no. 3, 2016.

[14] S. Bagheri, W. Konen, and T. Bäck, "Comparing Kriging and Radial Basis Function Surrogates," in *Proc. 27th Workshop on Computational Intelligence*, (Dortmund, Germany), pp. 243–259, 2017.

[15] R. G. Regis and C. A. Shoemaker, "Constrained global optimization of expensive black box functions using radial basis functions," *Journal of Global Optimization*, vol. 31, no. 1, pp. 153–171, 2005.

[16] M. Mathiesen, A. K. Meyer, and B. Kvingendal, "RE2014-002: Hywind Buchan Deep Metocean Design Basis," 2014.

[17] C. Audet and W. Hare, *Derivative-Free and Blackbox Optimization*. Springer Cham, 1 ed., 2017.

# B

# Reference Standards for DNV-OS-J103

| Standard no. | Title |
|---|---|
| IEC 60183 | Guide to the selection of high-voltage cables |
| IEC 60502 | Power cables with extruded insulation and their accessories for rated voltages from 1 kV (Um = 1,2 kV) up to 30 kV (Um = 36 kV) |
| IEC 60840 | Power cables with extruded insulation and their accessories for rated voltages above 30 kV (Um = 36 kV) up to 150 kV (Um = 170 kV) - Test methods and requirements |
| IEC 60228 | Conductors of insulated cables |
| IEC 60287-1-1 | Electric cables - Calculation of current rating - Part 1-1: Current rating equations (100% load factor) and calculation of losses - General |
| IEC 60287-2-1 | Electric cables - Calculation of current rating - Part 2-1: Thermal resistance - Calculation of thermal resistance |
| IEC 60287-3-2 | Electric cables - Calculation of current rating - Part 3-2: Sections on operating conditions - Economic optimization of power cable size |
| IEC 60300-1 | Dependability management - Part 1: Design requirements for offshore wind turbines |
| IEC 60793 | Optical fibres |
| IEC 60794 | Optical fibre cables |
| IEC 61400-3 | Wind turbines - Part 3: Design requirements for offshore wind turbines |
| IEC 62067 | Power cables with extruded insulation and their accessories for rated voltages above 150 kV (Um = 170 kV) up to 500 kV (Um = 550 kV) - Test methods and requirements |
| ISO 9001 | Quality management systems - Requirements |
| ISO 13628-5 | Petroleum and natural gas industries - Design and operation of subsea production systems - Part 5: Subsea umbilicals |
| ISO 14688-1 | Geotechnical investigation and testing - Identification and classification of soil - Part 1: Identification and description |
| ISO 14688-2 | Geotechnical investigation and testing - Identification and classification of soil - Part 2: Principles for a classification |
| ISO 19901-6 | Petroleum and natural gas industries - Specific requirements for offshore structures - Marine operations |
| ITU-T G.976 | Test methods applicable to optical fibre submarine cable systems |

Table B.1: Reference Standards for DNV-OS-J103 [45]

| Document no. | Title |
|---|---|
| API RP 2A | Recommended Practice for Planning, Designing and Constructing Fixed Offshore Platforms - Working Stress Design |
| API RP 2RD | Dynamic Risers for Floating Production Systems |
| CIGRÉ Technical Brochure 177 | Accessories for HV cables with extruded insulation |
| CIGRÉ Technical Brochure 279 | Maintenance for HV cables and accessories |
| CIGRÉ Technical Brochure 398 | Third-party damage to underground and submarine cables |
| CIGRÉ Technical Brochure 415 | Test procedures for HV transition joints for rated voltages 30 kV (Um = 36 kV) up to 500 kV (Um = 550 kV) |
| CIGRÉ Technical Brochure 476 | Cable accessory workmanship on extruded high voltage cables |
| CIGRÉ Technical Brochure 490 | Recommendations for testing of long AC submarine cables with extruded insulation for system voltage above 30 (36) to 500 (550) kV |
| CIGRÉ Technical Brochure 496 | Recommendations for testing DC extruded cable systems for power transmission at a rated voltage up to 500 kV |
| CIGRÉ Technical Brochure 560 | Guideline to maintaining the integrity of XLPE cable accessories |
| CIGRÉ Technical Brochure 610 | Offshore generation cable connections |
| CIGRÉ Electra 189 | Recommendations for tests of power transmission DC cables for a rated voltage up to 800 kV |
| DNV-OS-H102 | Marine Operations, Design and Fabrication |
| DNV-OS-H205 | Lifting Operations (VMO Standard Part 2-5) |
| DNV-OS-H206 | Loadout, transport and installation of subsea projects (VMO Standard - Part 2-6) |
| DNV-OS-J103 | Design of Floating Wind Turbine Structures |
| DNV-RP-F401 | Electrical Power Cables in Subsea Applications |
| DNVGL-RP-0360 | Subsea power cables in shallow water |
| GL-IV-2 | GL Rules and Guidelines - IV Industrial Services - Part 2 - Guideline for the Certification of Offshore Wind Turbines, Edition 2012 |
| ICPC Recommendation 3 | Criteria to be applied to proposed crossings between submarine telecommunications cables and pipelines/power cables |
| ICPC Recommendation 9 | Minimum technical requirements for a desktop study (also known as cable route study) |
| ICPC Recommendation 11 | Standardization of electronic formatting of route position lists |
| IMCA M 190 | Guidance for Developing and Conducting Annual DP Trials Programmes for DP Vessels |
| IMO MSC/Circ.645 | Guidelines for vessels with dynamic positioning systems |

Table B.2: Recommendations for DNV-OS-J103 [45]

# C

# Derivation of the Feasible Search Space Constraints

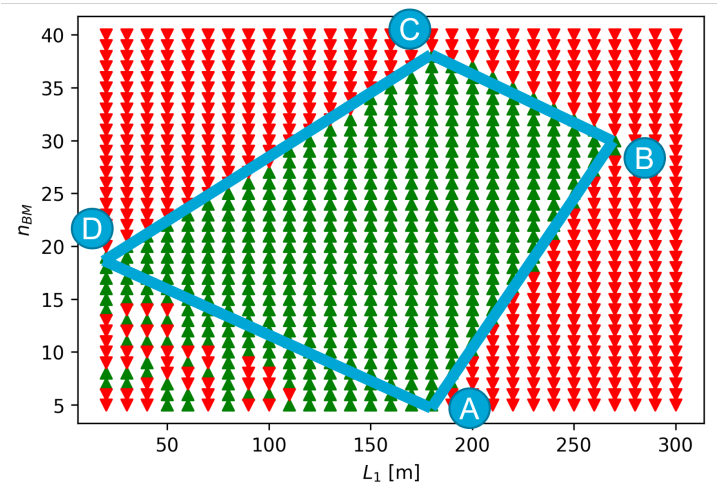


Figure C.1: Definition of the feasible search space vertices

| $D$ | $A_1$ | $A_2$ | $B_1$ | $B_2$ | $C_1$ | $C_2$ | $D_1$ | $D_2$ |
|---|---|---|---|---|---|---|---|---|
| 80 | 60 | 5 | 80 | 9 | 60 | 11 | 20 | 8 |
| 100 | 80 | 5 | 110 | 13 | 80 | 16 | 20 | 9 |
| 120 | 100 | 5 | 140 | 16 | 100 | 20 | 20 | 11 |
| 140 | 130 | 5 | 170 | 20 | 120 | 25 | 20 | 13 |
| 160 | 140 | 5 | 200 | 23 | 140 | 29 | 20 | 15 |
| 180 | 160 | 5 | 240 | 26 | 170 | 33 | 20 | 18 |
| 200 | 180 | 5 | 270 | 30 | 180 | 37 | 20 | 19 |
| 220 | 200 | 5 | 300 | 33 | 200 | 40 | 20 | 20 |

Table C.1: Vertices of feasible search space for different water depths

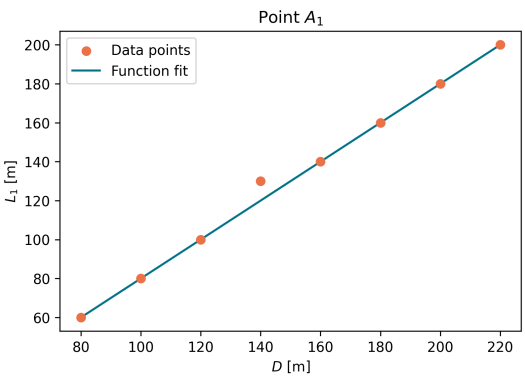


(a) $A_1 = D - 20$

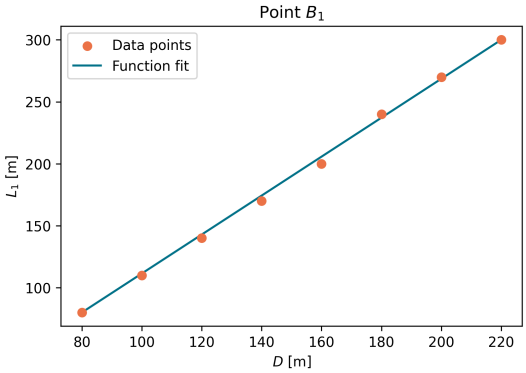


(b) $B_1 = \frac{11}{7}D - \frac{320}{7}$

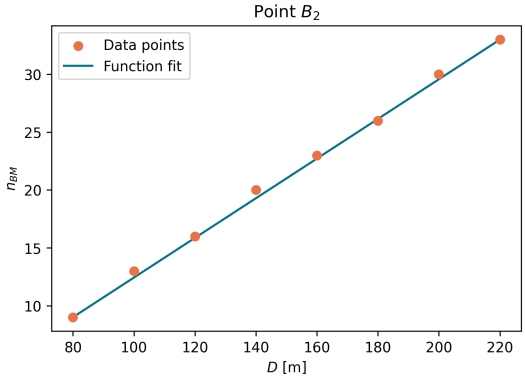


(c) $B_2 = \frac{6}{35}D - \frac{33}{7}$

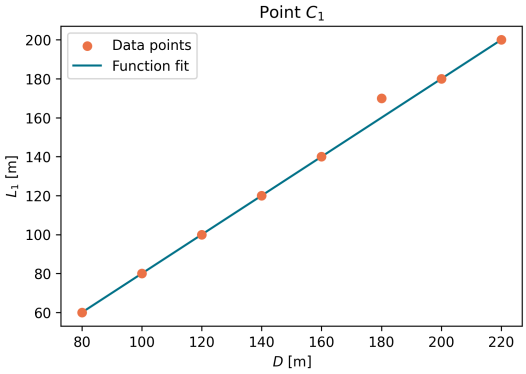


(d) $C_1 = D - 20$

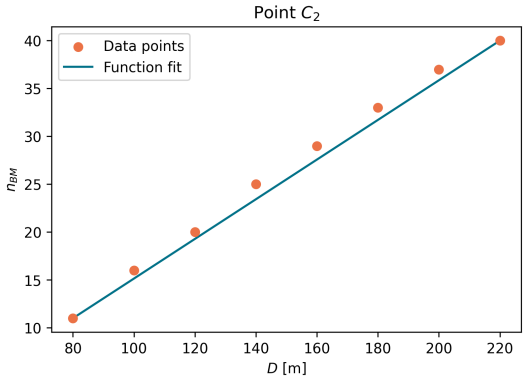


(e) $C_2 = \frac{29}{140}D - \frac{39}{7}$

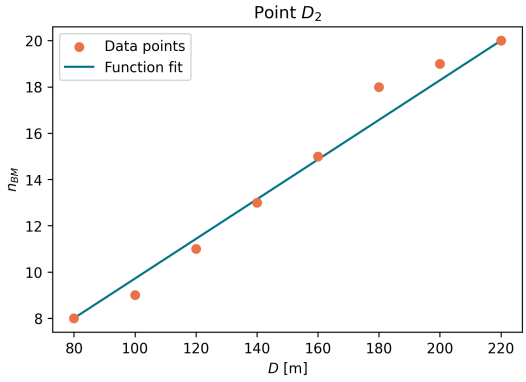


(f) $D_2 = \frac{3}{35}D + \frac{8}{7}$

Figure C.2: Data points from feasible search space analysis and fitted linear function

# D

# Feasible Search Space Verification

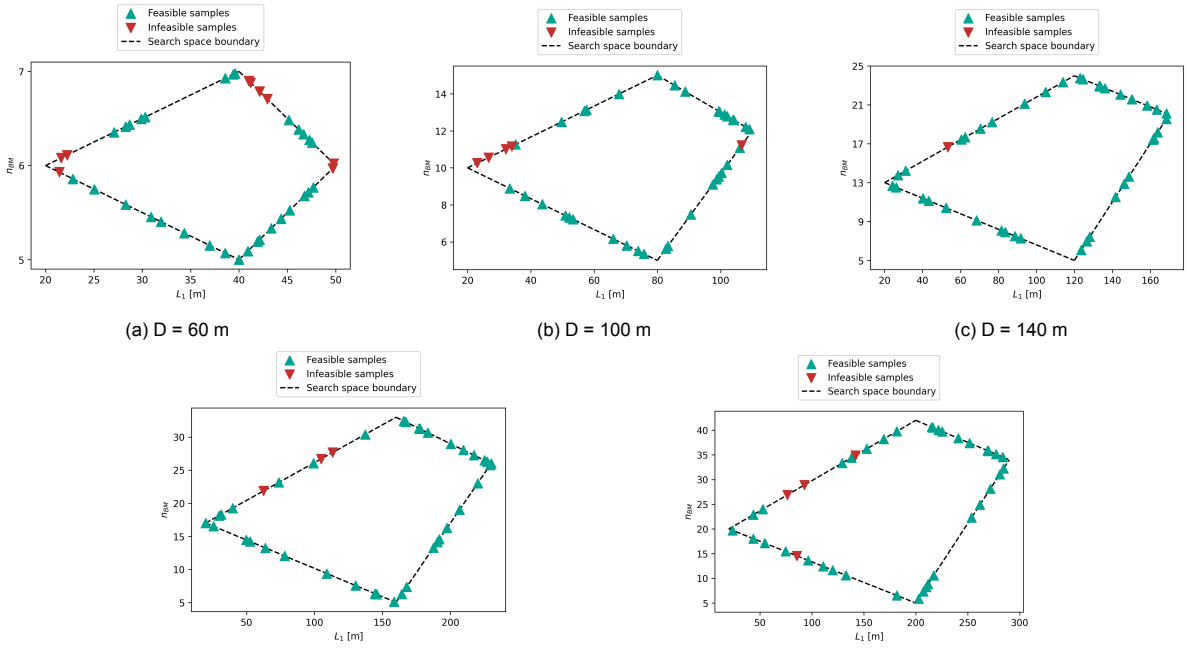


(a) D = 60 m

(b) D = 100 m

(c) D = 140 m

(d) D = 180 m

(e) D = 220 m

Figure D.1: Plotted results of the feasible search space verification step

# E

# Environmental Conditions at the HYWIND Floating Offshore Wind Farm

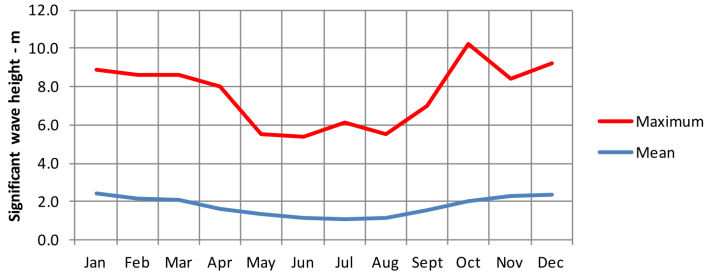


Figure E.1: Mean and maximum significant wave height at the HYWIND site [100]

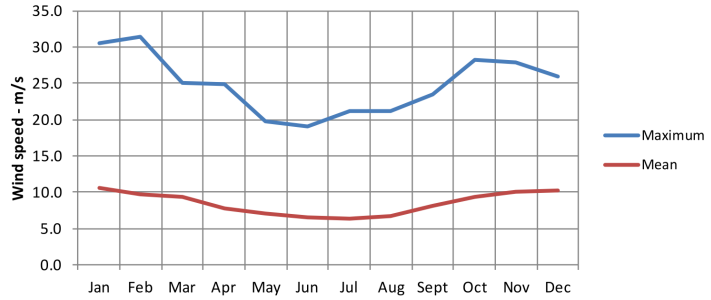


Figure E.2: Mean and maximum wind speeds at the HYWIND site [100]

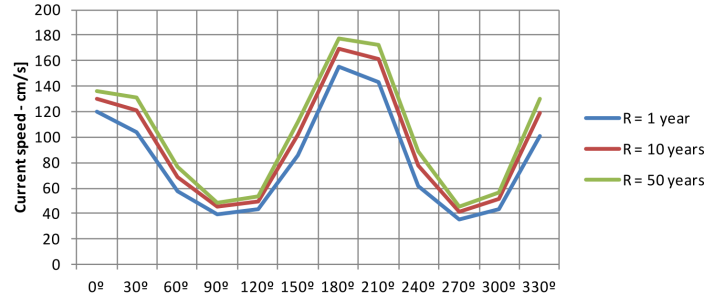


Figure E.3: Surface current velocities and direction at the HYWIND site [100]

| $H_S$ (m) | Spectral peak period ($T_p$) - (s) | | | | | | | | | | | | | | | | | | | | |
|---|---|---|---|---|---|---|---|---|---|---|---|---|---|---|---|---|---|---|---|---|---|
| | **2-3** | **3-4** | **4-5** | **5-6** | **6-7** | **7-8** | **8-9** | **9-10** | **10-11** | **11-12** | **12-13** | **13-14** | **14-15** | **15-16** | **16-17** | **17-18** | **18-19** | **19-20** | **20-21** | **21-22** | **22-23** | **Sum** |
| **0-1** | 177 | 3746 | 10423 | 9068 | 7551 | 4984 | 2983 | 2033 | 1142 | 626 | 309 | 167 | 63 | 38 | 12 | 3 | 4 | | | | | **43329** |
| **1-2** | | 57 | 5281 | 13966 | 12849 | 10034 | 7653 | 5074 | 3720 | 2476 | 1254 | 571 | 245 | 109 | 36 | 9 | 3 | | | | | **63337** |
| **2-3** | | | 32 | 1413 | 7085 | 7423 | 4826 | 3338 | 1985 | 1397 | 1132 | 582 | 228 | 125 | 31 | 12 | 7 | | | | | **29616** |
| **3-4** | | | | 4 | 599 | 2588 | 3559 | 2404 | 1332 | 553 | 388 | 204 | 141 | 63 | 20 | 5 | 2 | 1 | 1 | | | **11864** |
| **4-5** | | | | | 15 | 168 | 1046 | 1398 | 993 | 445 | 152 | 94 | 50 | 22 | 14 | 4 | | | 1 | | | **4402** |
| **5-6** | | | | | | 5 | 113 | 429 | 497 | 358 | 114 | 57 | 12 | 10 | 5 | | | | | | | **1600** |
| **6-7** | | | | | | | 3 | 55 | 132 | 166 | 103 | 43 | 13 | 3 | 2 | | | | | | | **520** |
| **7-8** | | | | | | | | 2 | 18 | 42 | 57 | 16 | 10 | 4 | 4 | | | | | | | **153** |
| **8-9** | | | | | | | | | 1 | 6 | 14 | 7 | 7 | 2 | 1 | | | | | | | **38** |
| **9-10** | | | | | | | | | | | | 1 | 2 | | | | | | | | | **3** |
| **10-11** | | | | | | | | | | | 1 | | | | | | | | | | | **1** |
| **Sum** | **177** | **3803** | **15736** | **24451** | **28099** | **25202** | **20183** | **14733** | **9820** | **6069** | **3524** | **1742** | **771** | **376** | **125** | **33** | **16** | **1** | **2** | **0** | **0** | **154863** |

Figure E.4: Wave scatter diagram at the HYWIND site [100]